ABSOLUTE DISTANCE (THICKNESS) METROLOGY USING WAVELENGTH SCANNING INTERFEROMETRY

by

Amit Ravindra Suratkar

A dissertation submitted to the faculty of
The University of North Carolina at Charlotte
in partial fulfillment of the requirements
for the degree of Doctor of Philosophy in
Optical Science and Engineering

Charlotte

2009

Approved by:

____
Dr. Angela Davies

____
Dr. Faramarz Farahi

____
Dr. Robert Hocken

____
Dr. Gregory Gbur

____
Dr. Shaozhong Deng

© 2009
Amit R Suratkar
ALL RIGHTS RESERVED

ABSTRACT

AMIT RAVINDRA SURATKAR. Absolute Distance (Thickness) metrology using wavelength scanning interferometry. (Under the direction of DR. ANGELA D. DAVIES)

Wavelength scanning interferometry offers a new dimension in precision metrology by measuring the cavity length (thickness), the cavity length variation over the cavity area (flatness), and the optical homogeneity within a transparent cavity; without any mechanical movement by implementing a tunable laser. This property is useful when the physical movement of an optic is not feasible using traditional phase shifting methods employing piezoelectric transducers and for characterizing solid optical cavities which require movement of one surface relative to the other. The cavity length that can be measured is limited by the wavelength scanning range - a smaller cavity requires a larger tuning range. Tunable lasers are now available with very large tuning ranges in the near infrared, potentially extending the measurement range significantly. The use of Fourier analysis on the intensity (interference) time history as a post processing step enables the measurement of cavity lengths without any 2π phase ambiguity. This study demonstrates absolute length (thickness) measurements of various artifacts such as the thickness of a transparent window, gauge blocks, and the diameter of transparent spherical cavities such as a ball lens on a commercial wavelength scanning Fizeau interferometer. A mathematical model of the measurement process is demonstrated along with a software simulation model to understand the impact of dynamic parameters such as tuning rate on the thickness. Finally, a custom built wavelength scanning interferometer is designed from an existing wideband tunable laser in-house to demonstrate the thickness of sub-mm windows.

ACKNOWLEDGEMENTS

I will always be indebted to my professor and advisor Dr. Angela Davies for her insights and inspiration during the course of my study and research. Coming from an engineering background, I have come to understand the depths of science (physics and optics in particular) under her able guidance. I would like to acknowledge the support and expertise from two other committee members Dr. Faramarz Farahi (chairman of the Department of Physics and Optical Science) and Dr. Robert Hocken (director for the Center for Precision Metrology and its affiliates which funded this research project). I am also grateful to my committee members Dr. Gregory Gbur and Dr. Shaozhong Deng for agreeing to sit on my committee. A special thanks to the Center for Optoelectronics and Optical Communications, its director Dr. Michael Fiddy and research operations manager Scott Williams for providing space and instrumentation for the project. This project would not have been possible for the technical and experimental inputs from Dr. Leslie Deck from Zygo Corporation, Dr. Joanna Schmit from Veeco Instruments, Dr. Awad Gerges from the Department of Physics and Optical Science at UNC Charlotte, David Jordan from National Instruments, Marc Hansen from Goodrich Corporation and Frank Buchanan from Agilent Technologies. I would also like to acknowledge the assistance from my colleague Dr. Young-Sik Ghim post doctoral student from KAIST (Korea Advanced Institute of Science and Technology) during the final phases of my research. A final thank you to my family and friends for having patience in me all these years.

DEDICATION

I would like to dedicate my studies at The University of North Carolina at Charlotte to my godparents.

TABLE OF CONTENTS

CHAPTER 1: MOTIVATION, GOALS AND OUTLINE OF STUDY 1

1. 1 Motivation 1

1. 2 Goals 2

1. 3 Outline 3

CHAPTER 2: INTERFEROMETRY IN METROLOGY 6

2. 1 Introduction to metrology 6

2. 2 Theory of interference 7

2. 3 Techniques for measuring Phase 11

2.3.1 Single Wavelength Interferometry 11

2.3.2 Multiple Wavelength (color) Interferometry 13

2.3.3 Frequency (Wavelength) Scanning Interferometry 14

2.3.4 Variable Synthetic Wavelength Interferometry 16

2.3.5 Broadband Interferometry : Phase measurements to measure thickness 16

2. 4 Review of techniques for absolute measurements: Thickness to distance 18

2. 5 Applications of interferometric measurements from Table 2-1 20

2. 6 Summary 21

CHAPTER 3 : MATHEMATICAL MODEL AND SIMULATION 22

3. 1 Introduction to wavelength scanning interferometry 22

3. 2 Theory of wavelength scanning interferometry 24

3. 3 Introduction to the MST: 29

3. 4 MST: Block diagram, Source, detectors, reference cavity specifics 31

3. 5 Example of a measurement 33

3. 6: OPD Transform 36

3. 7 Mathematical Model for the OPD of a cavity 38

3. 8 Simulation Model for the MST 40

3. 9 Uncertainty Analysis 45

3. 10 Measurements on a commercial interferometer 49

3. 11 Summary 56

CHAPTER 4: GAUGE BLOCK MEASUREMENTS 57

4. 1 Opaque Planar Artifacts using the MST 57

4. 2 Introduction to gauge blocks 58

4. 3 History of gauge block measurements 59

4. 4 Measurement theory 59

4. 5 Measurements 64

4. 6 Uncertainty Analysis 65

4.6.1 Effect of temperature on the OPL of test and reference cavity 67

4.6. 2 Effect of temperature on the Calibrated value of Reference 68

4.6.3 Effect of tuning rate non linearity 69

4.6.4 Effect of Phase Change on Reflection 70

4.6.5 Alignment 74

4. 7 Uncertainty Discussion 75

4. 8 Summary 77

CHAPTER 5: SUB-MILLIMETER METROLOGY 78

5. 1 Introduction to the sub mm project 78

5. 2 Hardware 79

5. 3 Optics 82

5. 4 Software 83

5. 5 Measurements of sub-millimeter thick windows 89

5. 6 Uncertainty Analysis 92

5. 7 Summary 96

CHAPTER 6: CONCLUSIONS AND CONTINUITY 98

6. 1: Conclusions 98

6. 2: Continuity (extension of the project to include surface profile measurements) 98

6. 3 Wavelength scanning and reflectometry techniques 100

REFERENCES 101

CHAPTER 1: MOTIVATION, GOALS AND OUTLINE OF STUDY

1. 1 Motivation

The project of determining absolute thickness of artifacts using wavelength scanning interferometry was initiated to determine the uncertainty sources in computing thickness (lengths) of various artifacts using the above mentioned technique. A successful addition to our project was the acquisition of a commercial wavelength scanning interferometer (the MST or Multiple Surface Transform from Zygo Corporation, tuning range: 4 nm) by the Center for Optoelectronics and Optical Communications. Although this instrument was designed for profiling, it was nevertheless decided to investigate the uncertainty sources in measuring thickness since it used the technique of wavelength scanning. In this regard, I am grateful for the correspondence with Dr. Leslie Deck from Zygo Corporation for providing me with insights into the measurement technique and the instrument. In addition to using this commercial instrument for measuring different artifacts (transparent planar, opaque planar and transparent spherical) and analyzing uncertainty contributions it was also decided to use existing tools in our department to build a customized interferometer to demonstrate the measurement of sub- millimeter cavities; the most important tools being a long wavelength tunable laser from Agilent technologies (tuning range 120 nm, 1460 nm to 1580 nm), a Sensors Unlimited Camera. The spectral response of the camera is from 900 nm to 1700 nm.

1. 2 Goals

The dissertation is divided into two parts: the first consists of measuring various artifacts mentioned above on a commercial interferometer and understanding the uncertainty sources. A mathematical model of the technique is provided to understand the measurement of thickness of a cavity using wavelength scanning. This is complimented with a software simulation model to understand the impact of dynamic parameters such as the tuning rate on the accuracy and precision of the measurement. The simulation uses experimental values for the tuning of the laser which are recorded using a wavemeter. Measurements of artifacts are accomplished in the reflection mode; i.e. the light reflected from the two ends of the cavity under test is used to determine the length (thickness). The measurement of different cavities is achieved using different configurations: a transparent cavity uses no additional optics and is placed simply in front of the instrument for measurement. A spherical cavity measurement is achieved using a transmission sphere and calculating the best focus position to place the artifact with a series of measurements to determine the Zernike defocus term. The distance corresponding to the lowest value of the Zernike term is used as the starting point in taking measurements. Opaque cavities are measured by using a two mirror Sagnac configuration along with a beam splitter to measure the two surfaces of the cavity. An uncertainty budget is provided to understand the limits in the instrument and which factor limits the measurement uncertainty. This information can be extrapolated to understand the limits in the measurement technique. This serves as a prerequisite in the design of the customized system with a predefined uncertainty goal. The next part of the dissertation is to use the knowledge gained from the simulation and experiments to

build an interferometer to measure sub-millimeter cavities. The samples which will be measured are fused silica wafers with thickness ranging from 400 microns to 60 microns. The need to design an interferometer to measure sub- millimeter cavities is pursued due to an absence of such an interferometer from literature and the need for measuring cavities in the sub-millimeter range from the sponsors of this project. A similar uncertainty budget is provided to help understand the dominating factors which limit the measurement uncertainty. Finally, this research can be used as a tool to understand which aspects of a measurement (source specifics, measurement technique, detector specifics) limit the thickness measurement for different artifacts using the technique of wavelength scanning interferometry.

1. 3 Outline

The dissertation is divided into four sections each involving the measurement of absolute thickness (distance) at a single pixel using the technique of wavelength scanning interferometry. The first section is a literature review of measurement techniques. In this section different types of measurement parameters such as absolute distance, absolute thickness, surface form are explored across different measurement scales using different techniques. The underlying aim is to show the absence of measuring the thickness of artifacts such as a thin transparent plate so widely used in the optics and semiconductor industries. The next section describes the technique of wavelength scanning interferometry which has moved from the laboratory to a commercial interferometer along with the measurement of various transparent artifacts such a transparent fused silica window and a transparent ball lens. A simulation describing the technique is added to the study to compliment the mathematical model of

measuring absolute thickness. A detailed uncertainty analysis is described to provide a measurement range to the estimated value of the thickness for the different windows as mentioned above. The third section describes the technique for measuring cavities by measuring the coarse length of a gauge block. Gauge blocks are length standards and use two measurements: a coarse and a fine measurement to provide measurement accuracies in the range of tens of nanometers for a measurements lengths of 1 2, 3 inches. While fine measurements use dynamic phase shifting techniques or comparators, coarse measurements are usually restricted to multiple wavelength interferometry where three wavelengths are used to determine the coarse lengths up to a tolerance of 140 to 300 micrometers. The technique of wavelength scanning and a special measurement geometry for measuring opaque objects is proposed and shown to improve on this tolerance. The average gauge block lengths for one, two, and three inch gauge blocks with this technique are shown to be within 40 micrometers (±20) of their absolute length. The fourth section covers the design of a broadband wavelength scanning system using a broadband tunable laser (1460 nm – 1580 nm) and a near infrared camera to demonstrate the technique of wavelength scanning to measure sub-millimeter artifacts. The thickness of various artifacts (25µm, 60µm and 450 µm) has been demonstrated with a custom built wavelength scanning interferometer. The final section describes future work as an ongoing project which aims to use data from the commercial interferometer and employ another technique of reflectometry (modeling) to obtain the absolute thickness over the entire footprint of the sample. A projected sketch of using this technique on the custom built broadband wavelength scanning

system for measure profiles and thickness over the sample is provided using color corrected optics as a future implementation.

CHAPTER 2: INTERFEROMETRY IN METROLOGY

2. 1 Introduction to metrology

Metrology as defined by the International Bureau of Weights and Measures (BIPM) is "the science of measurement, embracing both experimental and theoretical determinations at any level of uncertainty in any field of science and technology”.

The basic building block of an interferometric measurement consists of an interferometer to generate fringes between two surfaces or cavities, transform this fringe pattern into phase or frequencies (spatial or temporal) and finally compute the height profile (surface contour, volumetric thickness, single pixel thickness, distance) using this information as shown in Figure 2- 1. This concept is explained in the later sections.

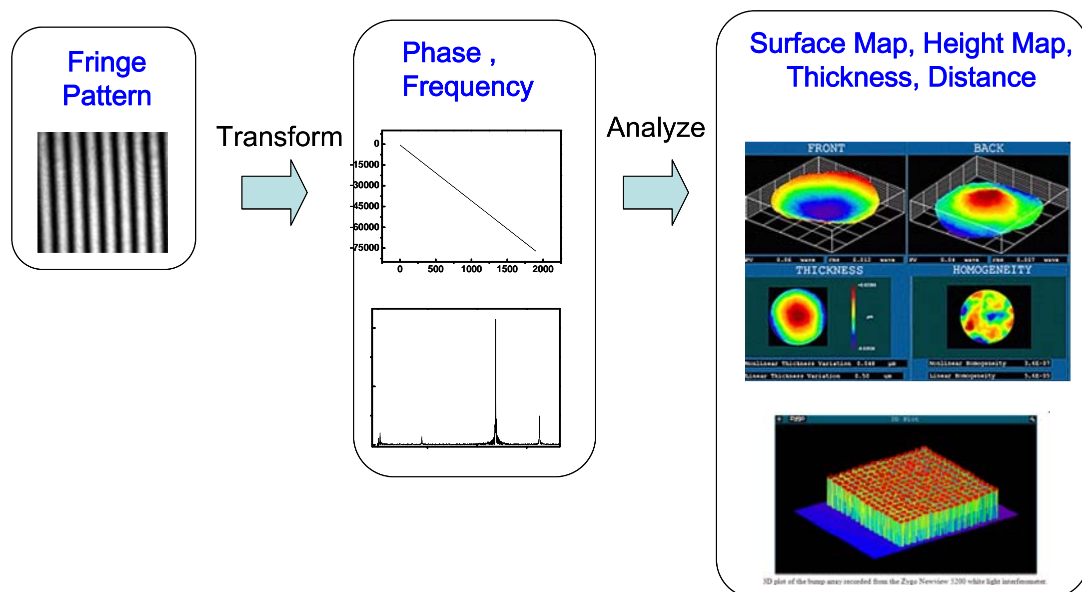

Figure 2- 1: Basic blocks in interferometry

2. 2 Theory of interference

The theory of interference is based on the principle of superposition and is the basis of all interferometric experiments [1]. The superposition principle states that the resultant displacement (at a particular point in space) produced by a number of waves having the same wavelength or frequency is the vector sum of the displacements produced by each one of the disturbances. In this context, a disturbance can be associated with an electric field having the form

$$E = E_0 cos(k \cdot x + \phi_0),$$

Equation 2- 1

where

E is the electric field amplitude at any point (x,y),

k is the wave vector along the x axis and is given as $2\pi/\lambda$ where λ is the wavelength and

ϕ_0 is the initial phase.

Although the resultant displacement vector using the principle of superposition can be applied to N different displacements where N represents the number of displacements at the given location *(x,y)*, let's consider the effect of two such displacements to understand the theory of interference. Consider two such electric fields described by Equation 2- 1 as

$$E_1 = E_{10} cos(k \cdot x + \phi_1) \text{ and } E_2 = E_{20} cos(k \cdot x + \phi_2)$$

Equation 2- 2

where all symbols have their usual meaning and δ represents the phase difference $(\phi_2 - \phi_1)$ between the two waves ($0 \leq \delta \leq 2\pi$).

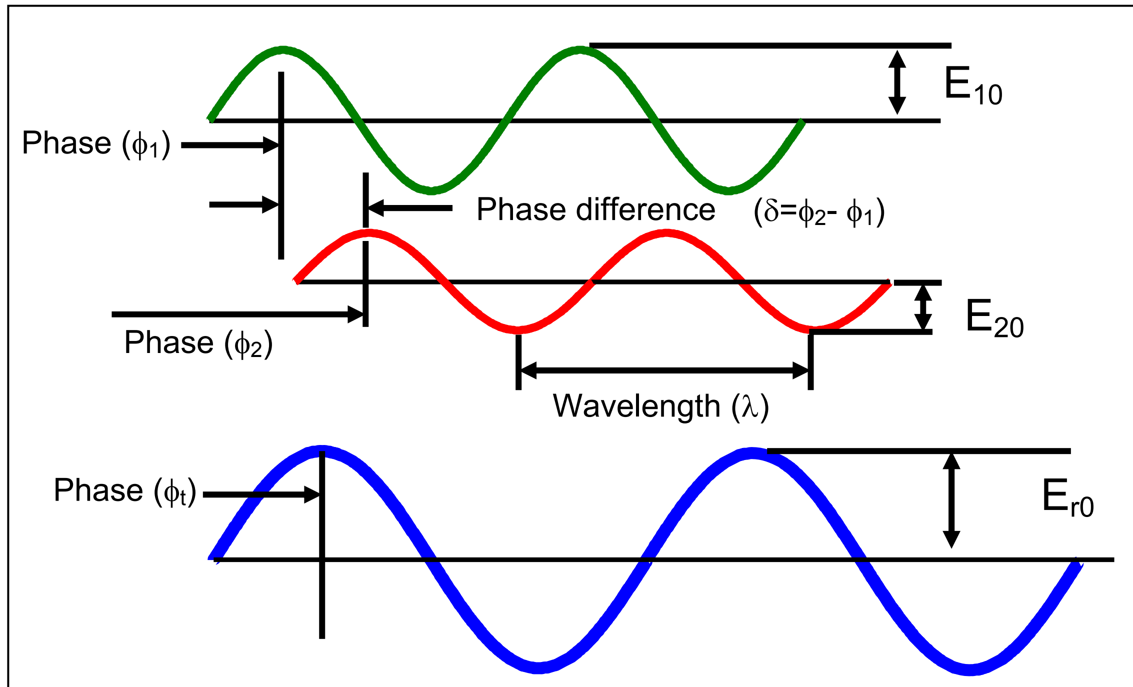

Figure 2- 2: Principle of superposition for two vectors along with resultant

Then according to the principle of superposition, the resultant electric field amplitude is given as

$$E_r = E_1 + E_2 = E_{10}\, cos(k \cdot x + \phi_1) + E_{20}\, cos(k \cdot x + \phi_2)$$

Equation 2- 3

which can also be written in the form

$$E_r = E_{r0} cos(k \cdot x + \phi_t)$$

Equation 2- 4

where the resultant amplitude and phase of the resultant are respectively

$$E_{r0} = \sqrt{E_{10}^2 + E_{20}^2 + 2E_{10}E_{20}cos(\delta)} \text{ and } \tan(\phi_t) = \frac{E_{10}\sin(\phi_1) + E_{20}\sin(\phi_2)}{E_{10}\cos(\phi_1) + E_{20}\cos(\phi_2)}.$$

Equation 2- 5

Since the detectors detect the intensity which is proportional to the square of the electric field, the resultant intensity is given by squaring Equation 2- 3 as

$$I = \left\langle (E_1 + E_2)^2 \right\rangle_T = (E_{10}\cos(k \cdot x + \phi_1) + E_{20}\cos(k \cdot x + \phi_2))^2$$

Equation 2- 6

which can be simplified to give the basic interference equation for two beams as

$$I = I_1 + I_2 + 2\sqrt{I_1 I_2}\cos(\delta)$$

Equation 2- 7

where $I_1 + I_2$ is the sum of irradiances of the two sources respectively and $2\sqrt{I_1 I_2}\cos(\delta)$ is the interference term. The intensity at the detector for a two beam (plane waves) interference would look similar to Figure 2- 3 where the bright lines correspond to constructive interference when the phase difference δ is an integer multiple of 2π (δ = 2πm where m = 0, ±1, ±2, ±3 ..) and the dark lines correspond to destructive interference when the phase difference is a odd multiple of π; (δ = πm where m = ±1, ±3, ±5 ..).

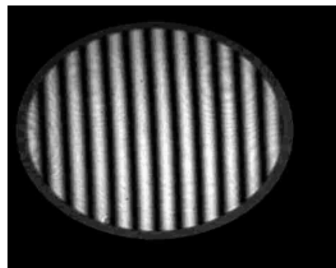

Figure 2- 3 : Intensity at the detector for two beam interference

In most cases the resultant phase difference may not be an exact multiple of π or 2π and this will result in the intensity to vary as shades of gray as shown in which represents multiple beam interference.

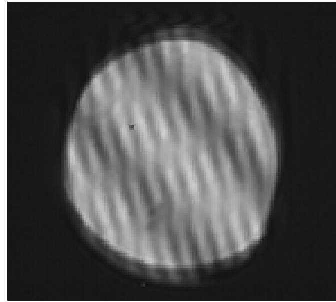

Figure 2- 4 : Intensity at the detector for multiple beam interference showing interference varying in shades of gray

In order to understand how the interference theory is related to the length, we start with the basic equation for the phase of a cavity which can written as

$$\phi = L \cdot k + \phi_0$$

Equation 2- 8

where L represents the length of the cavity and k is the wave vector ($k = 2\pi/\lambda$ where λ is the wavelength) and ϕ_0 is the initial phase. This equation represents the equation of a line in the form $y = a.x + b$ where a is the slope and b is the intercept along the y axis. The phase can be represented similarly as shown in Figure 2- 5 with the wave vector k as the abscissa and the phase ϕ as the ordinate.

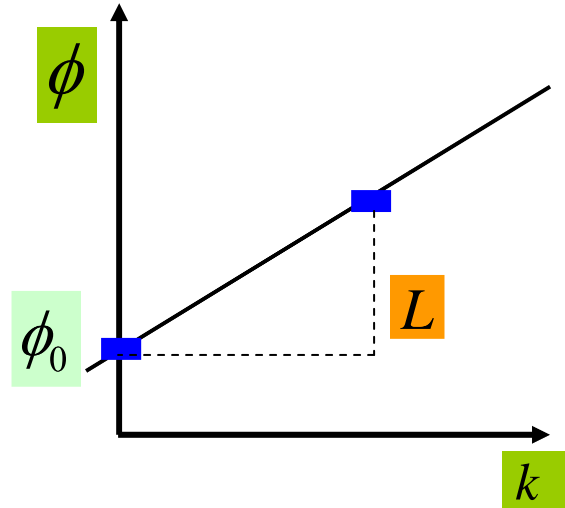

Figure 2- 5 : The equation for phase in the form of a straight line

2. 3 Techniques for measuring Phase

2.3.1 Single Wavelength Interferometry

It is possible to determine any quantity from Equation 2- 8 if the other parameters are known. For example, if the wavelength and the offset are known, the length (or height) can be obtained from the slope by varying the offset phase (ϕ_0) in equal increments and recording the intensity and using known algorithms. This is the basic feature of phase shifting interferometry and is used to determine the profile of a surface (height) for a single wavelength. Phase is a cyclic function i.e. it repeats after every 2π radians (modulo 2π).

$$\phi = \text{modulo} 2\pi \left[\frac{L}{\lambda}\right]$$

Equation 2- 9

Hence phase measurements for a single wavelength have been limited to a measurement range (height) of λ/2 or ± λ/4. From the electromagnetic spectrum shown in Figure 2-

6 and from Equation 2- 9, a microwave frequency (1 mm to 1 m) will be required to measure basic one inch artifacts used in the manufacturing and testing industry.

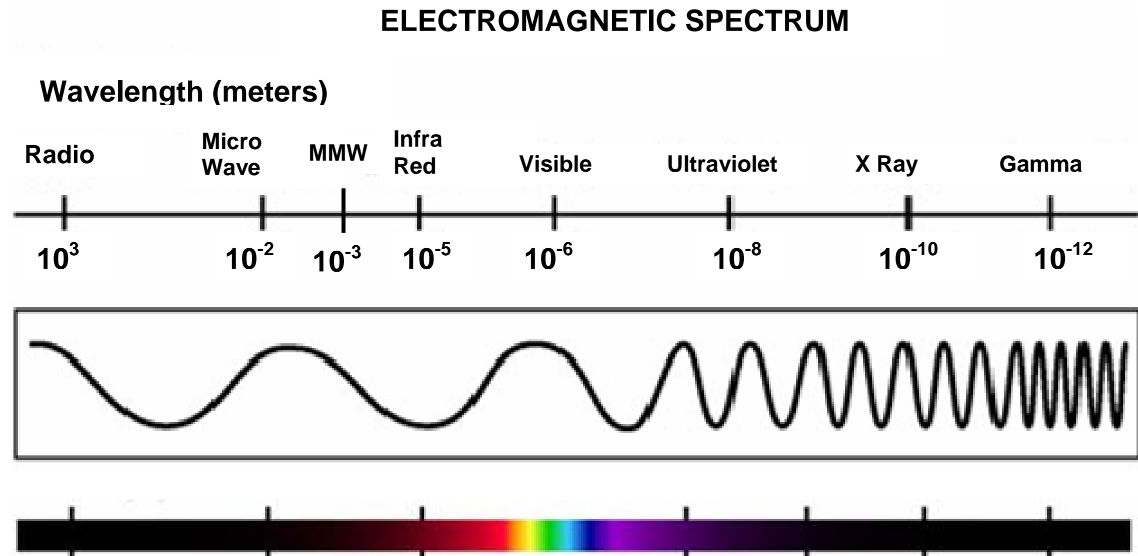

Figure 2- 6 : Electromagnetic Spectrum

Absolute distance measurements with single wavelength interferometry can be accomplished using the technique of displacement measuring interferometry (DMI) where changes in distance are measured, if the starting position or distance is known. Displacement measuring interferometry is sometimes also known as incremental interferometry [2]. Single wavelength interferometry has found itself in applications to phase shifting interferometry such as profilometry where the surface profile of artifacts is computed by changing the phase difference between a reference and test surface in a predefined manner using piezoelectric transducers [3]. The required phase profile of the artifact is computed using a combination of phase shifting methods and corresponding algorithms [4]. The procedure consists of determining the intensity at a

given pixel for a certain number of predefined phase shifts known as buckets and then solving a set of simultaneous equations to obtain the required phase. The phase resolution improves with the buckets but makes the algorithm for obtaining the phase more complex. Usually 4 to 11 buckets have been reported to determine the phase at a given pixel [5]. In recent years, piezoelectric transducers have been replaced by tunable lasers thereby eliminating mechanical movement and also by using different schemes and a larger number of buckets to obtain a more precise phase [6].

2.3.2 Multiple Wavelength (color) Interferometry

The challenge of increasing the measurement range (referred to as the unambiguity range) by using a single wavelength is increased by obtaining phase measurements for two, three or even four wavelengths and solving a set of simultaneous equations to obtain a range for the length L. In a two wavelength interferometry set-up, the process of using two wavelengths which are close to each other creates a virtual or synthetic wavelength (Λ) which is much larger than the individual wavelengths (λ_1, λ_2) and is given by

$$\Lambda = \frac{\lambda_1 \cdot \lambda_2}{\lambda_1 - \lambda_2}$$

Equation 2- 10

The use of effective wavelength was introduced in holography [7] [8] to test transparent media and aspherical optics thereby underlying the main advantages of using a combination of two wavelengths in the visible spectrum to obtain similar results equivalent to one measurement with a longer wavelength which would be invisible to the eye, could not be detected on film directly, would be unable to test ordinary refractive elements , and incur experimental difficulty due to its invisible radiation. The

use of equivalent or effective wavelength was then extended into the interferometry regime by Polhemus [9]. The detection schemes for the effective wavelength have been vastly different: measuring the phases individually at the given wavelengths [10] and determining the distances to more complex schemes of heterodyning in which the phase difference is directly measured by electronics [11]. One of the greatest advantages in using the multiple wavelengths is that the measurement range is greatly increased by using sources within the visible region thereby making alignment easier. . In [12] the authors use sub Doppler transitions from Iodine and Cesium atoms as their source for two wavelength interferometry to measure distances. A distance accuracy of 90 µm ($9/10^3$) is reported for an effective wavelength of 19 mm corresponding to a distance measurement of 9.5mm. In another case the authors use four wavelengths (one in the infrared) to increase the measurement range [13] and apply this measurement for the coarse measurement of length standards such as gauge blocks. Here the author reports a 100 mm gauge block measurement to within a tolerance limit of 140 micrometers. It is important to mention that gauge blocks are precision length standards which are accurate to within $1/10^{th}$ of a micrometer (or even better) and involve a coarse and a fine measurement to provide such accuracy. The author mentioned above reports a coarse measurement of gauge blocks using the effective wavelength in multiple wavelength interferometry

2.3.3 Frequency (Wavelength) Scanning Interferometry

Another approach uses a changing phase at different values of the wavelength (k) spaced over time or different values to measure the distance (thickness). This technique falls in the dynamic interferometry regime and is known as wavelength

scanning (frequency scanning) interferometry [14]- [19]. Coherent / optical frequency domain reflectometry, wavelength scanning interferometry, broadband tuning interferometry, swept-wavelength interferometry and frequency sweeping interferometry are all synonyms referred to at different periods of time in history. They all use a tunable laser source for their intended purpose. An earlier application used for free space ranging measurements was known as frequency modulated continuous wave radar [20]. Other applications included measurement of reflections and back scatter in optical fibers [21] - [23] where this technique was popularly known as Optical Frequency Domain Reflectometry (OFDR). OFDR was also used for measuring group delays and group velocity dispersion [24] [25], polarization maintaining dispersion [26] and temperature and strain sensing [27]. Wavelength (frequency) scanning interferometry employs a tunable laser source/s to compute the phase (or phase variation) to determine the thickness of a cavity. The phase can be easily unwrapped and is without any 2π ambiguity which makes this technique efficient in measuring absolute distance. The measurement range of wavelength scanning interferometry depends on the tuning range of the laser; a larger tuning range measures a smaller cavity. The use of tunable laser means that phase can also be measured at the two ends of the sweep individually [28] [29] and during the sweep to give a better and more accurate sweep interval for distance measurement. Some of the uncertainty sources with this technique include non linearity of the tune, sensitivity to motion during the experiment. Non-linear effects during the tuning have been reduced by using a reference cavity and measuring the test cavity as a function of the reference cavity specifics. Any change in the motion of the test cavity during the sweep is magnified by

a factor of Λ/λ , where Λ is the effective wavelength. Thus this technique cannot be used to measure large distances in air, however as we will show in the following chapters, this effect will cancel itself out when measuring the two ends of a window (transparent artifact).

2.3.4 Variable Synthetic Wavelength Interferometry

Variable synthetic wavelength interferometry employs two lasers. The main objective is to have a synthetic wavelength similar to multiple wavelength interferometry which will change over time (variable) as one or both lasers are scanned in frequency. This technique was introduced to reduce the sensitivity to movements (test cavity) since any change in the movement now affects both the lasers and if the tuning ranges are similar then the errors related to movements can be greatly reduced [30].

2.3.5 Broadband Interferometry : Phase measurements to measure thickness

The coherence length of a laser enables it as a precision tool for measuring long distances. Contrary to the use of a laser, a broadband source such as a white light source has a very short coherence length which means that the test and reference arms in the interferometer need to be equal (within the coherence length) for interferometric fringes to be observed. This property is actually useful for measuring the thickness of films of the order of microns (thick films) and even in the nanometer regime (thin film). Since good contrast for the fringes is obtained only when the paths (test and reference) are well matched, various techniques have been implemented to determine the peak of the intensity envelope which determines the thickness of the films [31]. In this process the sampled is scanned in the z direction and an interference envelope is obtained which is

then processed to obtain the phase and further the thickness. While the smallest cavity that can be measured with this technique relies on the ability of the fringe envelopes corresponding to the two layers to be resolved; the largest cavity that has recently been demonstrated is a plane parallel plate with nominal thickness of 1 mm [32]. This was the first demonstration of using a short coherence source to measure an artifact around this dimensions and more emphasis is shown on the technique of measurement. While the previous reference on white light interferometers employ a scanning method, a new type of white light interferometry which utilizes spectrally resolved information using a grating and a spectrometer (dispersive interferometry) and phase shifting to determine the thickness of thin films has been reported [33]-[35]. Thin films of the order of tens of nanometers have been reported by some of these techniques. In this technique instead of scanning the sample in the z direction and obtaining the intensities for all the wavelengths as a function of time, a spectrometer is made to split the intensity based on wavelengths on calibrated linear photo arrays of a CCD thereby providing intensity information based on wavelength contrary to distance as in the scanning case. The phase is obtained similar to the previous case and the thickness is computed accordingly. In both cases the thickness is modeled from the phase using non linear least squares fitting functions. Another case of spectral scanning is reported in [36] where an acousto-optical tunable filter is implemented to determine the thickness profile of an aluminum patterned sample along a line boundary. Finally dispersive interferometry using a femtosecond pulse laser has been reported in [37] to demonstrate the thickness of a 1 mm transparent BK7 part with a fractional uncertainty of 1/1000.

2. 4 Review of techniques for absolute measurements: Thickness to distance

Absolute distance measurement is a broader topic which can be divided into two types of measurement techniques: 1) pulse measurement techniques and 2) interferometric techniques. The pulse measurement technique is a time of flight measurement in which a pulse is sent out to a reflecting object and the round trip time for the pulse from source to the detector is recorded. Thus if t is half the round trip time and v is the speed of the pulse, then the unknown path length L is given as

$$L = v \cdot t$$

Equation 2- 11

For optical pulses the speed of the pulse is the speed of light c. This technique is used in different forms in radar, sonar etc. The uncertainty in measuring the length depends on the rise time uncertainty of the transmitted and received pulses. Current accuracies are usually limited to one millimeter because of the finite resolution in resolving the time differences [38].

Another technique uses an amplitude modulated carrier instead of a pulse and the distance is measured as a function of the difference in phase (time) between the reflected signal when compared with the modulation signal in a phase meter.

$$\phi = 2 \cdot \pi \cdot f_m \cdot t = 2 \cdot \pi \cdot f_m \cdot L / c = 2 \cdot \pi \cdot L / \lambda_m$$

Equation 2- 12

Authors in

[39] and [40] use different modulation frequencies to measure distances of several meters with a resolution of several micrometers. However the phase obtained is modulo 2π and hence *a priori* information of the length needs to be known within the

modulation wavelength rendering these techniques relative. Another technique is the use of a femtosecond pulse laser whose intensity is a train of sharp pulses. The frequency domain representation of a femtosecond pulsed laser consists of frequency modes repeating every 50 MHz (femtosecond pulse width of 180 fs) [41]. The distance is measured by determining the phase of the wave relative to the original wave for a given harmonic frequency in the received signal (which is a large multiple of the pulse repetition frequency) and is given by

$$(N+\frac{\phi}{2\pi})=\frac{2fn_gL}{c}$$

Equation 2- 13

where f is the high frequency harmonic, n_g is the group refractive index at that frequency (wavelength), ϕ is the fractional phase for the given frequency, L is the distance and N is the integer part of the phase. The integer part is obtained by mechanical movement or using two color (two wavelength) interferometry. The integer part can also be obtained very accurately if conditions for stability are met for the pulse repetition frequency and pulse to pulse carrier envelope as discussed in [42]. Another scheme involving choice of multiple wavelengths from the comb of a femtosecond laser has been proposed to measure distances in [43]. The authors propose selecting any two different wavelengths from the comb of a femtosecond laser to provide a synthetic wavelength just like in the multiple wavelength interferometry for distance measurements. Absolute distance measurements have also been reported by tuning a laser and counting the number of fringes for the test cavity and the number of free spectral ranges in a Fabry-Perot cavity by a technique known as frequency sweeping

interferometry [44]. The authors report an average tolerance of 10 μm for distances around 1 m. Some of the applications of interferometry are summarized below.

2. 5 Applications of interferometric measurements from Table 2-1

Table 2- 1: Summary of techniques for absolute measurements

Technique	Type of artifacts observed in literature	Parameter measured (Single pixel thickness, area, volume)	Limits in measurement
Phase shifting laser interferometer	Metal parts, mirrors, plain, spherical	Surface form, shape, roughness	Cannot determine thickness beyond (0.5 wavelength) between adjacent pixels
Phase shifting low coherence interferometer	Transparent glass plates	Surface profile of each surface with one measurement, homogeneity, optical thickness	Surface profile for front and back surface for a given thickness limited by scanning range
White light interferometry	Thin films (50 nm onwards) to thick films(2 μm)	Surface profile, topographic measurements,	Limit lies in separation between adjacent peaks between two cavities, Thickness limited to z range in z scanning and resolution of spectrometer in spectral scanning
Multiple Wavelength Interferometry	Distance, length of gauge blocks	Single pixel thickness	Length limited by half the effective wavelength. Stability of wavelengths also important.
Wavelength scanning with Fourier Analysis	Distance(length) of a cavity, transparent plate profile	Single pixel optical thickness, homogeneity, surface profile of all surfaces in one measurement	Length limited by tuning range, larger tuning range for a smaller cavity
Frequency sweeping with Fabry-Perot	Large distances	Single point measurement	Length accuracy limited by drift during measurement

cavity			
Femtosecond laser	Large distances,	Single point measurement	Stability of pulse

2. 6 Summary

From Table 2- 1, it can be inferred that although there are references for measuring the thickness of a cavity and distance (length of a large cavity) but no reference to window measurements such as transparent plates. There is also no detailed uncertainty analysis on the length of a cavity measurement using wavelength scanning interferometry. Most of the research in wavelength scanning interferometry has been to provide proof of concept that the technique is capable of providing distance measurements limited by a given set of parameters. One of the main objectives of this study is to provide a detailed uncertainty analysis of the parameters (using a mathematical model and an experimentally based simulation approach) and determine the limits in the measurement uncertainty and apply this analysis to the measurement of different artifacts (transparent planar window, transparent spherical window, opaque planar artifacts) not reported in the literature. The next objective is to apply this study in building an interferometer to measure sub-millimeter windows which are also not reported in literature.

CHAPTER 3 : MATHEMATICAL MODEL AND SIMULATION

(based on papers [90]-[91])

3. 1 Introduction to wavelength scanning interferometry

Wavelength scanning interferometry owes its origins to the tunability of a laser and has found great applications in the domain of phase shifting interferometry. Before the use of the tunable lasers, phase shifting interferometry was accomplished using mechanical forms of phase shifting such as piezoelectric transducers or PZT's. Although phase shifting has replaced mechanical forms of profiling due to non contact and area measurements compared to point by point measurements, it has been unable to measure some of the basic components in industry such as transparent plates which have found great applications in display, telecommunications and the optics industries. This is due to its inability in differentiating multiple beam interference from various optics or the artifacts itself. The phase shifting algorithms also assume a two beam interference and hence majority of the methods have been stated in [6] to suppress multiple beam interference. These include grating based interferometry, coating the obstructing surface with index matching lacquer, broadband interferometry, multimode laser diodes, grazing based interferometry and designing frequency specific algorithms using wavelength tuned phase shifting interferometry [45]- [49]. A recent publication in 2007 cited earlier [32] uses a low coherence source along with phase shifting interferometry to determine the front, back and the optical thickness profiles of transparent artifacts. Using a low coherence source, the length from a reference and the

front surface of the artifact is matched with another interferometer. Since the intensity is maximum when the paths are matched over a very small distance on account of a low coherence source the phase can be extracted for the surface of the artifact whose length matches with the interferometer. Other surfaces are mapped similarly by changing the reference interferometer length and measuring the phase using phase shifting methods.

The first tunable lasers were dye lasers and were discovered by Sorokin and Lankard [50] and Schäfer et al. [51] in 1966. Subsequent improvement in controlling the modes of the laser were provided with the invention of the continuous wave dye laser by Peterson *et al.* [52] in 1970. Most of the work of ultra-short pulse generation has its origin to the research done with dye lasers [53] - [57]. The growth of dye laser research has been impeded because of several factors chief among them being: limited output power, need for pumping with green or blue light making the pump sources expensive, rapid degradation during operation, handling of poisonous materials associated with dye lasers and the toxic nature of most dyes and their solvents [58].

Semiconductor lasers solve most of the problems associated with dye lasers: small, compact and rugged design, larger tuning range with no mod hop behavior, excellent repeatability, little intensity variation during tuning, more output power and the most important being that they can be fiber pigtailed and easy to tune by a variety of methods [6]. The tunability of the laser found itself in many applications as mentioned in the last chapter. The successive sections now describe the usability of a tunable laser in measuring absolute length, profiling various surfaces in one measurement etc.

One of the early references in wavelength scanning interferometry to measure absolute thickness of artifacts was proposed by Olsson et al [14] (1981) in which a dye

laser was implemented and tuned electronically and the distance measurement of a transparent artifact was determined from the period of the interference signal with a given tuning rate. This was later followed by distance measurements using the phase shift of the laser diode [15] [16] , the period of a beat signal produced by a frequency ramped laser diode [17] , from two consecutive harmonics of interference signal produced by sinusoidal phase modulation [18] and later by temporal Fourier Transform techniques on the intensity pattern [19]. The use of tunable lasers has greatly enhanced profilometry measurements compared to mechanical forms of phase shifting interferometry by eliminating moving parts such as piezo electric transducers. The Fourier Transform technique which is the most robust and widely used technique allows one to measure the phase profiles of all the cavities along with their optical thickness, physical thickness and the homogeneity: all in one single measurement [59]. Tunable lasers have also found themselves in applications to OCT [60]. This chapter will concentrate the discussion of single pixel thickness using the Fourier Transform technique and related uncertainty sources henceforth which is the main parameter of interest in this study.

3. 2 Theory of wavelength scanning interferometry

Consider a Fizeau interferometer setup as shown in Figure 3-1.

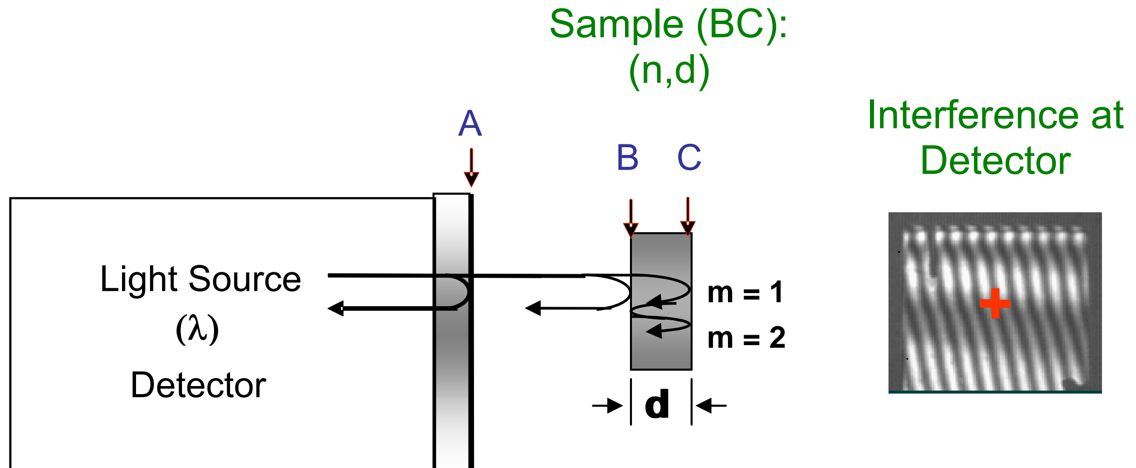

Figure 3-1: A Fizeau interferometer setup for measuring thickness

The objective is to measure the thickness of the sample (a transparent fused silica artifact) using wavelength scanning interferometry. The interference pattern at the detector shows the interference pattern between the various surfaces (A-B, A-C and B-C). Ideally three patterns should be seen but since one of them is weak only two interference patterns can be observed.

The electric fields on reflection from each of the three surfaces (A, B and C) can be represented respectively as

$$E_A = Ae^{i\phi_A}\ ,\ E_B = Be^{i\phi_B}\ ,\ E_C = Ce^{i\phi_C}\ .$$

Equation 3- 1

The total electric field is given by

$$E_T = E_A + E_B + E_C$$

Equation 3- 2

The intensity as seen at the detector is given by

$$I_T = E_T . E_T^{\ *}\ ,$$

Equation 3- 3

$$I_T = A^2 + B^2 + C^2 + 2AB\cos(\phi_A - \phi_B) + 2BC\cos(\phi_B - \phi_C) + 2AC\cos(\phi_A - \phi_C),$$

Equation 3- 4

$$I_T = S + 2AB\cos(\phi_{A-B}) + 2BC\cos(\phi_{B-C}) + 2AC\cos(\phi_{A-C}),$$

Equation 3- 5

where S = $A^2 + B^2 + C^2$ and the subscripts ϕ_{A-B}, ϕ_{B-C} and ϕ_{C-A} represent the phases between the respective surfaces. Let us now derive the equations for these phases as the wavelength is tuned.

The phase of a cavity at any point *P(x,y)* is represented from the generic phase equation

$$\phi(x, y, t) = \frac{2\pi}{\lambda(t)} \cdot m \cdot n(x, y, t) \cdot d(x, y, t) + \Omega(x, y, t)$$

Equation 3- 6

where *n* is the refractive index, *d* is the physical length or thickness in case of transparent materials, λ is the wavelength, *m* is the order of interference (*m= 1* for single reflection, *m=2* for double reflection and so on) and *Ω* is the difference in the phase change on reflection between the interfering surfaces .

As the phase is tuned w.r.t. time *t*, the equation of the phase variation can be represented as

$$\frac{\partial \phi}{\partial t} = -\frac{2 \cdot \pi \cdot m}{\lambda^2} \cdot n(x, y, t) \cdot d(x, y, t) \cdot (1 - \frac{\lambda}{n} \cdot \frac{\partial n}{\partial \lambda}) \cdot \frac{\partial \lambda}{\partial t} + \frac{\partial \Omega}{\partial t}$$

Equation 3- 7

where $\frac{\partial \lambda}{\partial n}$ is the dispersion of the medium over the tuning range. The dispersion coefficient term η is represented as

$$\eta = \frac{\lambda}{n} \cdot \frac{\partial n}{\partial \lambda}.$$

Equation 3- 8

The term $\frac{\partial \Omega}{\partial t}$ represents the variation in the phase change on reflection. Since the phase change on reflection is usually constant over the tuning range for most artifacts the term $\frac{\partial \Omega}{\partial t}$ is almost negligible.

As the phase changes due to the change in wavelength, the rate of change of the fringes with reference to the point P (x,y,t) over the measurement gives the frequency f corresponding to the fringe pattern. Since the angular frequency ω is defined as the rate of change of phase, Equation 3- 7 can be represented as

$$\omega = \frac{\partial \phi}{\partial N} = 2 \cdot \pi \cdot f$$

Equation 3- 9

where the frequency is represented as

$$f_C = \frac{m}{\lambda^2} \cdot n(x,y,t) \cdot d(x,y,t) \cdot (1-\eta) \cdot \frac{\partial \lambda}{\partial t} + \frac{1}{2\pi} \frac{\partial \Omega}{\partial t}$$

$$f_C = \frac{m}{\lambda^2} \cdot n(x,y,t) \cdot d(x,y,t) \cdot (1-\eta) \cdot \frac{\partial \lambda}{\partial t} + \frac{m}{\lambda^2} \cdot \delta_\Omega \cdot \frac{\partial \lambda}{\partial t}$$

$$f_C = \frac{m}{\lambda^2} \cdot OPD \cdot \frac{\partial \lambda}{\partial t}$$

Equation 3- 10

where the Optical Path Difference (OPD) is given as

$$OPD = n(x,y,t) \cdot d(x,y,t) \cdot (1-\eta) + \delta_\Omega$$

Equation 3- 11

where δ_{Ω} represents the optical length corresponding to the phase change on reflection. From Equation 3- 10, it is seen that the frequency of a cavity is a function of the Optical Path Difference (henceforth mentioned as OPD) and the tuning rate of the laser. Another parameter of interest is the OPD of a cavity. While mechanical forms of measurement directly compute the mechanical length or thickness, static forms of interferometry compute the optical length but require the refractive index of the artifact at the given wavelength to compute the physical length, dynamic forms of interferometry such as wavelength tuning require an additional term apart from the average refractive index and that is the dispersion coefficient η, for computing the physical length from the OPD. It is also important to mention that the dispersion coefficient is negative if we take the slope of refractive index with wavelength and so the contribution from dispersion is positive $(1+\eta)$. One of the clear advantages of pursuing this technique for measuring silicon wafers and industry parts made of different glass types (BK7, fused Silica etc) is that their refractive indices (equation of refractive index with wavelength) have been well documented in literature which makes the determination of the dispersion coefficient only a mathematical computation! As mentioned in the early sections of this chapter this study discusses the measurement of artifacts using the Fourier Transform technique.

As seen from Equation 3- 10, the frequency of a cavity will be constant only if the laser is tuned perfectly. This is never the case and so techniques have been implemented to account for the non linearity in the lasers. Some of them mentioned in [61] involve focusing on the design and execution of the tunable laser source to provide a tuning curve which is linear in time [62] - [65], using a reference interferometer as a

clock to trigger data acquisition [66] - [68], using an auxiliary interferometer to measure the tuning rate and correct it on the fringe data for equal samples [69] -[70].

Another approach used in this study [71], uses a special type of Fourier transform known as the OPD transform which uses phase information along the x axis to match with intensity information along the Y axis to compensate for the non linearities during the tune. A brief description of the instrument (the Multiple Surface Transform or the MST) which uses this technique is provided before discussing the mathematical model for obtaining the absolute length (thickness) of a cavity (window).

3. 3 Introduction to the MST:

The Multiple Surface Transform (MST) from Zygo Corporation was designed as a profiling instrument to measure the surface profile of the front and back surfaces of a cavity, the physical and optical thickness of the cavity and the homogeneity: all, in one single measurement using the theory of wavelength scanning interferometry or Fourier Transform phase shifting interferometry. The concept of determining the cavity lengths using a tuning laser and the Fourier transform method has been patented by them [72].

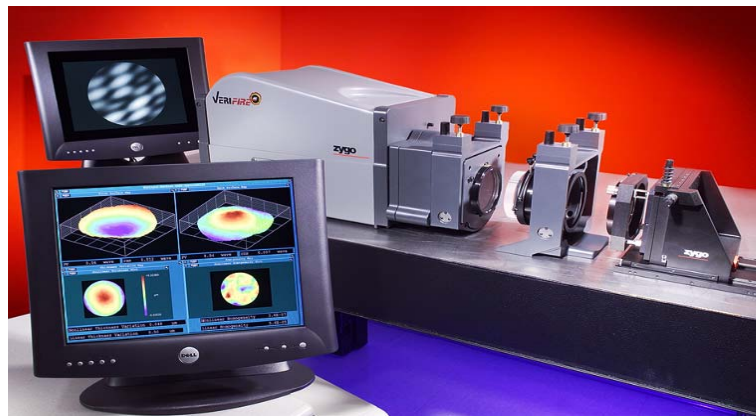

Figure 3- 2: The Multiple Surface Transform (MST) from Zygo Corporation is a profiling instrument using the concept of wavelength scanning interferometry

The MST uses a couple of applications but the one of interest to this study is the custom cavity application which has the ability to measure the different surface profiles of all windows and their cavity lengths in one measurement while the homogeneity requires an additional measurement as shown in Figure 3- 3.

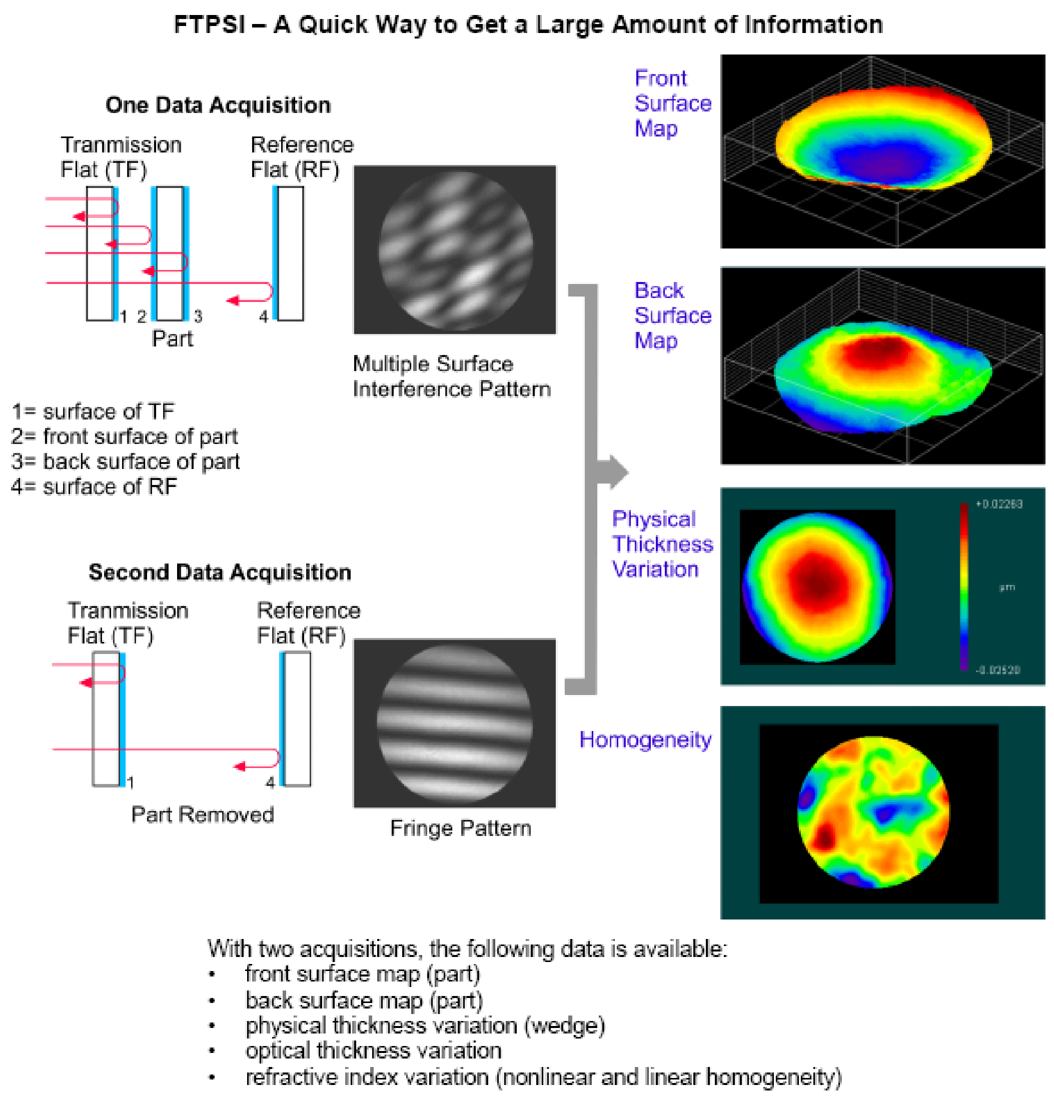

Figure 3- 3: MST in the Custom Cavity Application for measuring front and back surfaces, thickness variation and homogeneity

3. 4 MST: Block diagram, Source, detectors, reference cavity specifics

The basic building blocks of the MST [73] are shown in Figure 3- 4 . The source, detector and the reference cavity are described in the following sections.

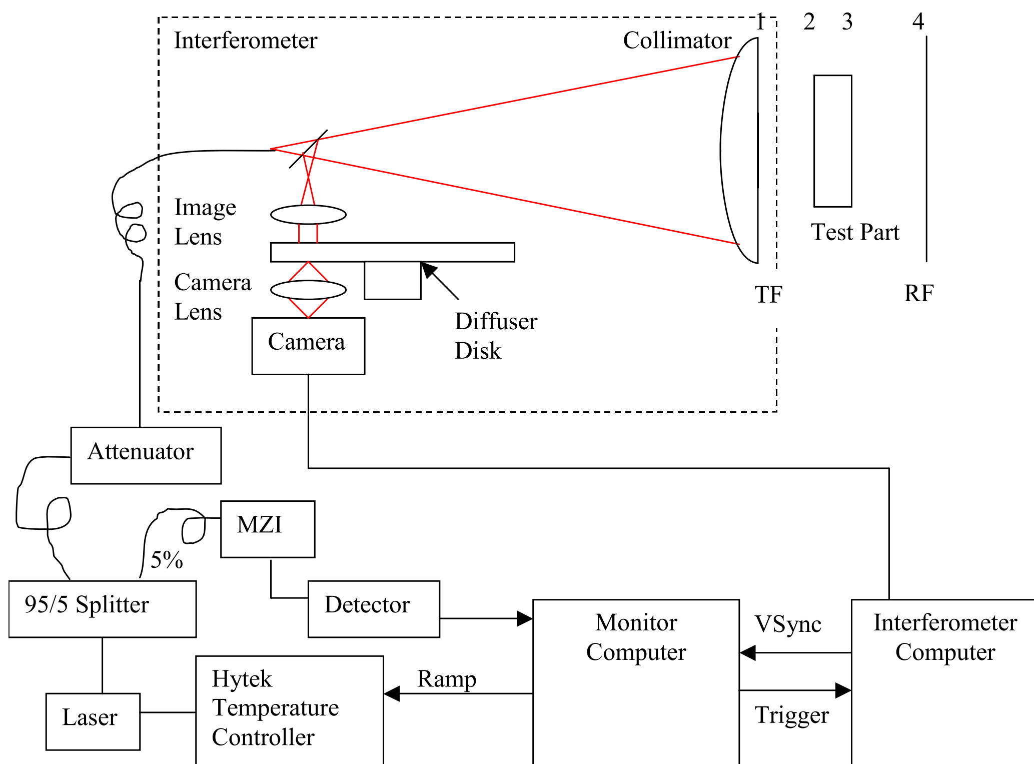

Figure 3- 4: Basic building blocks of the MST

The MST uses a thermally tuned semiconductor distributed feedback laser diode which is tuned by changing the injection current to the diode, which in turn changes the temperature and finally the wavelength. The tuning range of the diode is around 4 nanometer. An integrated thermoelectric cooler is used for heating and cooling the laser chip and for thermal tuning by varying the temperature from 0 to 40° Celsius over a range of 4 nanometers [74] . The temperature of the diode is initially set at 0° Celsius

and varied to a maximum of over 4 nanometers with every 10° Celsius corresponding to a change in 1 nanometer. The laser is fiber coupled and the output fiber is inserted into a 95/5 fiber beamsplitter with the 5% leg inserted into a fiber Mach-Zehnder interferometer (MZI) which is the reference cavity, while the 95% leg is routed to the interferometer. The output of the MZI is directed to a New Focus InGaAs photodetector connected to the DAC card input. The camera (second detector) is a Sensors Unlimited SU320M-1.7RT camera containing a 320x240 InGaAs array. The camera operates at 60Hz and has a 12 bit digital output. The camera data is acquired by a Matrox Pulsar framegrabber. The two detectors are time synchronized by providing the Pulsar board with a trigger generated by the DAC card.

The reference cavity in the MST is a fiber Mach-Zahnder interferometer with an optical path difference (OPD) of around 7.34153 m with a temperature uncertainty of ± 2 ° Celsius. The reference cavity is calibrated against an in-house Fabry-Perot cavity of around 238 mm with an accuracy of 500 nanometers. The major uncertainty in the calibrated value of the reference cavity lies in the temperature uncertainty between calibration on site and inside the laboratory where measurements are taken. This uncertainty effect is evaluated for different measured cavities in the uncertainty budget. The MST uses two detectors, a camera to get two dimensional data for the test sample and a photo detector to measure the phase variation of the reference cavity. The OPD for any given length is determined using the two dimensional intensity information from the camera along with one dimensional data (reference phase variation) from the reference cavity to generate a special Fourier transform known as the OPD transform which is explained later in this section and is represented mathematically as

$$\text{OPDS(D)} = \left| \sum_{j=0}^{N-1} I_j W_j \exp\left(i\phi_{Rj} \frac{D}{D_R} \right) \right|^2$$

Equation 3- 12

where I_j is the intensity information from the external cavity (two dimensional information from the camera), W_j is the Fourier weight to band limit the signal, ϕ_{Rj} is the reference phase variation from an internal reference cavity (one dimensional information from the photo detector), D_R is the calibrated value of the reference cavity and D is any cavity of interest.

The MST uses a long focal length lens to provide a 4 inch beam for testing purposes. The return beam from the artifacts passes through a small aperture about 1 mm in diameter. An important mention is that the MST uses two beams of light, one is the alignment beam with its detector and the other is the measurement beam (1550 nm) both coaxially aligned. A monitor for the alignment beam captures the image of the aperture and aids in visually getting the reflected beams from the artifacts into the system by using tip tilt arrangements for the artifacts.

3. 5 Example of a measurement

A four surface geometry is demonstrated in Figure 3- 5 to determine the cavity lengths in the MST using the Custom Cavity Application. Surface 1 is the transmission flat, surfaces 2 and 3 are the two surfaces of a transparent cavity such as Zerodur and surface 4 is a plane mirror.

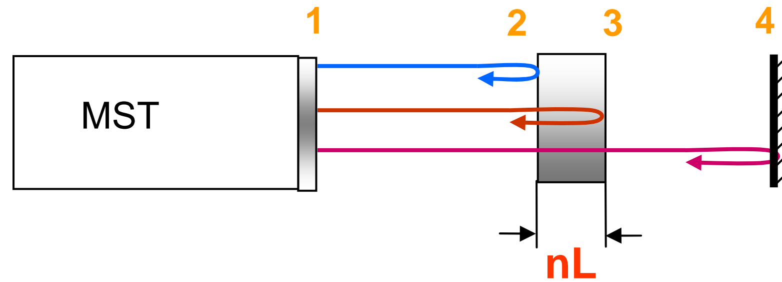

Figure 3- 5: A four surface geometry setup

Once the cavities are aligned a test pixel is marked on the interference pattern. The path lengths of all cavities will be measured at the test pixel as shown in Figure 3- 6.

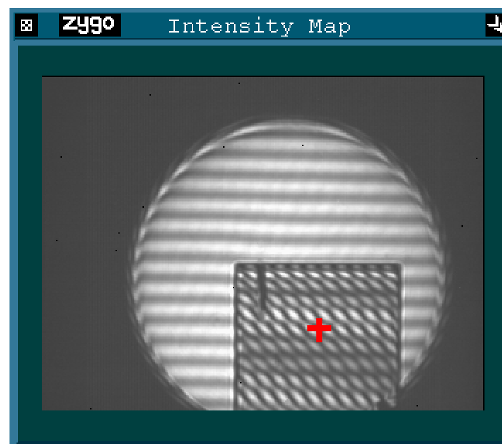

Figure 3- 6: Marking the test pixel for cavity length measurements

The light level intensity is adjusted for getting optimum contrast from the measurement by adjusting the optical power to the laser source. This is digitized in the Zygo software and an optimum value of 28 is found to be sufficient enough in our the laboratory to avoid saturation of the camera. One such measurement result is shown along with the intensity data in Figure 3- 7.

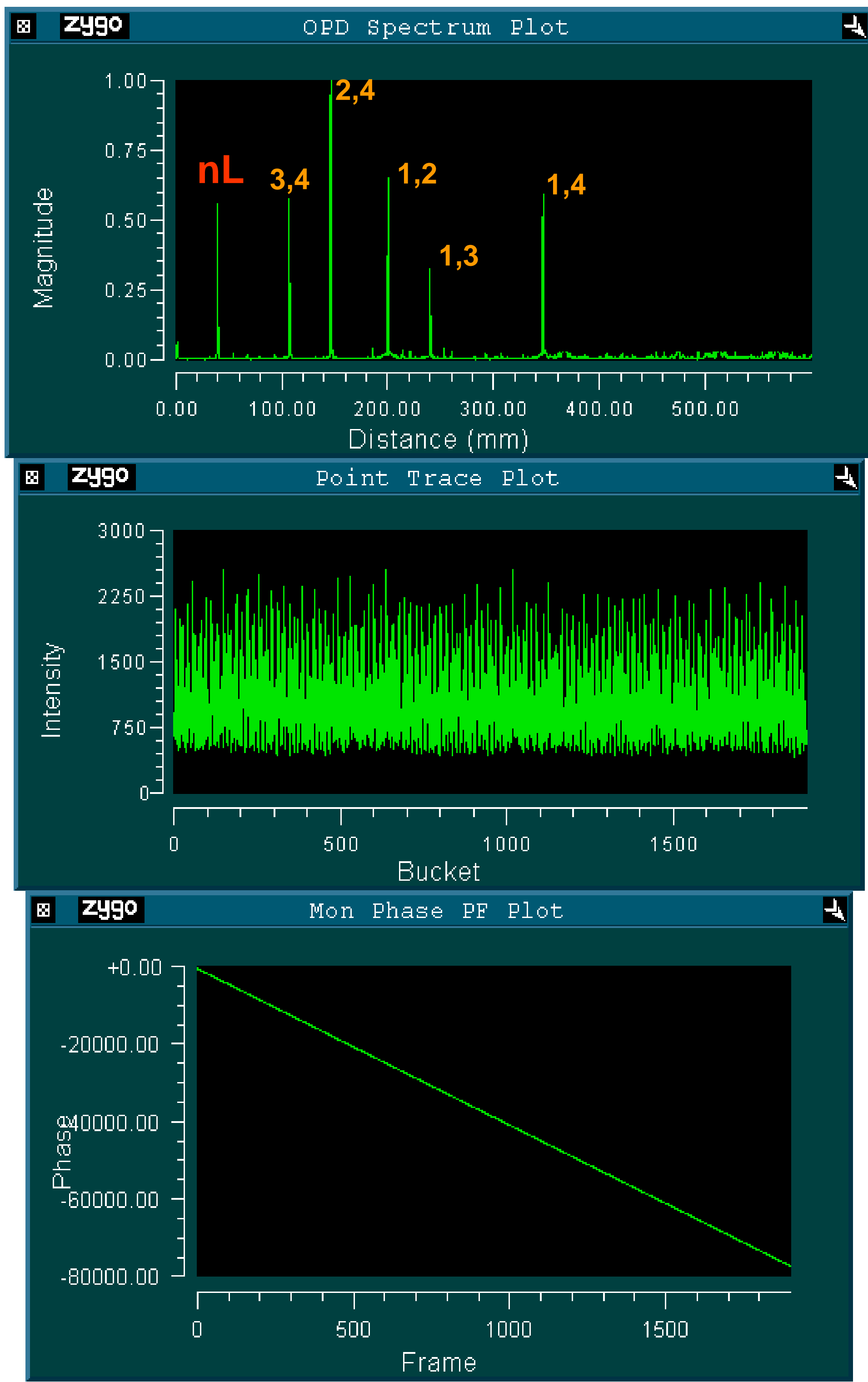

Figure 3- 7 : OPD measurement using intensity data from external cavity and phase data from the internal reference cavity (Fiber Mach-Zehnder interferometer)

3. 6: OPD Transform

Let's rewrite the equation for the intensity and frequency of a cavity using wavelength scanning interferometry

$$I = A + B\cos(\frac{2\pi}{\lambda} \cdot OPD + \phi_0) \text{ and}$$

$$f_C = \frac{m}{\lambda^2} \cdot OPD \cdot \frac{\partial \lambda}{\partial t}$$

Equation 3- 13

A Fourier Transform on the intensity pattern would be described as

$$\mathrm{F}(f) = \int_{-\infty}^{\infty} I(t)W(t)\exp[i\varphi(t)]dt$$

Equation 3- 14

where $I(t)$ is the intensity variation, $W(t)$ is the window function and $\varphi(t)$ is the Fourier kernel and is typically represented as the phase evolution of a particular frequency where $\varphi(t) = 2\pi ft$. Rewriting in discrete notation, the general discrete Fourier transform (DFT) can be written as

$$\mathrm{DFT} = \sum_{j=0}^{N-1} I_j W_j \exp[i\varphi_{Tj}]$$

Equation 3- 15

where φ_{Tj} is the interferometric phase shift for the test cavity at camera sample j. The most important feature of the Fourier Transform is that it assumes constant samples or a constant tuning rate for the wavelength which means that the x axis controlled by ϕ_{Tj} should have a perfect slope for the wavelength at each and every sample j.

$$\varphi_{Tj} = \sum_{j=1}^{N-1} (\frac{2\pi}{\lambda^2} \cdot OPD \cdot [\frac{\partial \lambda}{\partial j}]_{CONSTANT})\Delta j$$

Equation 3- 16

However the wavelength characteristics from the laser are far from perfect for any given sample variation Δj. The OPD transform which is a special Fourier Transform determines the phase ϕ_{Tj} as a function of the actual wavelength variation along each sample by using an internal reference cavity. Consider a reference cavity having a known fixed OPD D_R. The interferometric phase shift of the test cavity with optical path length D_T for time sample j can also be determined from the reference phase variation φ_{Mj} as

$$\varphi_{Tj} = \frac{D_T}{D_R} \varphi_{Rj}$$

Equation 3- 17

where D_R is the monitor cavity OPD. The OPD transform (OPDT) for a given length D can now be computed by using Equation 3- 17 and Equation 3- 15 as

$$\text{OPDT(D)} = \sum_{j=0}^{N-1} I_j W_j \exp\left(i\varphi_{Rj} \frac{D}{D_R} \right)$$

Equation 3- 18

The OPD Spectrum (OPDS) can now be generated as

$$\text{OPDS(D)} = \left| \sum_{j=0}^{N-1} I_j W_j \exp\left(i\phi_{Rj} \frac{D}{D_R} \right) \right|^2$$

Equation 3- 19

Each data or peak in the OPD spectrum corresponds to the optical length of the cavity over the given tuning range. Since the intensity and reference phase data was available

in csv (comma separated values) format, a snippet of code was written in Matlab software using Equation 3- 19 and the OPD spectrum was plotted as shown in Figure 3-8.

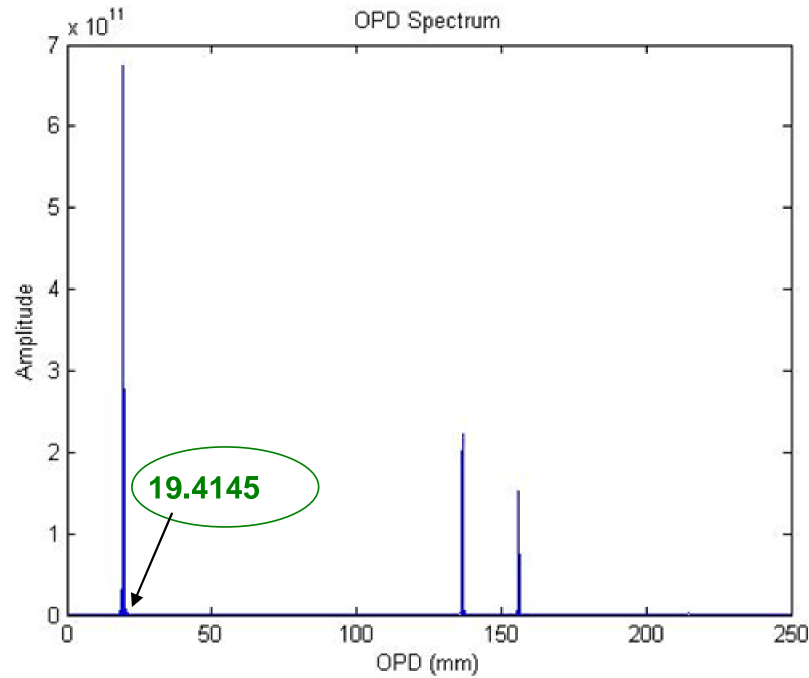

Figure 3- 8 : OPD Spectrum obtained by reading the intensity and phase information data from the MST (commercial wavelength scanning interferometer) and using Equation 3- 19 and Matlab Software

3. 7 Mathematical Model for the OPD of a cavity

The OPD of a cavity OPD_T can be modeled as

$$OPD_T = \frac{\Delta\phi_T}{\Delta\phi_R} \cdot OPD_R + \beta + \varepsilon_{Tuning}$$

Equation 3- 20

where all the parameters have their usual meaning as defined earlier and β represents an estimate of the error in the OPD of a cavity and is a measure of the precision of the phase of the reference cavity and test cavity. Ideally, Equation 3- 20 can be rewritten as

$$OPD_T = \frac{\Delta\phi_T}{\Delta\phi_R} \cdot OPD_R$$

$$OPD_T = \frac{\frac{1}{\lambda^2} \cdot 2\pi(OPD_T) \cdot \frac{\partial\lambda}{\partial N}}{\frac{1}{\lambda^2} \cdot 2\pi(OPD_R) \cdot \frac{\partial\lambda}{\partial N}} \cdot OPD_R$$

$$OPD_{T_\beta} = \frac{(OPD_T)_{measured}}{(OPD_R)_{measured}} \cdot OPD_R$$

Equation 3- 21

where the final equation in Equation 3- 21, OPD_{T_β} represents how well the OPD of the two cavities $(OPD_T)_{measured}$ and $(OPD_R)_{measured}$ is measured using their respective phases for a perfectly linear tuning range.

$$\beta = | OPD_T - OPD_{T_\beta} |$$

Equation 3- 22

The term β represents the difference in the OPD values for a cavity when the ideal value of the OPD of a test cavity is compared to the process of obtaining the OPD of a cavity by any given process with the given reference cavity specifics for a perfect wavelength sweep. In most cases such a parameter is easily determined from experimentation or simple analysis and would be treated as a bias but in this case β is treated as a random estimate due to limited access to some of the parameters (such as reference cavity samples over the sampling time) and controls of the instrument. β thus

represents an estimate of the technique used to extract phase, sampling, window size and analysis to extract the peak OPD location etc used to obtain the OPD of a cavity. In this analysis β is estimated with a computer based simulation for different OPDs. By having an estimate of β for a given OPD or a range of OPDs, it is possible to provide a range of uncertainty for any measured value of OPD obtained from the experiment. ε_{Tuning} represents the repeatability in the instrument and is mostly a measure of the different tuning slopes encountered during different runs and is range variant which means a larger cavity has a larger ε_{Tuning}.

3. 8 Simulation Model for the MST

The simulation model to describe the wavelength scanning is three-tier in the sense that the method of determining the OPD from the given equations is first verified by obtaining necessary information (intensity data and reference phase variation) from the instrument and comparing measurement values with the equations describing the process. The next tier relates to determining the value of β for a perfect sweep for any given cavity length. using the basic equations for phase and intensity of the test and reference cavities using the necessary parameters. The parameters governing the measurement include measurement time, number of buckets for reference and test cavities, sampling frequencies and lengths for the test and reference cavities, source specifics such as tuning range and wavelengths. The final tier consists of varying the slope (from experimental values) to explain repeatability in the instrument. The variation in the tuning of the laser for ten different measurements was determined from the reference cavity variation and also from wavelength data using a wavelength meter.

The average variation in the computed slopes is used to vary the slope in our simulation. The block diagram of the simulation model is as shown in Figure 3- 9

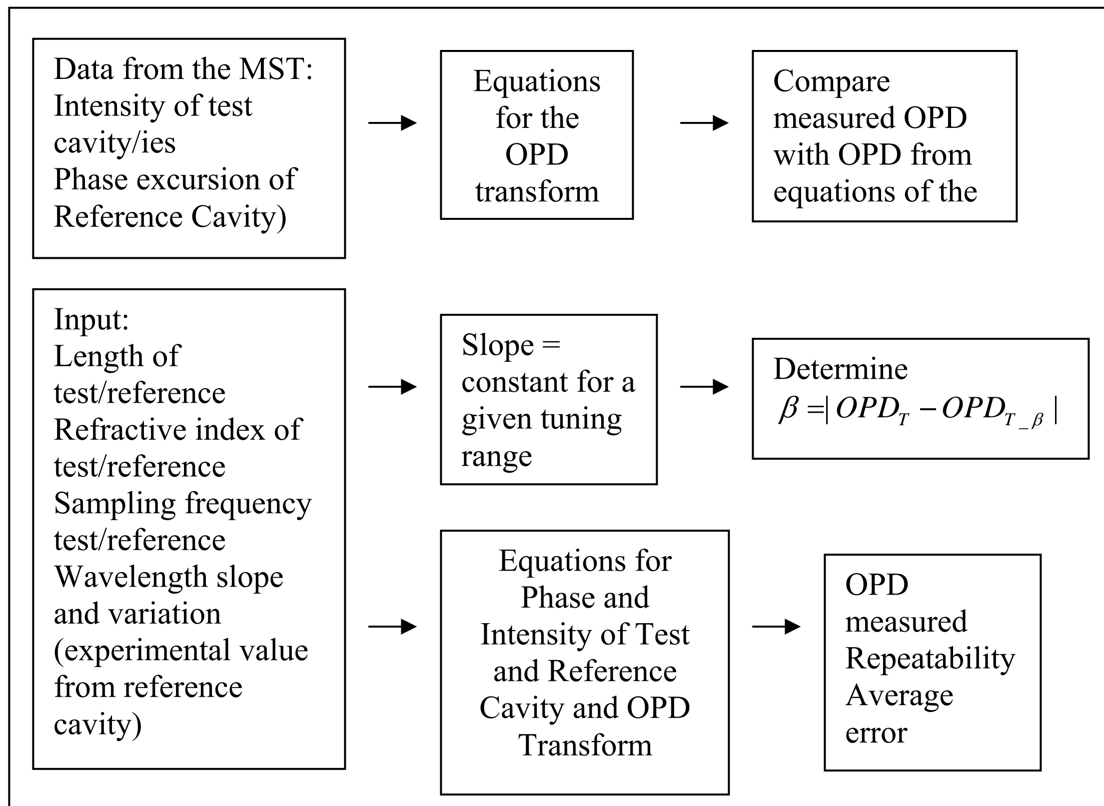

Figure 3- 9 : A three tier simulation model for wavelength scanning interferometry using the OPD transform of the MST

Step 1: to verify the OPD transform equations

The measurement of the OPD as explained using the OPD transform is implemented to obtain the OPD of a cavity. In order to verify the simulation model, intensity data and reference phase (two parameters needed) are obtained from the instrument (MST) and the OPD obtained using the simulation model is verified with the measurement result.

The variation between the two readings results from sampling effects, algorithms to determine peak location etc..

Table 3- 1: OPD values using the MST software (Metropro) and our model using MATLAB software and intensity and reference data from the instrument

OPD (mm) from measurement (peak location)	OPD(mm) from model using data (intensity and reference phase) from the instrument
19.416	19.4155
19.416	19.4152
19.415	19.4147
19.415	19.4142
19.415	19.4139
19.415	19.4144
19.415	19.4140
19.415	19.4146
19.415	19.4142
19.415	19.4142

Step 2:

In this step for a perfect sweep of the laser for a given cavity length the error in measuring the OPD of a cavity using the simulation and theory is computed.

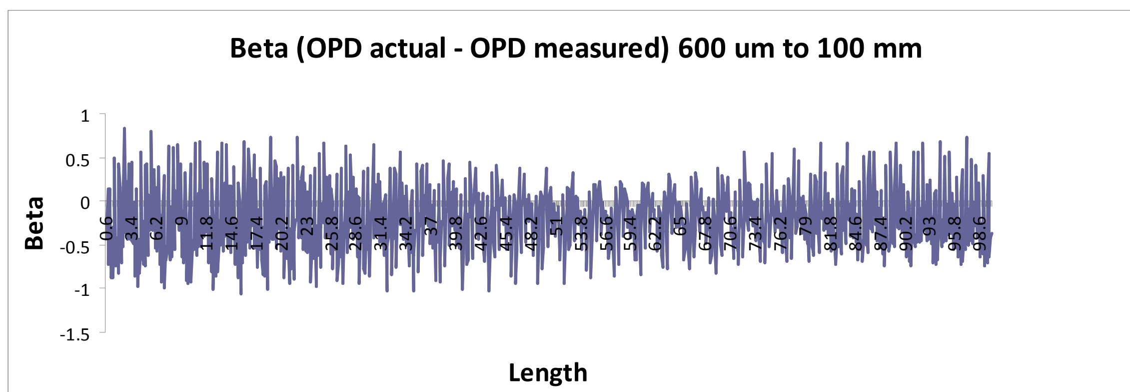

Figure 3- 10 : Plot of Beta (OPD True – OPD measured) from a length of 600 micrometers to 100 millimeters in steps of 100 micrometers

Figure 3- 10 estimates the value of β for a cavity range of 600 micrometer to 100 millimeter in steps of 100 micrometers. The value of β lies between ± 1µm for the given thickness range (600 µm to 100 mm). This value of β is added to the uncertainty estimate.

Step 3: In this step the value of the slopes is computed for the tune using a wavemeter and also from the phase variation of the reference cavity for the same measurement reading. An HP 86180 C wavemeter is placed in front of the MST by launching light from a 50X microscopic objective into a fiber which feeds into the wavemeter as shown in Figure 3- 11.

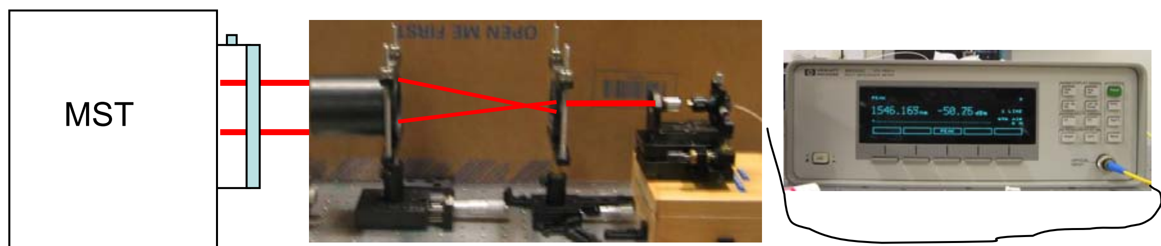

Figure 3- 11 : Wavelengths measured (using a wavemeter) in the MST during a measurement

The wavelength slope variation from the reference cavity phase was computed using Equation 3- 23 and the phase values from the monitor phase plot of the MST.

$$\frac{\partial \phi}{\partial N} = \frac{2\pi(OPD_R)}{\lambda^2} \cdot \frac{\partial \lambda}{\partial N}$$

Equation 3- 23

Since the OPD transform relies on measuring the phase variation of the test cavity as a function of the phase variation of the reference cavity on a sample by sample basis, it is

advantageous to compute the slope between two successive samples to determine the maximum and minimum slopes for a given measurement. Since the wavemeter samples at approximately 1 second (0.925 seconds to be precise) there are less samples (34) from the wavemeter then when compared to the reference cavity phase variation which is 1900 samples. Table 3- 2 shows the wavelength slopes obtained from the reference cavity with the scaled values from the wavemeter (nm/0.925 second converted to nm/sample) along with minimum and maximum values of slopes per sample for each of the ten measurements.

Table 3- 2: Wavelength slopes from wavemeter and reference phase variation for the same measurement. All quantities are in nm/sample.

Average slopes from reference cavity using **Equation 3- 23**	Scaled Average slopes from **Wavemeter**	Minimum Slope value from successive samples from reference phase plot	Maximum Slope value from successive samples from reference phase plot
2.10E-12	2.09446E-12	2.15E-12	2.04E-12
2.09666E-12	2.09554E-12	2.15222E-12	2.04467E-12
2.09659E-12	2.09392E-12	2.15019E-12	2.03919E-12
2.09668E-12	2.0968E-12	2.1437E-12	2.04041E-12
2.09692E-12	2.0977E-12	2.14735E-12	2.04156E-12
2.09665E-12	2.09374E-12	2.15222E-12	2.0467E-12
2.09688E-12	2.09554E-12	2.14451E-12	2.03483E-12
2.09669E-12	2.09572E-12	2.15608E-12	2.04731E-12
2.09645E-12	2.09644E-12	2.15303E-12	2.04183E-12
2.09678E-12	2.09626E-12	2.15892E-12	2.03737E-12
AVG	**AVG**	**AVG**	**AVG**
2.097E-12	**2.096E-12**	2.151E-12	2.041E-12

From Table 3- 2, it is clear that the slopes as obtained from the wavemeter and those computed from the reference cavity for the same measurement are similar. The last two columns indicate the range of slope variation per sample which can be used in the simulation to change the slope values between measurements.

3. 9 Uncertainty Analysis

The uncertainty estimate for the OPD of a cavity can be now represented as

$$OPD_T = \frac{\Delta\phi_T}{\Delta\phi_R} \cdot OPD_{R_Calib} + \beta + \varepsilon_{Tuning} .$$

Equation 3- 24

The individual terms are

$$\Delta\phi_T = \frac{2\pi}{\lambda^2} \cdot OPD_T \cdot \frac{\partial\lambda}{\partial N}$$

Equation 3- 25

where

$$OPL_T = n_T L_T (1 + \eta_T) + \delta_\Omega$$

Equation 3- 26

and n_T, L_T *and* η_T represent the refractive index, physical length and dispersion for the test sample.In measuring cavity thickness, the term δ_Ω is the same for the front and back surface of the cavity and can be neglected, but it is important when measuring cavities formed from different surfaces. The reference cavity specifics can be determined as

$$\Delta\phi_R = \frac{2\pi}{\lambda^2} \cdot OPD_R \cdot \frac{\partial\lambda}{\partial N}$$

Equation 3- 27

$$OPL_R = n_R L_R (1+\eta_R)$$

Equation 3- 28

$$OPL_{R_calib} = OPL_{R_Zygo} + \delta_{\Delta T_Cal}$$

Equation 3- 29

where n_R, L_R *and* η_R represent the refractive index, physical length and dispersion for the reference cavity. OPL_{R_Zygo} is the calibrated value of the reference cavity measured by Zygo Corporation which is 7.34153 m with a calibration uncertainty, while $\delta_{\Delta T_Cal}$ represents the error in the OPL due to different average temperatures between the calibration and the actual measurement environments. It is assumed that both environments have an average temperature of 22°C with a ± 2°C possible difference. Equation 3- 24 can be rewritten as

$$OPD_T = \frac{[OPD_T]_{meas}}{[OPD_R]_{meas}} \cdot OPD_{R_Calib} + \beta + \varepsilon_{Tuning}$$

or $$OPD_T = \frac{[n_T L_T (1+\eta_T)]_{meas}}{[n_R L_R (1+\eta_R)]_{meas}} \cdot OPD_{R_Calib} + \beta + \varepsilon_{Tuning}$$

Equation 3- 30

Although the phase terms for both the external and reference cavities contain the tuning rate of the laser, these do not completely cancel out completely [75] [76] and increase as a function of distance. The effect of non linearity in the slopes on cavity length has been studied in [75] with the help of simulation and experiment to explain the repeatability effects caused by non linearity but no account of absolute length has been mentioned, only a relative slope ratio is provided. This study accounts for all possible sources of uncertainty on the absolute thickness of a window using a detailed simulation approach,

experimental results and verification of the results with comparison with two traceable micrometer screws

Since the measured values for the test and reference are dependent on material parameters which change with temperature, the individual uncertainties of the test and reference cavities with temperature can be determined as

$$U_{OPD_{T_Temp}} = \frac{\partial OPD_T}{\partial T} = OPD_T\left(\frac{1}{L_T}\cdot\frac{\partial L_T}{\partial T} + \frac{1}{n_T}\cdot\frac{\partial n_T}{\partial T}\right)$$

Equation 3- 31

where OPD_T represents the test cavity as usual and the differentiable ∂T represents change in temperature. The reference cavity variation with temperature is represented as

$$U_{OPD_{R_Temp}} = \frac{\partial OPD_R}{\partial T} = OPD_R\left(\frac{1}{L_R}\cdot\frac{\partial L_R}{\partial T} + \frac{1}{n_R}\cdot\frac{\partial n_R}{\partial T}\right).$$

Equation 3- 32

Equation 3- 31 and Equation 3- 32 are simplified versions when differentiating Equation 3- 26 and Equation 3- 28 with temperature.

OPD_{R_calib} is a constant value (used in Equation 3- 17- Equation 3- 19 as D_M) which is multiplied with the reference specifics to determine the OPD of the test sample. This value has a temperature uncertainty of ± 2° C as mentioned earlier and its effect on the test sample can be estimated by determining the range of values for OPD_R over a temperature difference of 4 degrees averaging at the room temperature.

$$U_{OPD_{R_Calib}} = \frac{[OPD_T]_{meas}}{[OPD_R]_{known}}\cdot\delta_{\Delta T_calib}$$

Equation 3- 33

where *[OPD$_T$]$_{meas}$* is the value obtained from the OPD peak in the OPD spectrum or any known value obtained from another measurement (knowledge of the physical length refractive index and the index variation) and *[OPD$_R$]$_{known}$* is 7.34153 (obtained from the configuration file in the Metropro software of the MST).

The final uncertainty equation can be determined by performing a Taylor series expansion using Equation 3- 30 and is given by

$$U_{OPD_T} = OPD_T \sqrt{(\frac{U_{OPD_T_Temp}}{OPD_T})^2 + (\frac{U_{OPD_R_Temp}}{OPD_R})^2 + (\frac{U_{OPD_R_Calib}}{OPD_T})^2 + (\frac{\beta}{OPD_T})^2 + (\frac{\varepsilon_{Tuning}}{OPD_T})^2}$$

which can be simplified as

$$U_{OPD_T} = \sqrt{(U_{OPD_T_Temp})^2 + (\frac{U_{OPD_R_Temp}}{OPD_R})^2 + (U_{OPD_R_Calib})^2 + (\beta)^2 + (\varepsilon_{Tuning})^2}\ .$$

Equation 3- 34

Equation 3- 34 is applied to all the measurements to compute the contributions from each uncertainty source.

Most of the research and analysis using wavelength scanning interferometry has been based on measuring distances in air using a retroreflector using different techniques. In such cases a small change in the optical path length of the retroreflector (sometimes referred to as drift) can cause a large change in the final readings thereby limiting the length measuring capacity of the technique. However the drift does not affect the measurement of a transparent artifact where the optical path difference is measured as a difference in frequency measurements from the front and back surfaces. Hence any change in the length of the arm between the front and back surfaces is equally affected and is eliminated due to the difference measurement.

3. 10 Measurements on a commercial interferometer

Transparent planar (half inch fused silica cavity)

Transparent planar cavities are easily measured in the MST by simply placing them in front of the MST and taking measurements. A set of 10 readings were taken on a half inch fused silica window (double sided) from Thorlabs. The average of the 10 readings was 19.4152 mm with a standard deviation of 0.000420 mm. The extended uncertainty analysis consists of considering all the uncertainty sources mentioned in Equation 3- 34.

Table 3- 3: Uncertainty budget for a fused silica cavity using the MST

Main Parameter	Secondary Parameters	Absolute Uncertainty	Fractional Uncertainty
OPD_{T_Temp}	$n_T = 1.444045$ $\partial n_T / \partial T = 1.28 \times 10^{-5}/°C$ $L_T = 13.275$ mm $\partial L_T / \partial T = 5.5 \times 10^{-7}/°C$	125 nm	$9.4/10^6$
OPD_{R_Temp}	$n_R = 1.444045$ $\partial n_R / \partial T = 1.28 \times 10^{-5}/°C$ $L_R = 7.34153$ mm $\partial L_R / \partial T = 5.5 \times 10^{-7}/°C$	125 nm	$9.4/10^6$
OPD_{R_calib}	Temp (20°C - 24°C)	688 nm	$35/10^6$
β	Simulation	1000 nm	$51/10^6$
ε_{Tuning}	Repeatability	420 nm	$32/10^6$
Combined Uncertainty for single pixel thickness		819 nm	$70/10^6$

By using the minimum and maximum values of slopes for the tune from Table 3- 2, it was possible to obtain the repeatability in the MST. The average value for a 19.415 mm cavity for 10 and 100 readings was 19.4154 mm and 19.4153 mm respectively with standard deviations of 403 nm and 330 nm (for 10 and 100 measurements respectively).

Another simulation also computed the average and standard deviations for ten separate measurements for the given tuning variation as listed in Table 3- 4 .The average estimates and standard deviation in the simulation compare well with the experimental result of 19.4152 mm and standard deviation of 420 nm..

Table 3- 4: Average OPD values and standard deviations for 10 readings for a 19.415 mm window

Average of OPD Values (mm) for 10 readings	**Standard Deviation (nm) for 10 readings**
19.4154	403
19.4155	363
19.4154	245
19.4154	364
19.4156	316
19.4154	343
19.4154	307
19.4156	272
19.4154	292
19.4156	385
AVG	**AVG**
19.4155 (mm)	**329 (nm)**

The combined uncertainty is calculated using a Taylor series expansion using Equation 3- 34. The major contribution from the uncertainty comes from the uncertainty in the reference cavity OPD which has a temperature uncertainty of ± 2°C over the calibration temperature range 22 °C as obtained in correspondence from the Zygo staff. Another major contribution is the repeatability in the instrument which can be reduced by taking more runs. The refractive index and dispersion were determined using Malitson's

equation [77] for fused silica. Using the average value of the refractive index for fused silica 1.444045609 and the dispersion coefficient 1.012853686, the physical thickness of the fused silica sample was computed using $OPL_T = n_T L_T (1+\eta_T)$ to be 13.274 mm ± 0.0008 mm. In order to extend the measurement uncertainty to any pixel over the surface, the peak to valley (PV) information from the OPD filled plot was used as shown in Figure 3- 12. The average of 10 peak to valley values from the OPD filled plots was computed to be 1.1 μm. The corresponding physical thickness variation over the whole surface was computed to be 0.752 μm.

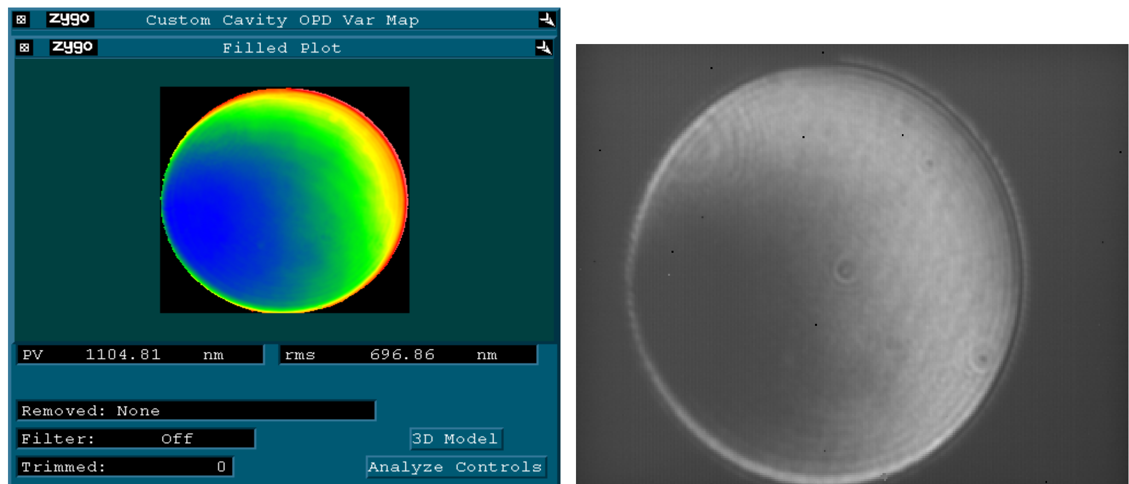

Figure 3- 12: OPD filled plot for fused silica cavity along with the fringe pattern

The physical thickness of the fused silica window computed from the MST was within the manufacturer's tolerance of 11.2 mm – 14.2 mm (12.7 mm ± 1.5 mm). Another measurement procedure was followed by using two calibrated micrometer screws, one handheld and the other a tabletop. The two micrometers were first made to measure a 13 mm gauge block. Since both the micrometers were digital, any bias on the instruments

was corrected with a reset switch. The fused silica window was then measured at 10 different positions by each of the micrometer screws. The average physical thickness as measured by the handheld was 13.274 mm ± 0.0005 mm and for the tabletop version was 13.274 mm ± 0.0014 mm. Table 3- 5 lists the average thickness and its variation over the entire sample for the three methods.

Table 3- 5 : Average and standard deviation values of a Fused Silica window over the entire sample using the MST and calibrated micrometers

	MST	**Micrometer 1 (handheld)**	**Micrometer 2 (tabletop)**
Average (mm)	13.274	13.274	13.274
Standard Deviation (mm)	0.0007	0.0005	0.001

The fractional uncertainty for the physical thickness of the fused silica window is 70 ppm.

<u>Spherical Ball Lens Measurements:</u>

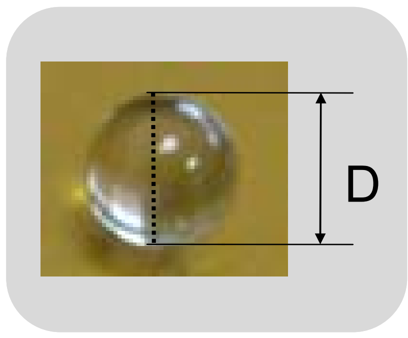

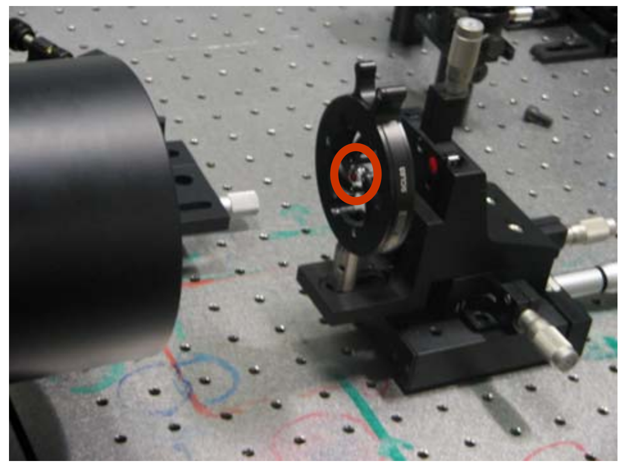

Figure 3- 13: Setup for measuring the diameter of a transparent spherical ball lens

In order to measure a spherical ball lens, a transmission sphere (f / 1.5) is used and the OPD of the ball lens is measured at the confocal position. In this arrangement all the rays converging on the ball lens are reflected from the back surface and travel along the same path which defines the diameter of the ball. The OPD spectrum in the confocal arrangement is then similar to a planar arrangement since any ray travels the same distance (the diameter of the ball lens). The best estimate of the diameter is computed from the best estimate of the confocal position which is determined using the Zernike term Defocus (Focus as mentioned in the application).

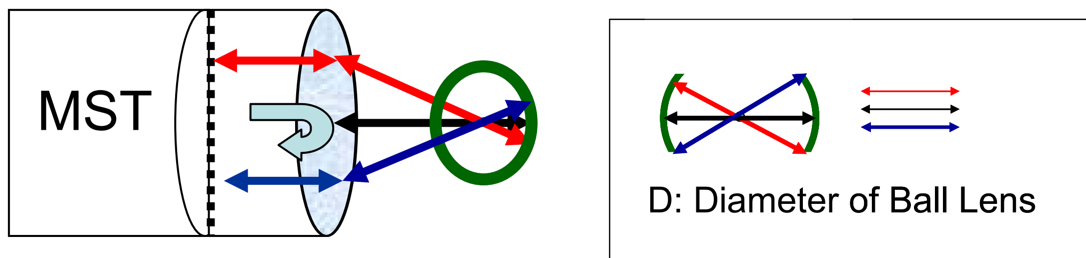

Figure 3- 14: Spherical ball lens measurement in the MST

A 10 mm uncoated ball lens (BK7) was purchased from Edmund Optics with a tolerance of ± 5 μm. An f / 1.5 Zygo transmission sphere was used to determine the diameter of the ball lens. In order to measure the spherical ball lens, it is required to determine the precise confocal position and then determine the diameter of the ball. In this case the Zernike application was used to determine the best confocal position by looking at the defocus term at the reference pixel (on the interference fringe pattern) of the test sample. Translational stages were incorporated to ease the process of obtaining a precise confocal position. The process of obtaining the defocus term involved moving

the translational stage, taking a measurement and determining the OPD map of the front surface of the ball lens and determining the Zernike term Defocus from the Zernike application. The objective was to repeat the above process till the Defocus term (Focus as mentioned in the application) is close to zero which then represents the best estimate of focus. The best estimate of the confocal position was obtained at a defocus of about 0.000 at the test pixel as given by the Zernike application as shown in Figure 3- 15.

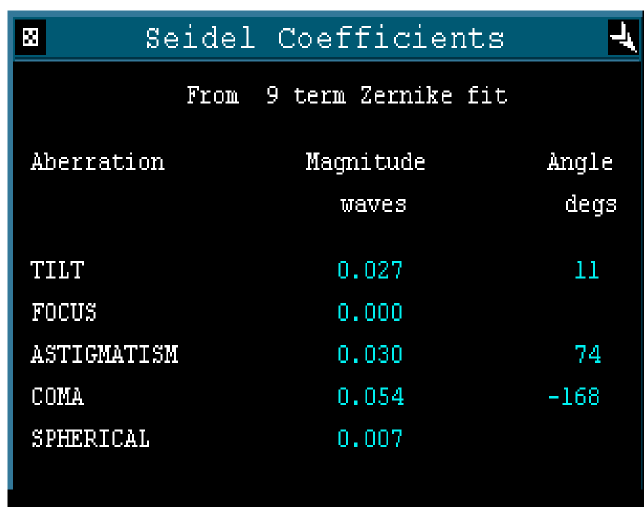

Figure 3- 15: Best estimate of confocal position from the focus term

Twenty readings were taken at this position and the mean optical path length of the ball lens was computed to 15.203 mm with a one sigma deviation of 0.0003 mm. No change in temperature to within 0.1 degree was observed during the measurement. The dispersion (η) was computed from the Sellmeier equation (with BK7 constants) by determining the refractive index variation of n with wavelength (frequency). The wavelength was obtained by using a wavelength meter to record values for different tuning ranges. η was computed to $0.012934 \pm 3 \times 10^{-6}$ (from the uncertainty of the

wavelength meter: 4 picometer / 1550 nm and from the Sellmeier equation). By using this value and the refractive index of BK7 at 1550 nm i.e. 1.500069, the absolute diameter of the ball was computed to be 10.001 mm.

Table 3- 6 : Uncertainty Budget for Spherical ball lens (Specs: 10.000 mm ± 0.005 mm)

Main Parameter	**Secondary Parameters**	**Absolute Uncertainty**	**Fractional Uncertainty**
OPD_{T_Temp}	$n_T = 1.500069$ $\partial n_T / \partial T = 2.4 \times 10^{-6}/°C$ $L_T = 10.001\ mm$ $\partial L_T /(L_T . \partial T) = 7.1 \times 10^{-6}/°C$	87 nm	$8.7/10^6$
OPD_{R_Temp}	$n_R = 1.444045$ $\partial n_R / \partial T = 1.28 \times 10^{-5}/°C$ $L_R = 7.34153\ mm$ $\partial L_R /(L_R . \partial T) = 5.5 \times 10^{-7}/°C$	125 nm	$9.4/10^6$
OPD_{R_calib}	Temp (20 °C -24 °C)	500 nm	$33/10^6$
β	Simulation	1000 nm	$65/10^6$
ε_{Tuning}	Repeatability	300 nm	$20/10^6$
Combined Uncertainty for single pixel thickness		**1.2 µm**	**$76/10^6$**

The combined uncertainty for the OPD of the BK7 ball lens at an estimated average OPD of 15.203 mm is 1.2 μm from Table 3- 6. The uncertainty in the diameter of the ball lens is computed after dividing by the dispersion contribution and the refractive index i.e. n(1+η). The final uncertainty in the diameter of the ball lens is 10.001 mm ± 0.0007 mm.

The ball lens was also measured at 10 different positions with the MST and also with two calibrated micrometers like the previous measurements and all the values are found to be agreeing satisfactorily as shown in Table 3- 7.

Table 3- 7: Average and standard deviation values of a BK7 ball lens for 10 different positions using the MST and calibrated micrometers

	MST	Micrometer 1 (handheld)	Micrometer 2 (tabletop)
Average (mm)	10.001	10.001	10.001
Standard Deviation (mm)	0.0006	0.0005	0.0008

3. 11 Summary

The thickness of a transparent planar window and a transparent spherical window has been measured using the concept of Fourier transform phase shifting interferometry using a commercial interferometer along with a detailed uncertainty estimate. The average measurements for both the artifacts has been compared and verified by two micrometer screws when calibrated to a traceable gauge block of 13 mm. A simulation model is described to understand the effect of tuning non linearities using experimentally obtained values. For a perfect sweep the simulation shows that the measurements lie between a ± 1 μm range which also forms the chief contributor towards the uncertainty in the measurement, followed by the uncertainty in knowing the calibrated value of the reference cavity for a given temperature and the repeatability in the instrument.

CHAPTER 4: GAUGE BLOCK MEASUREMENTS

4. 1 Opaque Planar Artifacts using the MST (based on papers [92]-[93])

Gauge block measurements have changed dramatically since their advent when static interferometric techniques and comparators were used. Current scenarios include dynamic interferometric techniques like phase shifting interferometry and time-of-flight methods using femtosecond lasers. All techniques on gauge block measurement use prior information about the approximate length of the gauge block (coarse measurement) which is computed mainly by static multiple interferometry techniques and this information is used to determine the absolute length of gauge block to tens of nanometers (fine measurement). In this chapter, a Sagnac interferometer in described in conjunction with a commercial Fizeau wavelength scanning interferometer (MST) as shown in Figure 4- 1 to determine the coarse lengths of a one, two and three inch gauge blocks. Preliminary results of the measurement are discussed along with uncertainty sources.

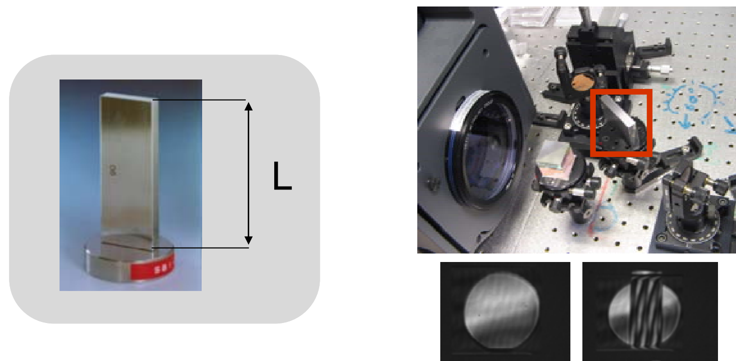

Figure 4- 1: A two mirror Sagnac configuration in conjunction with the MST to measure coarse lengths of gauge blocks

4. 2 Introduction to gauge blocks

Gauge blocks are used as precision and lapped standards in diverse areas in the industry from measuring parts loosely on the factory floor to measuring parts accurately to a millionth in an environmentally controlled laboratory. Since the patenting of the gauge block by Swedish inventor Carl Edvard Johansson in 1901, gauge blocks have changed little with respect to their design, application or even accuracy as compared to the way they are measured. A set of gauge blocks with the right combinations are wrung to accurately determine the length of an artifact. As a result of the wringing process, the length of a gauge block in the ISO 3650 "Geometrical Product Specifications – Length standards – Gauge Blocks" is defined as "the perpendicular distance between any particular point of the measuring face and the planar surface of an auxiliary plate of the same material and surface texture upon which the other measuring face has been wrung". This is illustrated in Figure 4- 2.

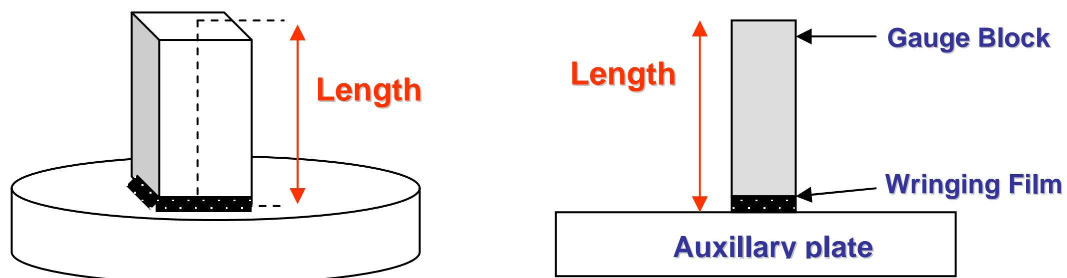

Figure 4- 2: The length of a gauge block as defined by ISO 3650

Wringing involves a lot of skill, decreases throughput, and prevents automation of the measurement process and is not completely understood. In recent years however, most techniques have measured gauge blocks without wringing them onto the platen.

4. 3 History of gauge block measurements

Gauge blocks are measured in two steps: one is a coarse measurement which gives the gauge block length to within a couple of 100 micrometers and the other is a fine measurement which uses the coarse measurement to provide the gauge block length to within tens of nanometers. While fine measurements have improved dramatically from using mechanical comparators [79] to using static multiple wavelengths [80][81] to the more dynamic forms of interferometry such as phase shifting [82][83] and femtosecond lasers [84], coarse measurements have used mechanical means like a micrometer and non-contact methods such as multiple wavelength interferometry have also been reported to determine the gauge block to within a given tolerance (140 μm – 300 μm)[13][84]. Since the gauge block is a length standard, techniques such as multiple wavelength interferometry provide a means for measurement of a step height as discussed by authors in [13]. The focus of this chapter is to improve the coarse length measurements of gauge blocks along with a detailed uncertainty analysis thereby providing an estimate of measuring different step heights. Since the object measured is opaque, the approach involves a unique configuration and measurement sequence where light is reflected from both ends of the object and the two end faces of the gauge block serve as boundaries of independent optical cavities. Absolute coarse length of one, two and three inch gauge blocks is demonstrated along with uncertainty sources.

4. 4 Measurement theory

In order to measure an opaque cavity such as a gauge block, a two mirror Sagnac configuration is used in conjunction to the MST, as shown in Figure 4- 3. The two mirror Sagnac geometry avoids beam inversion for the empty cavity and the cavity

with the gauge block. The length of the gauge block is then measured in two steps outlined as follows:

(a) Using a multi-axes stage, the two mirrors of the Sagnac are adjusted to give minimum fringes for the empty cavity (usually 1 fringe over the surface), as shown in the left part in Figure 4- 4.

(b) The gauge block is then placed and aligned to give a similar fringe pattern for the front and back surfaces. Since the empty cavity is aligned to give minimum fringes and the gauge block surfaces are flat, a similar fringe pattern for the front and back surface indicates that the two surfaces are fairly parallel with respect to each other, as in Figure 4- 4. A multi axes stage for the mirrors and the gauge block greatly helps in the alignment and reproducibility of the fringe pattern.

(c) The front and back surfaces of the gauge block are then determined from the OPL spectrum discussed in the earlier sections.

(d) The gauge block is removed and the empty cavity is measured similarly.

The length (thickness) of the gauge block is then given by

$$L_{GaugeBlock} = L_{EmptyCavity} - (L_{Front\ Surface} + L_{Back\ Surface})$$

Equation 4- 1

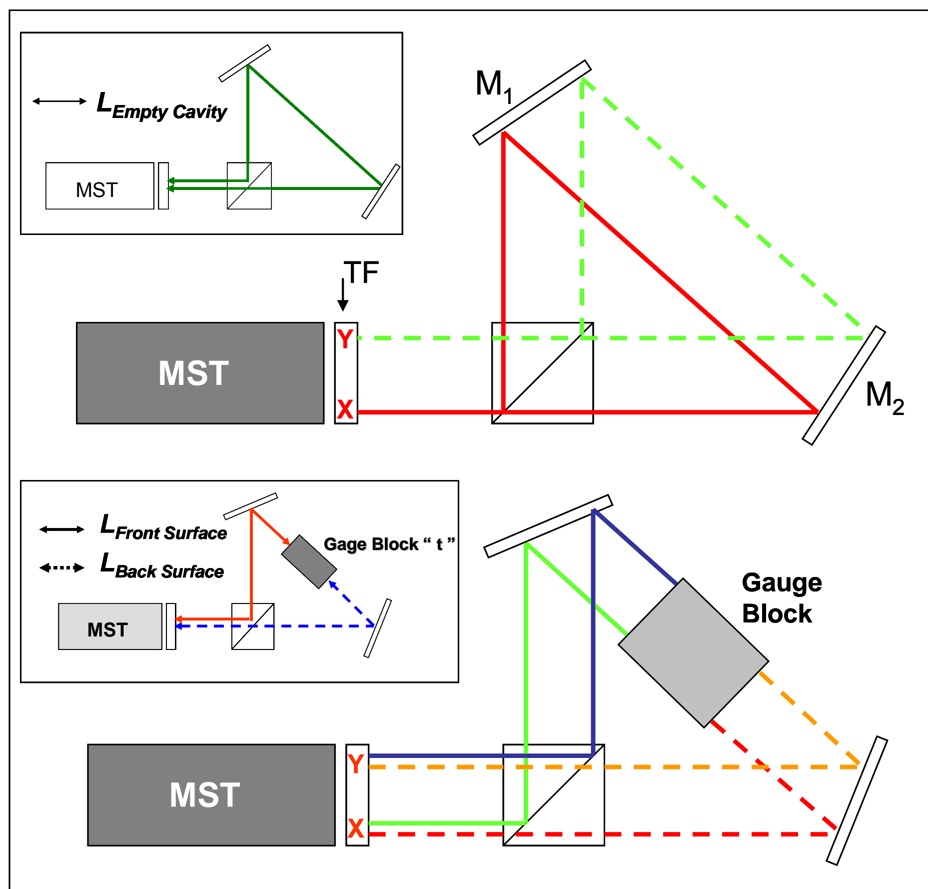

Figure 4- 3 : A two mirror Sagnac configuration to measure a gauge block with the MST

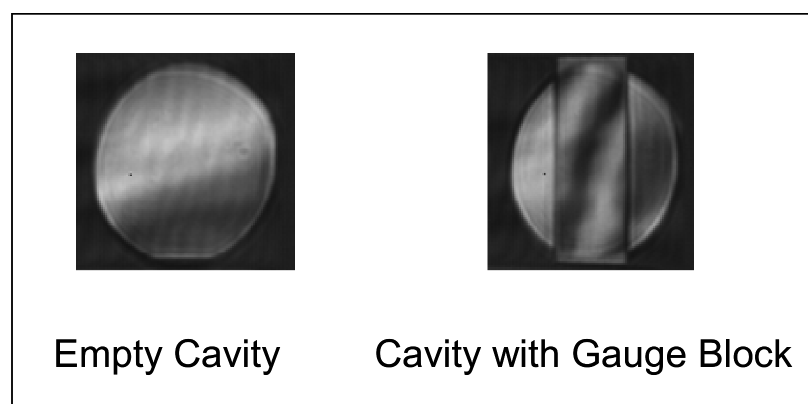

Figure 4- 4 : Fringes for empty cavity and gauge block (front and back). In order to ease the alignment of the gauge block (almost parallel front and back surfaces) the empty cavity fringes are made to a minimum.

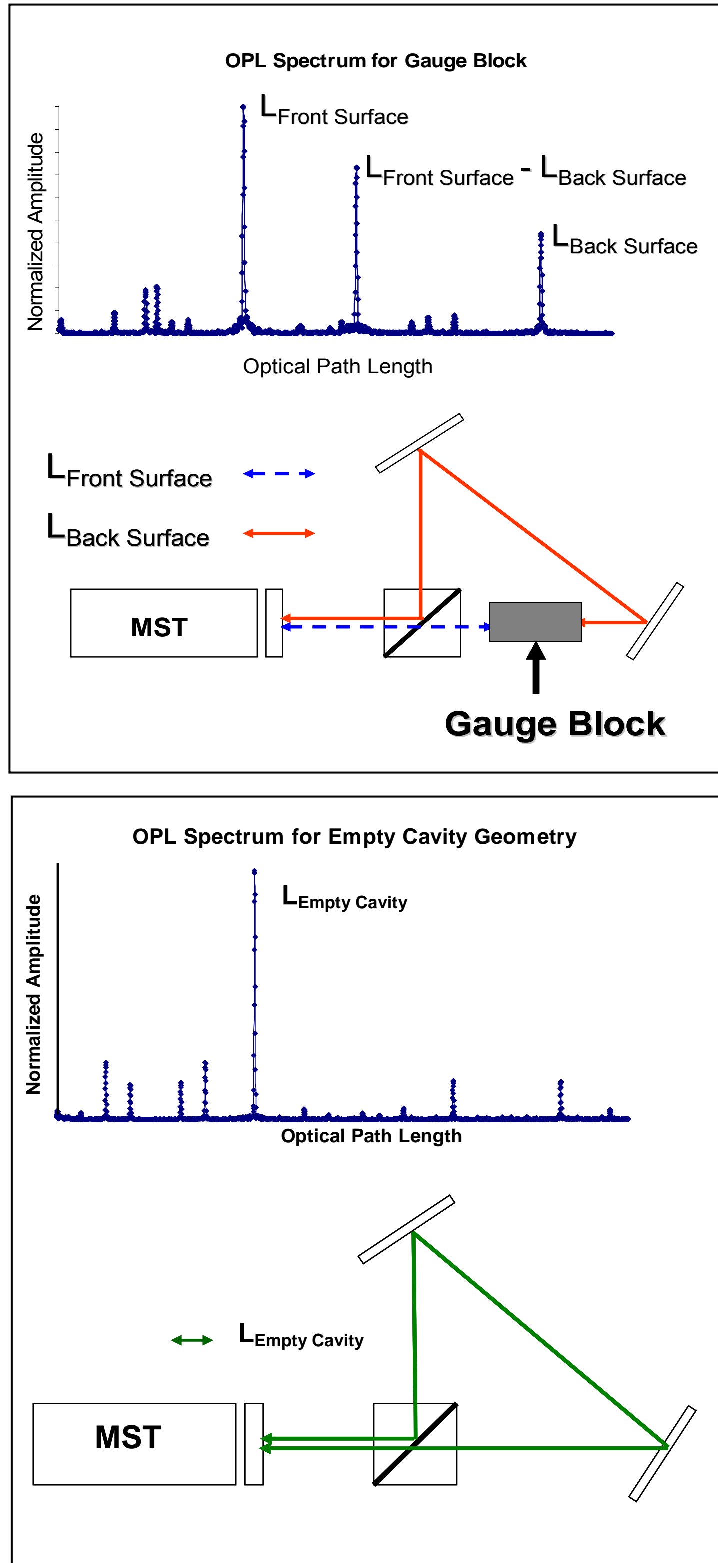

Figure 4- 5 : OPD Peaks for the empty cavity and the gauge block surfaces (front/back)

The peaks of interest in the OPL spectrum and therefore the cavity lengths must be identified with care to carry out the analysis. With a standard Fizeau configuration each cavity measurement is double-pass; therefore a cavity's measured optical path difference is twice the cavity's physical optical length. The data processing in the MST takes this into account and automatically divides all optical path lengths by two. This division is correct when the gauge block is in one arm of the Sagnac; however the empty cavity measurement is a single pass configuration and the empty cavity peak will appear at half the cavity length. It must be multiplied by a factor of two to recover the cavity optical length. Also, the software normalizes the OPD spectrum with respect to the largest amplitude so identification and comparisons of peaks between measurements must be done with care. For example, the empty cavity and the two cavities corresponding to the front and back surfaces of the gauge block have the largest fringe contrast; therefore these peaks will have the largest amplitudes. Smaller peaks in the spectra are from irrelevant cavities such as the front and back surfaces of the beam splitter, the beam cavity, and multiple reflection combinations. Care must be taken to ensure that these peaks and significant multiples thereof are well-separated from the peaks of interest. The next section discusses the components of the system and the measurement results. This is followed by an uncertainty assessment of the measurement. A certain amount of expertise was gained while setting up the optics and with time and preliminary results a reduced geometry with multi-axes alignment stages were incorporated as shown in Figure 4- 6. All measurements reported are for the setup on the far right in Figure 4- 6.

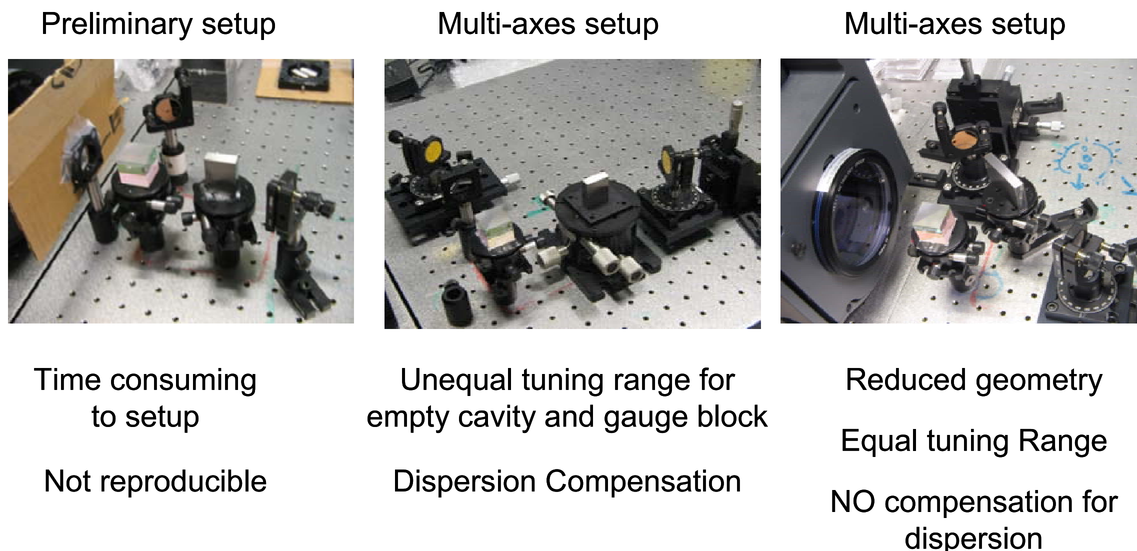

Figure 4- 6 : Improvements in the gauge block setup over time. Measurements described in the chapter are for the rightmost setup.

4. 5 Measurements

Three different gauge block lengths (1 inch (25.4 mm), 2 inch (50.8 mm) and 3 inch (76.2 mm)) were measured in four sets, each set comprising of twenty measurements for the geometry in Figure 4- 6. The total OPD of the empty cavity is approximately 556 mm so as to utilize the full tuning range of the laser 500 GHz. The gauge block is first measured and then the empty cavity. The length of the gauge block is then determined as per Equation 4- 1 with the empty cavity OPD being the average of the empty cavity measurement. Table 4- 1 lists the average and standard deviation of the three gauge block lengths (one, two and three inches) for four sets, each set comprising twenty measurements. It is observed that for any given set of measurement and for any of the given lengths, the average value of the length of the gauge block is accurate to ± 20 μm of the value provided by the manufacturer. The discussion of the

combined uncertainty, which takes all uncertainty sources into account, is discussed below.

Table 4- 1: Gauge Block measurement for 1,2 and 3 inch blocks

1 inch (25.4 mm)				
	Set 1	Set 2	Set 3	Set 4
Average value (mm)	25.404	25.380	25.413	25.412
Standard Deviation (μm)	26	30	32	27
2 inch (50.8 mm)				
	Set 1	Set 2	Set 3	Set 4
Average value (mm)	50.816	50.803	50.804	50.797
Standard Deviation (μm)	31	30	31	36
3 inch (76.2 mm)				
	Set 1	Set 2	Set 3	Set 4
Average value (mm)	76.207	76.182	76.191	76.184
Standard Deviation (μm)	40	42	32	38

4. 6 Uncertainty Analysis

The OPL of a cavity for a given set of measurements can be described as

$$OPD_C = \frac{[n_C L_C (1+\eta_C)]_{meas}}{[n_R L_R (1+\eta_R)]_{meas}} \cdot OPD_{R_Calib} + \varepsilon_{Tuning}$$

Equation 4- 2

where all the terms have their usual meaning as explained earlier and ε_{Tuning} is the standard deviation of the measurement results for a given set of measurements. The effect of β is not considered in this scenario since cavities are measured instead of a window as in the previous chapters. The exact position of a cavity cannot be estimated from the OPD peaks however since a window is measured as a difference between two

cavities and its thickness can be estimated from other forms of mechanical measurements β can be determined. In this study the absolute length of a gauge block is determined from a sequence of cavity measurements and so the uncertainty analysis focuses on determining the range of uncertainty from known average readings, standard deviation and primary parameters such as refractive index, length variations with temperature. The uncertainty in the OPL of a cavity using the MST can be expressed as a Taylor series expansion of the individual terms in Equation 4- 3 as

$$U_{OPL_C} = \sqrt{[U_{OPL_Tuning}]^2 + [U_{OPL_C_Temp}]^2 + [\frac{OPL_C}{OPL_R} \cdot U_{OPL_R_Temp}]^2 + [U_{OPL_R_Cal}]^2}$$

Equation 4- 3

where U represents the uncertainty in the measurement and the corresponding subscripts represent the parameters. The gauge block measurement is modeled below as

$$L_{GaugeBlock} = L_{EmptyCavity} - (L_{Front\ Surface} + L_{Back\ Surface}) + \delta_{Alignment} + \delta_{\Omega}$$

Equation 4- 4

where $\delta_{Alignment}$ and δ_{Ω} represent the length errors that may result from cavity misalignment and effects from phase change on reflection. Since the gauge block measurement consists of two independent measurements taken one after another, similar conditions of temperature throughout the measurement process are assumed. This means that the average temperature conditions measured during a set of measurements (twenty readings for gauge block and empty cavity) are the same. As a result; the value of OPL_{R_Cal} remains the same during the measurement. The effect of having a different OPL_{R_Cal} value between measurement and calibration environments on the gauge block measurement still needs to be estimated. The only factor which will

be different between the gauge block and empty cavity measurements is the tuning rate non-linearity. Since the temperature variations are assumed to be similar for the empty cavity and gauge block measurements but the tuning rate will be different for the two measurements, the uncertainty in the gauge block measurement can be written similar to Equation 4- 3 as

$$U_{GB} = \sqrt{[U_{GB_Tuning}]^2 + [U_{GB_C_Temp}]^2 + [U_{GB_R_Temp}]^2 + [U_{GB_R_Cal}]^2 + [\delta_{Alignment}]^2 + [\delta_{\Omega}]^2}$$

Equation 4- 5

where the subscript OPL from Equation 4- 3 is replaced to represent gauge block or (GB) along with additional terms from Equation 4- 4. The following section now estimates the effects of all the parameters in the OPL of the gauge block using Equation 4- 2 and Equation 4- 5.

4.6.1 Effect of temperature on the OPL of test and reference cavity

Although the average temperature variations for the empty cavity and gauge block measurements are similar, it is more logical to assume the scenario in which the temperature may be steadily increasing during one measurement set (twenty readings) say the empty cavity and steadily decreasing during the other (with the gauge block). This encompasses a more general scenario and so the root sum square approach is used in determining the uncertainty in the gauge block due to temperature variations in both the test and reference cavities. The equations are as shown below.

$$U_{GB_C_Temp} = \sqrt{(U_{Empty_Temp})^2 + (U_{Front_Temp})^2 + (U_{Back_Temp})^2}$$

Equation 4- 6

$$U_{GB_R_Temp} = \sqrt{(\frac{OPL_{Empty}}{OPL_R} \cdot U_{Empty_Temp})^2 + (\frac{OPL_{Front}}{OPL_R} \cdot U_{Front_Temp})^2 + (\frac{OPL_{Back}}{OPL_R} \cdot U_{Back_Temp})^2}$$

Equation 4- 7

4.6. 2 Effect of temperature on the Calibrated value of Reference

Since the reference cavity is known to an uncertainty in temperature of ± 2° Celsius, the effects of different temperatures between measurement and calibration environments is now considered to estimate the uncertainty in the gauge block measurement. Considering a refractive index variation for fused silica due to temperature to be 1.28 x 10^{-5} ° C, a one degree change in temperature causes the reference cavity OPL to vary as much as 65 microns, so a temperature difference of 4 degree Celsius between measurement and calibration environments would cause an error in the calibrated value of the OPL of the reference cavity of 260 microns. Since the ratio of the phase is equal to the ratio of the OPL of the cavities as seen from equation 6, the average values along with their uncertainty for each cavity (empty, front and back) are determined from the measurement, and multiplied with different values of the reference cavity for the temperature range from 20° C to 24° C to estimate the uncertainty for each cavity. The uncertainty in the gauge block due to the reference cavity calibration can then be expressed as

$$U_{GB_R_Cal} = [\frac{OPL_{Empty}}{OPL_R} - \frac{OPL_{Front}}{OPL_R} - \frac{OPL_{Back}}{OPL_R}] \cdot U_{R_\Delta T}$$

Equation 4- 8

where $U_{R_\Delta T}$ = 260 µm. Since the average temperature variations (0.2°C) during the experiment are found to be constant and small compared to the maximum temperature

difference of 4°C between calibration and measurement environments, the effect of the calibrated value of the reference cavity due to average temperature fluctuations on the gauge block measurement is considered to be negligible and therefore its effect is ignored. Table 4-2 lists the uncertainty in the gauge block measurements for various lengths (1 inch, 2 inch and 3 inch) due to the uncertainty in the reference cavity calibration.

Table 4-2 : Uncertainty contribution to gauge block due to calibration uncertainty in the reference cavity

Gauge Block Length (inch/mm) ± σ_{AVG} (mm)	**Uncertainty due to reference cavity calibration (μm)**
1 /(25.4) ± 29	0.9
2 /(50.8) ± 32	1.8
3 /(76.2) ± 38	2.7

4.6.3 Effect of tuning rate non linearity

Although the phase terms for both the external and reference cavities contain the tuning rate of the laser, these do not completely cancel out completely [75] [76] and increase as a function of distance. The standard deviation (σ) for a given number of measurement readings is considered as an uncertainty contributor towards tuning in the measurand equation.

$$U_{OPL_Tuning} = \sigma$$

Equation 4- 9

Since the average empty cavity measurement is used in computing the gauge block measurement from every measurement of the front and back cavity, the uncertainty in

the gauge block due to the tuning rate can be expressed as the sum of the standard deviations for the front and back surfaces for any given set of readings as

$$U_{GaugeBlock_Tuning} = U_{Front_Tuning} + U_{Back_Tuning}$$

Equation 4- 10

This can be validated by looking at the 12 measurement sets in Figure 4- 7 where the uncertainty in the gauge block (standard deviation) is compared and verified from measurements with the sum of the standard deviations of the front and back surfaces from Equation 4- 10 for the three gauge blocks. The empty cavity represents the average of 20 readings and is constant for the gauge block measurement.

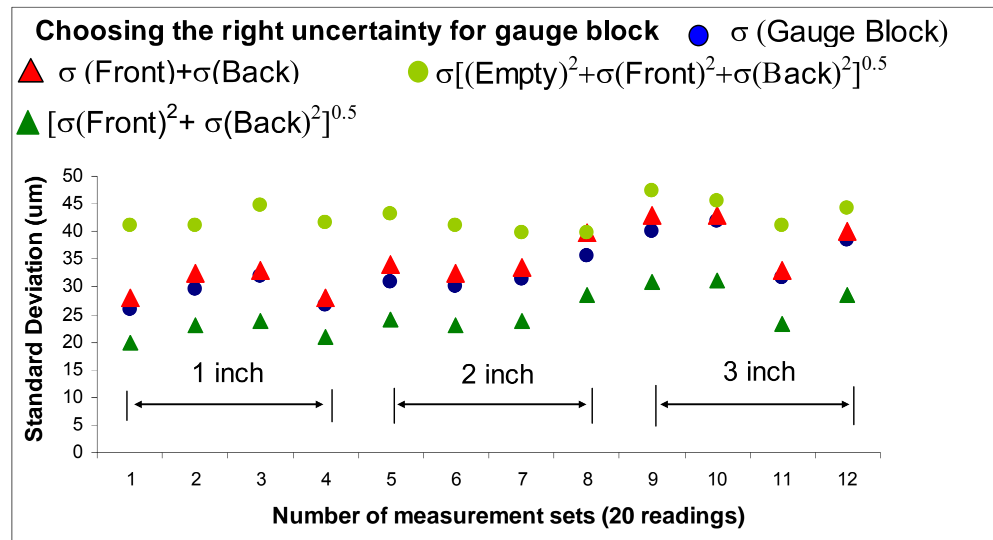

Figure 4- 7: Choosing the right uncertainty for the gauge block due to tuning effects from a combination of uncertainty contributions

4.6.4 Effect of Phase Change on Reflection

Revisiting basics, the phase equation between two cavities in the MST separated by a distance L and refractive index n at wavelength λ is given by

$$\Phi_{A-B} = \frac{2\pi \cdot 2m \cdot nL}{\lambda} + \Omega$$

Equation 4- 11

where Ω represents the phase change on reflection of surface A compared to surface B. In this case, it will be the phase change on reflection of each surface of the gauge block with respect to the transmission flat and is given by

$$\Omega = \frac{4\pi}{\lambda} z,$$

Equation 4- 12

where z is the length corresponding to the phase change on reflection for the given wavelength. There is an additional factor of two in this equation to represent the double-pass nature of the measurement.

Since the phase of the cavities is varied during wavelength scanning differentiating Equation 4- 11 with respect to time gives the phase variation as

$$\frac{\partial \Phi_{A-B}}{\partial t} = -\frac{4\pi}{\lambda^2}\frac{\partial \lambda}{\partial t} mnL + \frac{\partial \Omega}{\partial t} .$$

Equation 4- 13

In order to model the effect of the phase change on reflection on the OPL of a given cavity, Equation 4- 12 is differentiated with respect to time as follows:

$$\frac{\partial \Omega}{\partial t} = \frac{4\pi}{\lambda^2}[\lambda \frac{\partial z}{\partial t} - z \frac{\partial \lambda}{\partial t}]$$

$$\frac{\partial \Omega}{\partial t} = \frac{4\pi}{\lambda^2}[\lambda \frac{\partial z}{\partial \lambda}\frac{\partial \lambda}{\partial t} - z \frac{\partial \lambda}{\partial t}]$$

$$\frac{\partial \Omega}{\partial t} = -\frac{4\pi}{\lambda^2}\frac{\partial \lambda}{\partial t}[z - \lambda \frac{\partial z}{\partial \lambda}]$$

Equation 4- 14

From Equation 4- 14 it is seen that the term $-4\pi/\lambda^2(\partial\lambda\partial t)$ is common to the numerator and the denominator which contains the phase variation for the reference cavity as a result of which it will cancel out. The term inside the brackets, $[z-\lambda(\partial z/\partial\lambda]$, then represents the length contribution to the optical length of a cavity due to the phase change on reflection which is denoted as δ_Ω and is represented as

$$\delta_\Omega = z - \lambda \frac{\partial z}{\partial \lambda}.$$

Equation 4- 15

The value of δ_Ω to the gauge block measurement can be computed by looking at the values for n and k for steel (gauge block material) and their variation over the wavelength range of interest. From reference [85] , the expression for the phase change on reflection for an air/material boundary with a material complex refractive index, $\tilde{n} = n + ik$, is

$$\Omega = \tan^{-1}\left(\frac{2k}{(n^2 + k^2 - 1)}\right).$$

Equation 4- 16

The refractive index values for n and k was obtained from [86] for the wavelength regime of 1 μm to 2.25 μm in steps of 0.25 μm and the values of the phase change on reflection and its length effect at the given wavelengths from Equations 20 and 23 were determined respectively. These values are presented in Table 4- 3. The value of z for a wavelength of 1.5 μm was selected from this table, then $\partial z/\partial\lambda$ was computed from Figure 4- 8 over the tuning range of interest from 1.5 μm to 1.75 μm (in steps of 0.25 μm) and finally δ_Ω was determined from these values to be 13 nm. In case of single wavelength interferometry for a wavelength of 1550 nm, the length contribution from

the phase change would be 29.3 nm as recorded in Table 4- 3 . The technique of wavelength scanning interferometry reduces the length contribution from the phase change on reflection as compared to single wavelength interferometry.

Table 4- 3: Length contribution for phase change on reflection from steel

Wavelength (μm)	**n**	**k**	**Arg = $2k/(n^2 + k^2-1)$**	**Ω = $\tan^{-1}$(Arg)**	**δ_Ω (nm)**
1	3.19	4.43	0.3076	0.2984	23.75
1.25	3.45	5.08	0.2768	0.2700	26.86
1.5	3.71	5.75	0.2509	0.2459	29.35
1.75	3.88	6.32	0.2341	0.2299	32.02
2	4.02	6.88	0.2202	0.2167	34.49
2.25	4.14	7.41	0.2086	0.2056	36.82

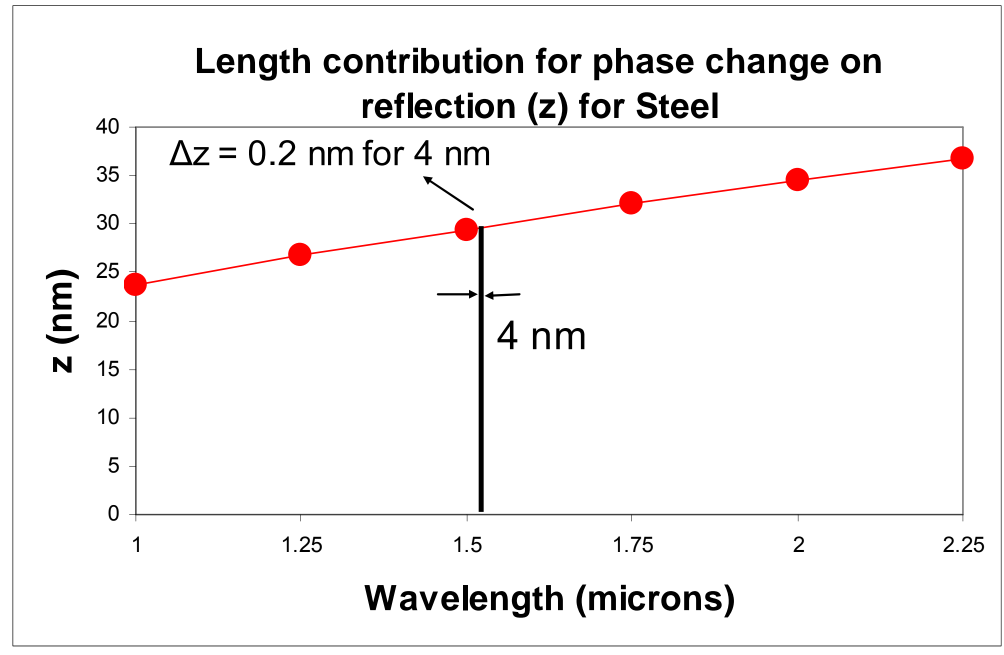

Figure 4- 8 : Length contribution obtained from the phase change on reflection for steel

4.6.5 Alignment

Since the measurement of the gauge block involves two measurements, one for the empty cavity and one with the gauge block in place, it is important to have all the cavities appropriately aligned. The length measurement occurs at a reference pixel at the ends of the gauge block, and ideally the rays traveling through the empty cavity at this location are the same rays that reflect from the gauge block ends when the gauge block is in place. Tilt in the cavities makes this condition approximate, and an additional path length because of this effect must be estimated.

Since the beams in the Sagnac travel in opposite directions before meeting at the beam splitter, it is necessary to determine the overlap by aligning the empty cavity first. Although a single peak for the empty cavity determines the optical length at the reference pixel, the fringe pattern over the entire aperture is a better indicator to determine beam overlap, as shown in Figure 4- 9. Once the empty cavity is aligned, the gauge block is inserted into one of the arms and aligned.

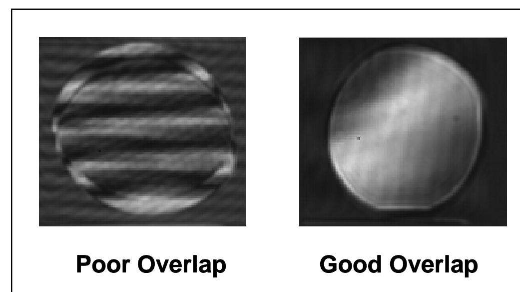

Figure 4- 9: Multi axial stages help in aligning the two cross beams for the empty cavity

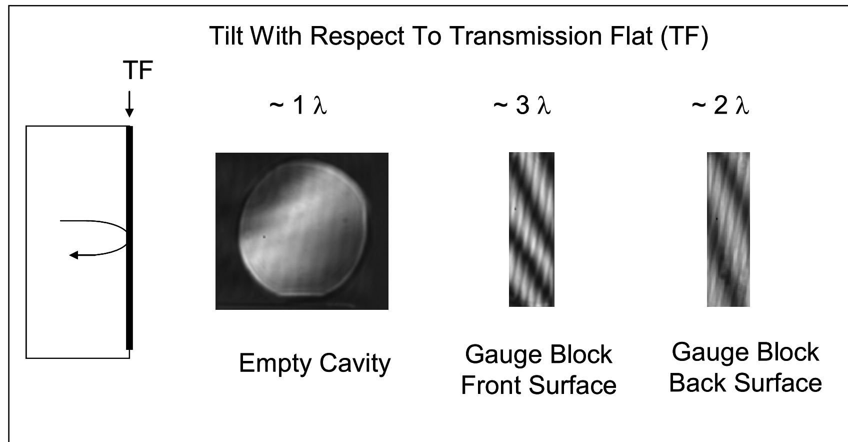

Figure 4- 10: Estimating the effect of tilt on the gauge block measurement from the empty cavity, front and back surface tilt contributions

The effect of alignment on the absolute length of a cavity at the reference pixel can be understood by estimating the amount of tilt in the interferograms and from the length of the cavity from the OPL Spectrum. As shown in Figure 4- 10, the amount of tilt for each cavity (front and back surfaces of the gauge block and the empty cavity) with respect to the transmission flat is determined by knowing the corresponding average cavity lengths and by estimating the error in the lengths at the reference pixel by using simple geometric ray tracing. The errors in the absolute length were estimated to be 0.02 μm and 0.02 μm for the front and back surfaces of the gauge block and 0.04 μm for the empty cavity (approximately 600 mm) geometry. The overall tilt contribution to the gauge block is a root sum square of the individual contributions and is estimated to be 0.05 μm.

4. 7 Uncertainty Discussion

A list of uncertainty sources for the empty cavity, front and back surfaces of the gauge block are listed in Table 4- 4. The major contributor towards the uncertainty in

the measurement is from the repeatability in the instrument which is a function of distance. The setup for the empty cavity and gauge block measurement was optimized based on the size of the available mechanical components. A smaller empty cavity length may be possible by using smaller components for the given setup. The next uncertainty contribution comes from the temperature effects of the reference cavity, which include random variations during the measurement and the calibration uncertainty caused by the unknown temperature during calibration. The calibration uncertainty could be reduced if the exact temperature during calibration be known. It is not possible to calibrate the reference cavity because of the unavailability of the reference cavity data from the commercial instrument. The combined expanded uncertainty for one, two and three inch gauge blocks on average is around 40 micrometers and is an improvement in the 100-300 micrometer tolerance limits used for non contact coarse length measurements of gauge blocks.

Table 4- 4: Uncertainty Budget for coarse measurements of gauge blocks. Values in brackets are for a temperature of 1°C as against 0.2 °C (experiment)

Parameter	**Uncertainty in the Length of Gauge Block (μm)**		
	1 inch	2 inch	3 inch
$U_{GB\ Tuning}$	29	32	38
$U_{GB\ C\ Temp}$	0.1(0.6)	0.14 (0.7)	0.14 (0.7)
$U_{GB\ R\ Temp}$	1(5)	1.2 (6)	1.2 (6)
$U_{GB\ R\ Calibration}$	0.9	1.8	2.7
δ_{Ω}	0.013	0.013	0.013
$\boldsymbol{U_{L\ GB}}$	**29 (29.4)**	**32 (32.6)**	**38 (38.6)**

4. 8 Summary

A simple geometry involving a two mirror Sagnac configuration in conjunction with a commercial wavelength scanning interferometer has been presented to determine the absolute coarse length of an opaque parallel object by measuring three gauge blocks (one, two and three inches). The average value of the gauge block for four sets of twenty readings was found to be accurate to within a combined uncertainty of 40 μm improving tolerance limits on previous non contact coarse length measurements.

CHAPTER 5: SUB-MILLIMETER METROLOGY

5. 1 Introduction to the sub mm project

The main purpose of building an interferometer to measure the thickness of sub-millimeter artifacts was the absence of such a system from literature, in-house source and detector, optics, hardware and software and interest from the sponsors of this project. The goal was to demonstrate single pixel thickness of samples from 25 micrometers to around 600 micrometers in physical thickness. The measurement range of the instrument can be extended to demonstrate the surface profile, front and back surface measurements of artifacts in the future with additional optics and analysis. The basic system described here can also be made to function as an interference microscope by using different parabolic reflectors as lenses to vary the beam size and magnification for a future setup. Each of the blocks are discussed in more detail. The system can be divided into the following components

1) The hardware
2) The software
3) The optics

A bird's eye view of the system design is represented in Figure 5 - 1

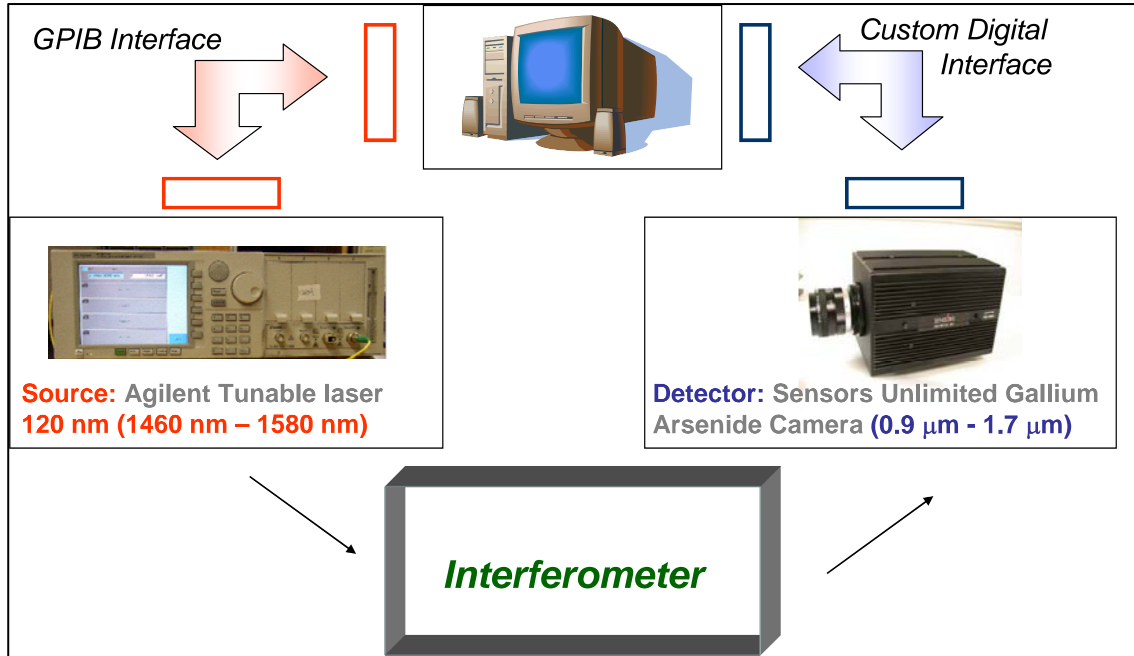

Figure 5 - 1: Block Diagram of Sub-millimeter Metrology System

5. 2 Hardware

One of the financial advantages to the setup which uses an expensive tunable laser and camera was the fact that these were in-house already and ready to use. A new computer system with 2 Gigabyte (GB) memory was bought to facilitate as a stand alone computer for this project. Apart from the source and detector additional hardware included a digital frame grabber PCI (Peripheral Component Interconnect) card (for the computer) along with a custom cable to connect the camera with the computer and a GPIB PCI card and GPIB cable to connect the tunable source with the computer. A wavemeter from HP model HP 86180 C was also incorporated just to check the tuning rate. A single mode fiber was deigned from Fiber Instrument Sales with a 95/5 split ratio the 95 percent being used for the interferometer and the 5 percent to be diverted to

the wavemeter. The source end of the fiber was connected to the high output (angled connector) of the tunable laser source. A helium neon laser was also incorporated to be used in the experiment so as to keep the visible and invisible (infra-red) beam coaxial as possible over the given design length of the experiment.

The camera is a digital camera with an analog output and so a digital frame grabber board from National Instruments NI PCI- 1422 was purchased to get frames from the camera into the computer for processing. A customized cable interface was built to interact with the camera. This was done due to a custom pin-out and connector configuration (DB37-S) for the camera (37 pins) and a general purpose frame grabber board from National Instruments (100 pins). A set top box was also purchased from National Instruments (NI) to be used as an intermediate coupler to connect the appropriate pins from the frame grabber and the camera. A customized cable was made in-house to connect the camera with the set-top box. The interface pin-out between the camera and the frame grabber board is as shown in Figure 5 - 2

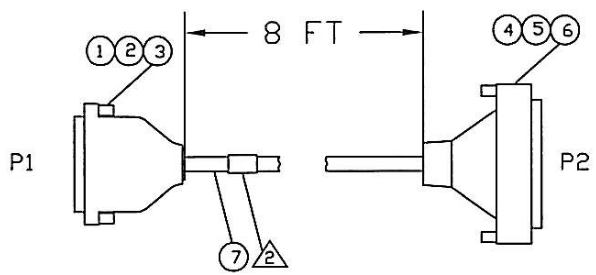

← Camera   Frame Grabber Board in the Computer →

P1 DB37M	P2 HD100M
HOOD	HOOD
1	23
2	24
3	21
4	22
5	19
6	20
7	17
8	18
9	15
10	16
11	13
12	14
13	11
14	12
15	9
16	10
17	7
18	8
19	5
36	6
20	49
21	50
22	44
23	43
24	42
25	41
28	37
29	39
30	35
31	33
32	2
33	1
34	4
35	3
37	99
	100

Figure 5 - 2: Interface pin-out between camera and the frame-grabber board (courtesy Sensors Unlimited Inc)

5. 3 Optics

Two interferometric configurations were considered in the design a) Fizeau setup and (b) Twyman Green Setup.

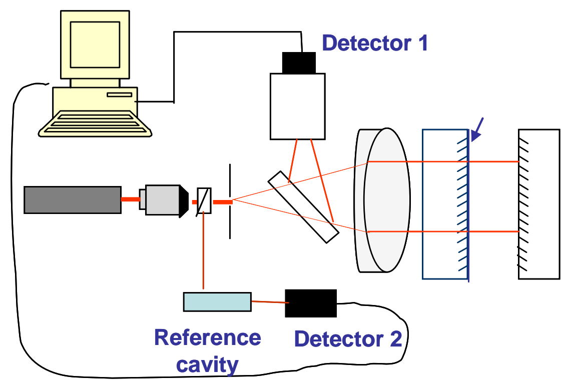

(a) Fizeau Setup similar to the MST

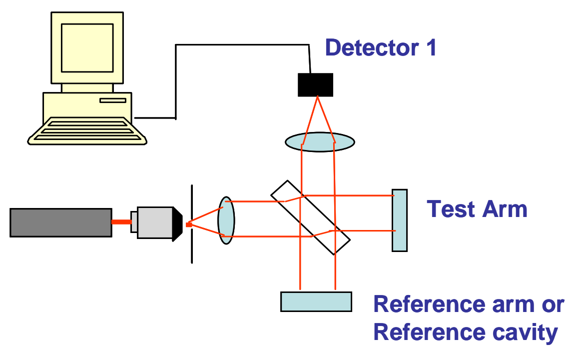

(b) Twyman Green setup

Figure 5 - 3: Fizeau and Twyman Green setups

The Fizeau setup in the MST uses two separate detectors compared to the Twyman Green setup with one detector. Also, the Fizeau setup uses a very expensive transmission flat, more electronics and control compared to a simple optical setup of a Twyman Green and so the choice of a Twyman Green configuration was implemented.

Since the objective of this study is to demonstrate the capability of system to measure sub-millimeter artifacts a simple setup such as Twyman Green was found to be more economical. A collimator lens for the tunable source was found to show enough collimation over the length of the experiment for the given tuning range. The collimation of the laser was found to be sufficient over a length of 2m for a tune of 120 nm to facilitate single pixel thickness measurements.

5. 4 Software

The design of the sub-millimeter system consists of the interferometer (Twyman-Green), a wideband tunable source (120 nm tuning range from 1460 nm to 1580 nm) from Agilent, a near infra red camera SU 320 1.7 RT-V (spectral range 0.9 μm to 1.7 μm) from Sensors Unlimited and a computer which acts as the main control unit to tune the laser and get frames from the camera. There are two software programs which were used, 1) LabVIEW to interact with the tunable laser and the camera and Matlab as a post processing software module to analyze the intensity data from the camera for computing the thickness of artifacts.

A GPIB (General Purpose Interface Bus) interface was used to send and receive commands from the laser and a GPIB PCI card was used in the computer. The LabVIEW driver to be used in software to send and receive commands to the instrument was provided by Agilent technologies.

The software module consists of using a combination of LabVIEW and Matlab to compute the thickness of artifacts. LabVIEW is used as the main driving engine to tune the laser for a given tuning range, monitor the wavelength sweep from a wavemeter and grab frames from the camera which are later used by the Matlab software for analysis.

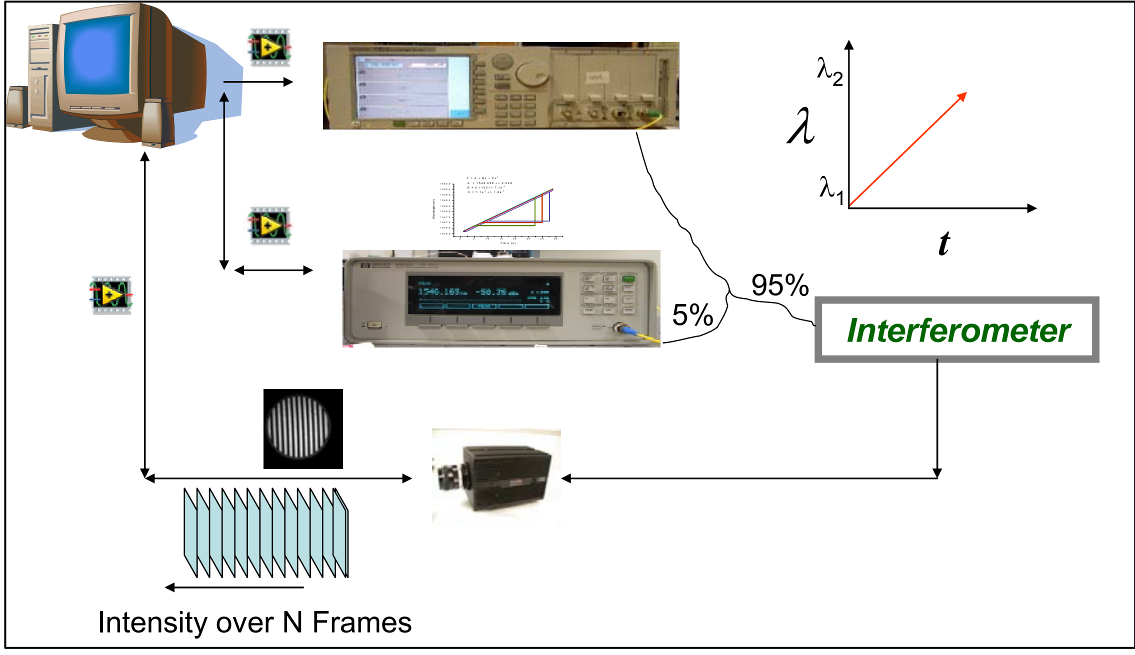

Figure 5 - 4: LabVIEW as a driving engine for real time control and acquisition of data

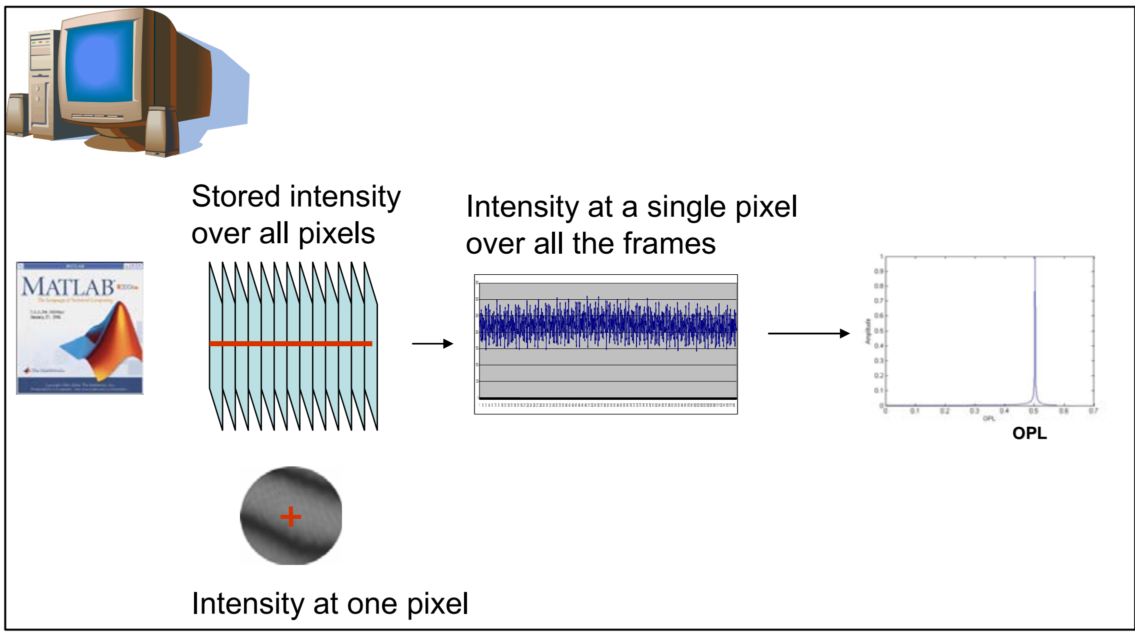

Figure 5 - 5: Matlab as a post-processing tool for analysis and computing the thickness of artifacts

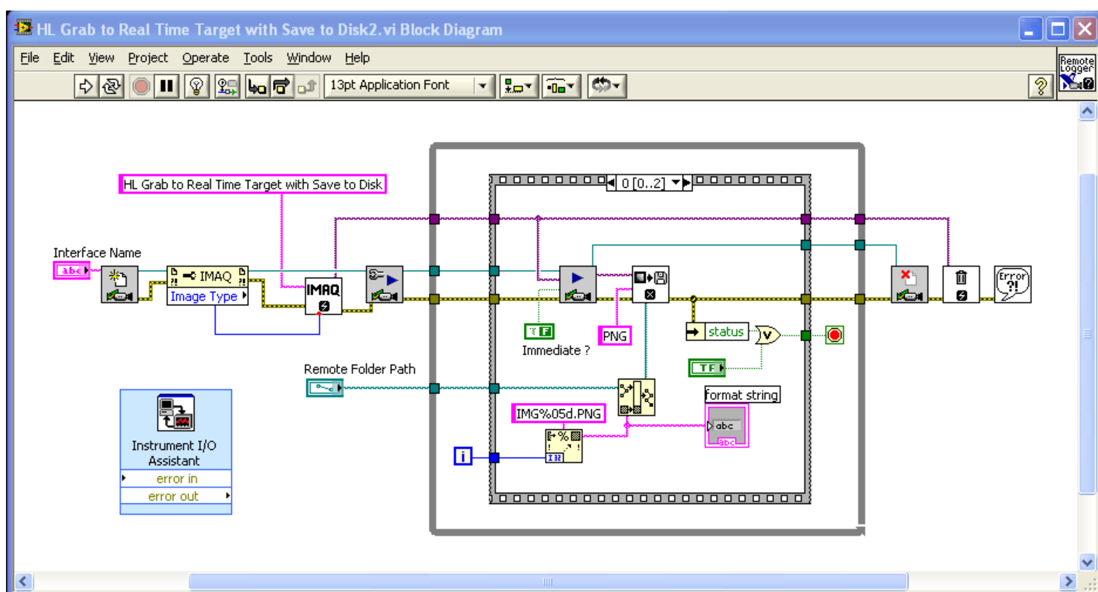

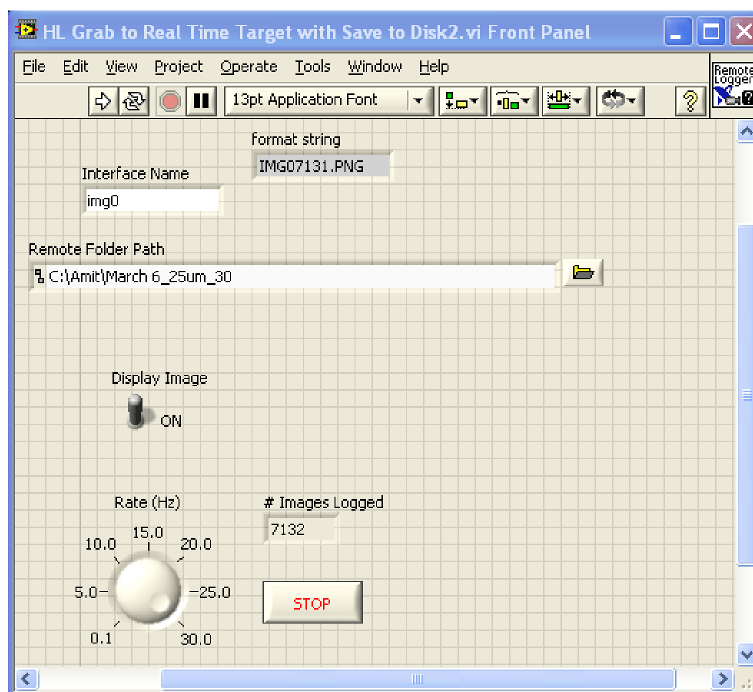

Figure 5 -6: Front Panel and Functional Block diagram in Labview to grab frames and tune the laser

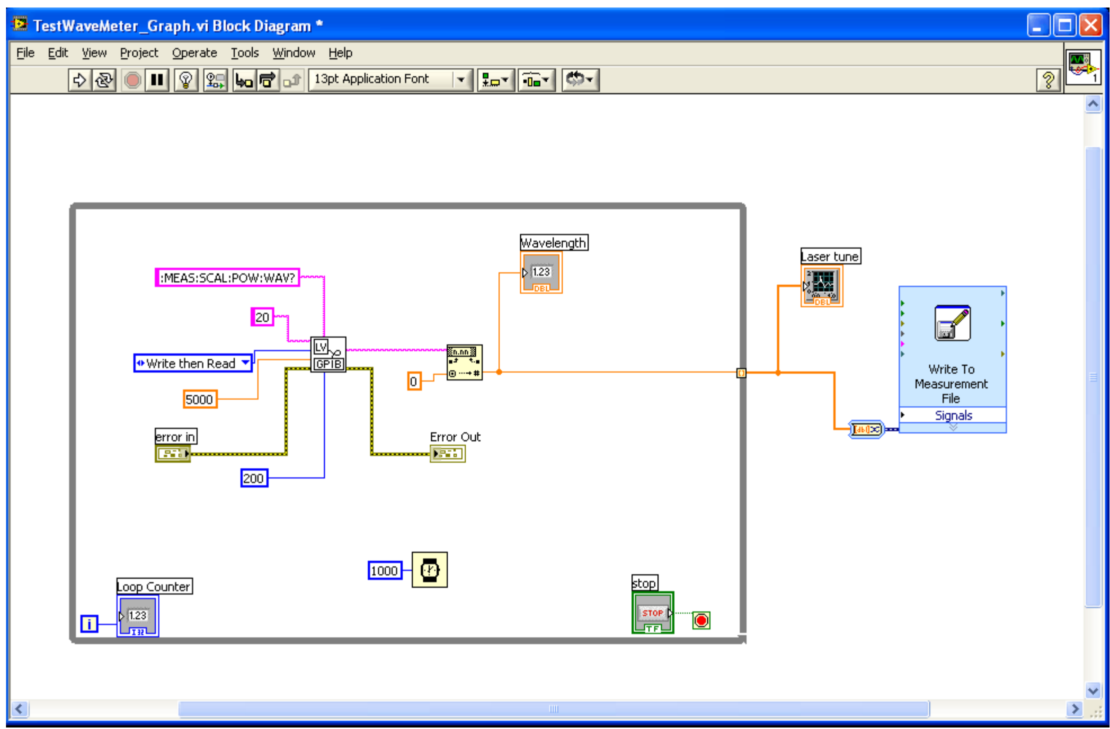

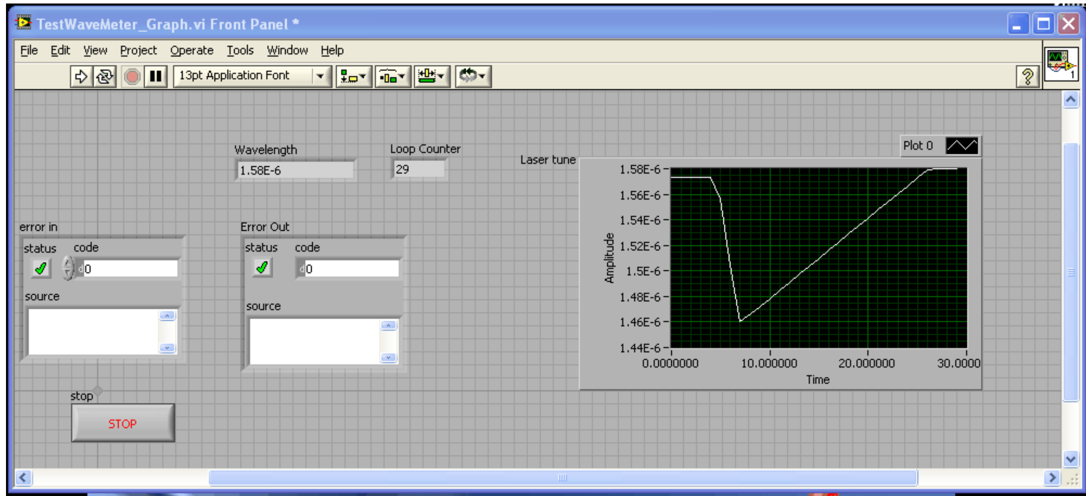

Figure 5 - 7: Functional Block Diagram and Front Panel for determining slope from wavemeter for review purposes only (not used in experiment)

The experimental setup for the sub-millimeter system as per the Tywman Green configuration is as shown in Figure 5 - 8 and Figure 5 - 9.

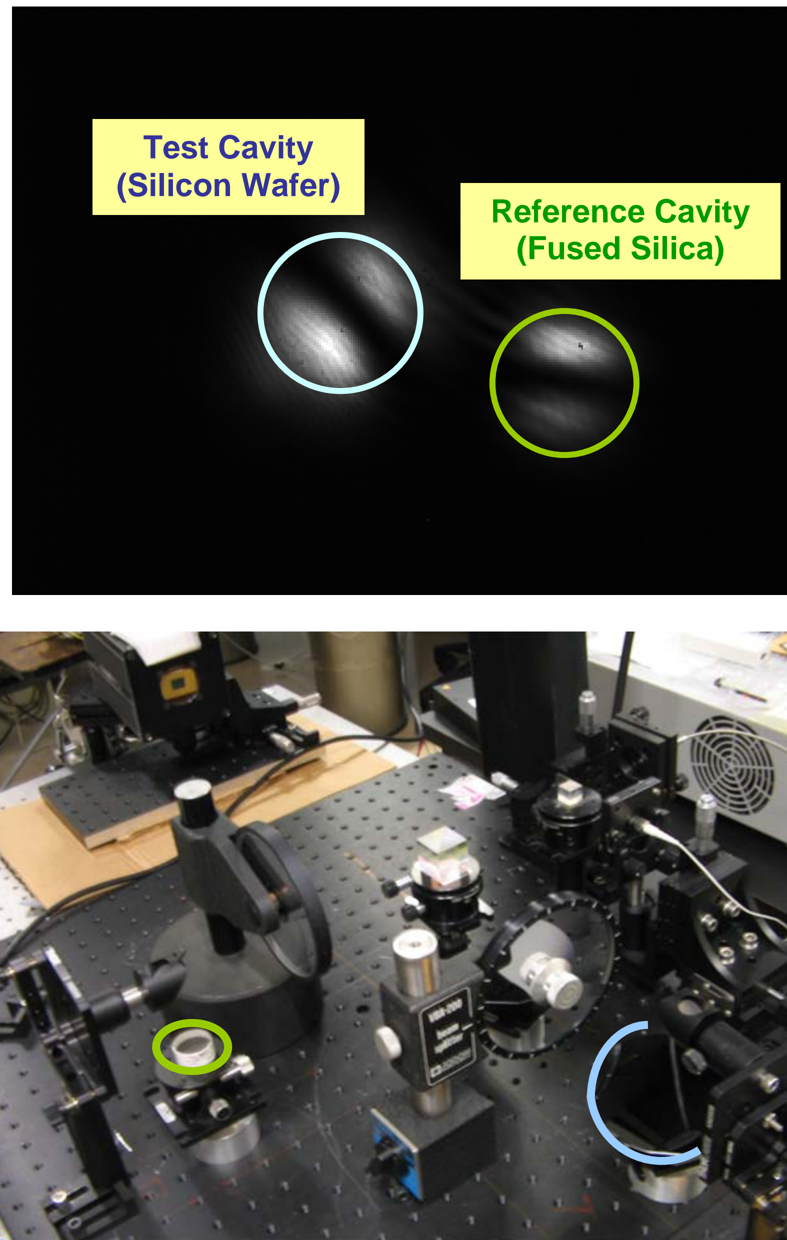

Figure 5 - 8: Experimental setup for sub-millimeter system along with interferometric fringes for the test and reference cavity (19 mm fused silica cavity) change picture

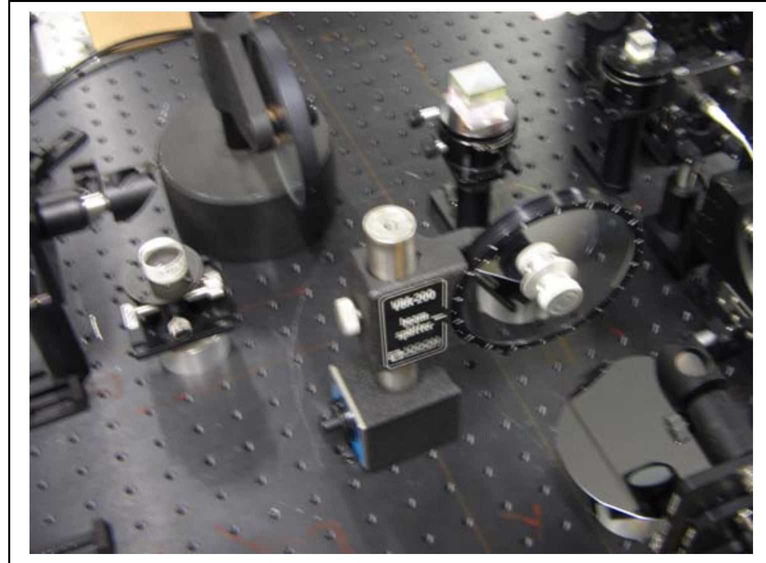

(a)

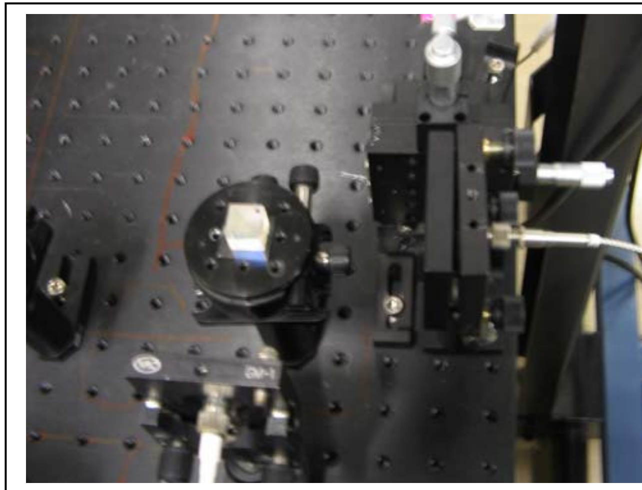

(b)

(c)

Figure 5 - 9: a) Test and reference cavity b) infrared (measurement beam) and visible light (alignment beam) and c) detector

5. 5 Measurements of sub-millimeter thick windows

The smallest window size measurable with a tuning rage of 120 nm (wavelength from 1460 nm to 1580 nm) is around 10 micrometers by using the formula for equivalent wavelength which is $\lambda_1\lambda_2 /(\lambda_2-\lambda_1)$. The equivalent wavelength represents a length corresponding to one full cycle for the give tuning range using a Fourier based analysis. This can also be proved by looking at the equation for the frequency of a cavity shown in the earlier chapters.

$$f_C = \frac{OPD}{\lambda_1\lambda_2} \cdot \frac{\partial\lambda}{\partial N}$$

Equation 5- 1

where fc is the frequency per sample, $\partial\lambda$ is the tuning range and ∂N is the total number of samples. The smallest frequency for the given number of samples will be fc/∂N or fc/N Since N and ∂N are one and the same, the smallest OPD measured can then be represented as

$$OPD_{MIN} = \frac{\lambda_1\lambda_2}{\partial\lambda} = \frac{\lambda_1\lambda_2}{\lambda_2 - \lambda_1}.$$

Equation 5- 2

Any OPD smaller than the minimum will need another technique of modeling the intensity to determine the thickness as is done in reflectometry which will be the continuing project for this study and is discussed in the following chapter. The largest cavity which can be measured is limited by the length corresponding to the Nyquist frequency. For a camera sampling at 30 Hz, the maximum optical path difference (OPD) that can be measured is around 70 mm. The reference cavity chosen in this case is a 19.415 mm (± 0.001 mm) fused silica window measured from the MST. Three

different windows were measured a 25 (± 5) micrometer window a 60 (± 5) micrometer window purchased from Virginia Semiconductor corporation and a 450 (± 10) micrometer was obtained from the center for Optoelectronics and Optical Communications and their physical thicknesses is shown in Table 5- 1. A set of 10 readings were taken for each window and the OPD transform was computed. By computing the refractive index and the dispersion contribution for the reference window (fused silica) [77] and test window (silicon) [87] in Figure 5 - 11, the physical thickness was computed. Figure 5 - 10 shows one such peak for the 25 micrometer window similar to the OPD transform in the previous chapters.

Table 5- 1: Thicknesses for 25 μm ± 5 μm,60 μm ± 10 μm,450 ± 10 μm silicon windows

Physical Thickness (25 μm ± 5 μm)	**Physical Thickness (60 μm ± 5 μm)**	**Physical Thickness (450 μm ± 10 μm)**
27.5268	49.1802	460.7719
27.607	49.4374	460.4787
27.6419	48.9327	460.1856
27.6935	48.87	460.1869
27.7071	49.1169	460.7716
27.7118	48.6742	460.4838
27.6922	49.1304	459.5994
27.7023	49.0686	460.4838
27.6475	49.0626	460.094
27.6968	48.975	460.1236
27.662 μm (AVG)	**49.045 μm (AVG)**	**460.318 μm (AVG)**
0.059 μm (STD_DEV)	**0.203 μm (STD_DEV)**	**0.354 μm (STD_DEV)**

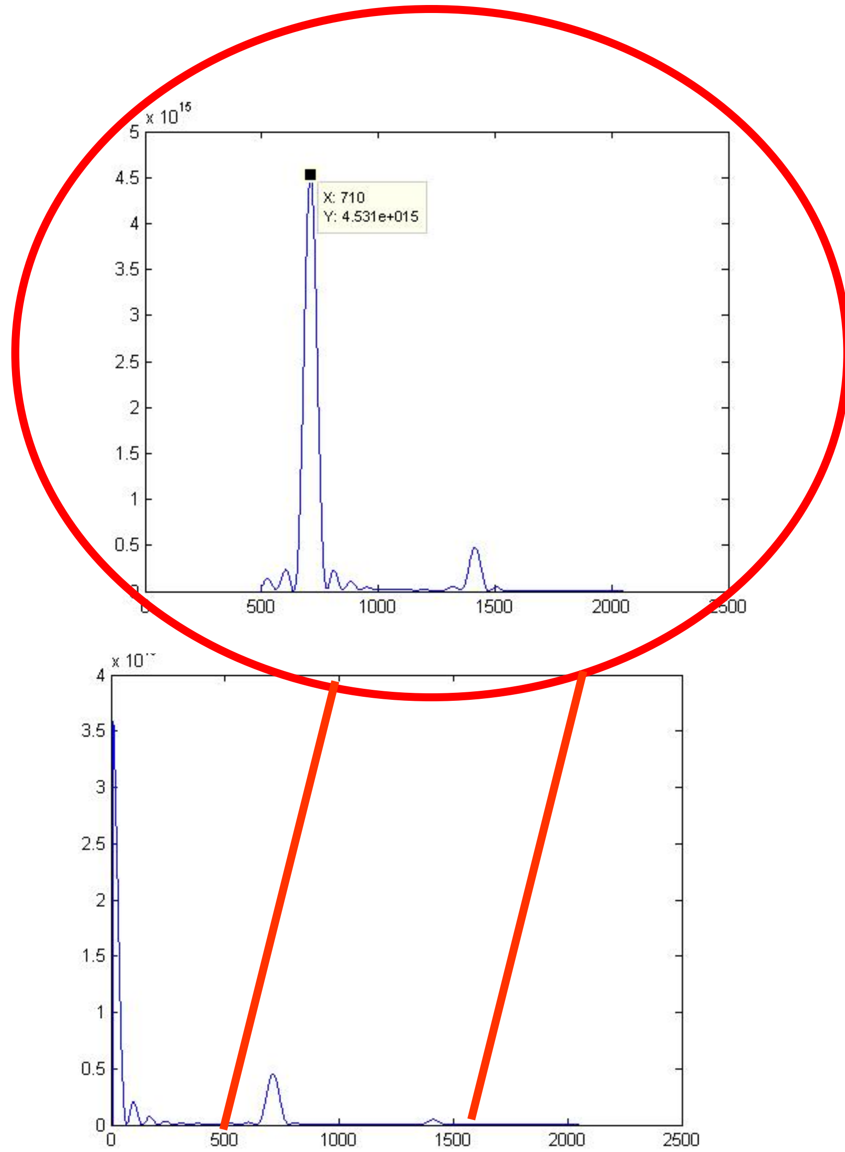

Figure 5 - 10: Large OPD peak (uppermost figure) corresponding to a 25 µm ± 5 µm cavity along with double reflection from a smaller peak at twice the location

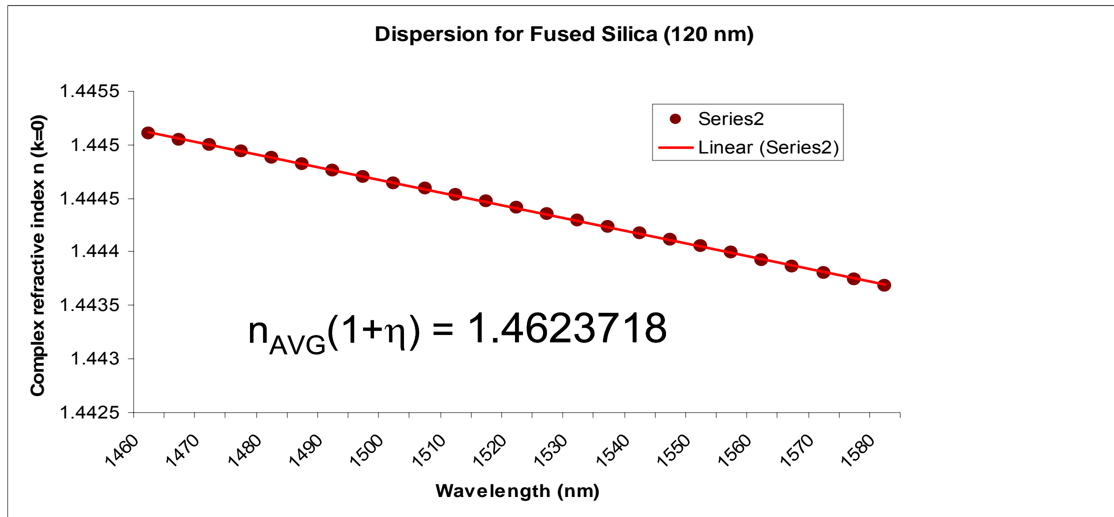

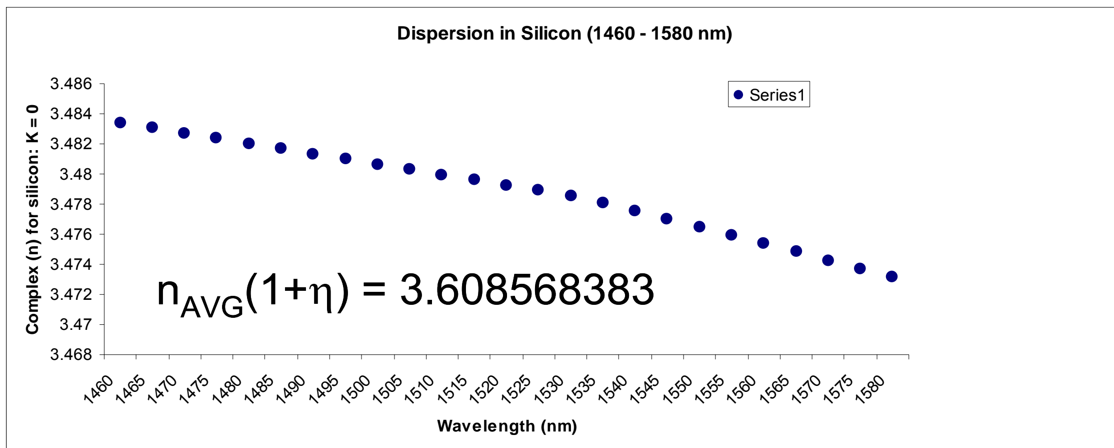

Figure 5 - 11: Dispersion for Fused Silica and Silicon

5. 6 Uncertainty Analysis

A similar simulation for β was used by changing the starting wavelength ending wavelength, tuning range etc over the tolerance limits for the two windows namely 25 μm ± 5 μm and 60 μm ± 5 μm. The value of β for the 25 micrometer (±5 μm) window in the range from 20 μm to 30 μm is around ± 5.5 μm while the β for the 60 μm (± 5 μm) window over the tolerance range of 55 μm to 65 μm is around ± 10 μm and the

value of β for the 450 μm window in the range from 440 μm to 460 μm is around ± 8 μm.

Table 5- 2: Uncertainty budget for 25 μm ± 5 μm window

Main Parameter	Secondary Parameters	Absolute Uncertainty	Fractional Uncertainty
OPD_{T_Temp}	$n_T = 3.48314$ $\partial n_T / \partial T = 1.87 \times 10^{-4} /℃$ $L_T = 25 \mu m$ $\partial L_T /(L_T . \partial T) = 4.6 \times 10^{-6} /℃$	1.5 nm	$60/10^6$
OPD_{R_Temp}	$n_R = 1.444045$ $\partial n_R / \partial T = 1.28 \times 10^{-5} /℃$ $L_R = 19.415\ mm$ $\partial L_R /(L_R . \partial T) = 5.5 \times 10^{-7} /℃$	182 nm	$9.4/10^6$
OPD_{R_calib}	± 1.1 μm	1.4 nm	$56/10^6$
β	Simulation	5.5 μm	$22/10^2$
ε_{Tuning}	Repeatability	59 nm	$2.3/10^3$
Combined Uncertainty for single pixel thickness		**5.5 μm**	**$22/10^2$**

Table 5- 3: Uncertainty budget for 60 μm ± 5 μm window

Main Parameter	Secondary Parameters	Absolute Uncertainty	Fractional Uncertainty
OPD_{T_Temp}	$n_T = 3.48314$ $\partial n_T / \partial T = 1.87 \times 10^{-4} /℃$ $L_T = 60 \mu m$ $\partial L_T /(L_T . \partial T) = 4.6 \times 10^{-6} /℃$	3.5 nm	$60/10^6$
OPD_{R_Temp}	$n_R = 1.444045$ $\partial n_R / \partial T = 1.28 \times 10^{-5} /℃$ $L_R = 19.415\ mm$ $\partial L_R /(L_R . \partial T) = 5.5 \times 10^{-7} /℃$	182 nm	$9.4/10^6$
OPD_{R_calib}	± 1.1 μm	3 nm	$50/10^6$
β	Simulation	10 μm	$17/10^2$
ε_{Tuning}	Repeatability	203 nm	$3.3/10^3$
Combined Uncertainty for single pixel thickness		**10 μm**	**$17/10^2$**

Table 5- 4: Uncertainty budget for 450 μm ± 10 μm window

Main Parameter	Secondary Parameters	Absolute Uncertainty	Fractional Uncertainty
OPD_{T_Temp}	$n_T = 3.48314$ $\partial n_T / \partial T = 1.87 \times 10^{-4}/°C$ $L_T = 450 \mu m$ $\partial L_T / (L_T . \partial T) = 4.6 \times 10^{-6}/°C$	26 nm	$60/10^6$
OPD_{R_Temp}	$n_R = 1.444045$ $\partial n_R / \partial T = 1.28 \times 10^{-5}/°C$ $L_R = 19.415$ mm $\partial L_R / (L_R . \partial T) = 5.5 \times 10^{-7}/°C$	182 nm	$9.4/10^6$
OPD_{R_calib}	± 1.1 μm	26 nm	$58/10^6$
β	Simulation	8 μm	$18/10^3$
ε_{Tuning}	Repeatability	354 nm	$8/10^4$
Combined Uncertainty for single pixel thickness		**8 μm**	**$18/10^3$**

In one measurement, two 450 micrometer (physical thickness) thick samples were measured on the commercial wavelength scanning interferometer (MST) and one was used a reference (457.618 μm) and the other as test (457.009 μm) was measured on the sub millimeter system. The average of ten readings for the test sample was 455.586 μm with a repeatability of 0.064 μm. Measuring similar artifacts for the test and reference does reduce the repeatability by almost an order of magnitude (64 nm) when compared to the repeatability of a larger reference (354 nm). The β in this case is about 9 micrometers which is similar to the β for the larger reference about 8 micrometers. However the uncertainty in knowing the optical thickness from the MST is dominated by β which is around 1 μm and since the reference and the test samples are similar in their thickness and material properties the absolute uncertainty contribution for the test sample is also 1 μm. Hence, although two similar samples give a lower repeatability

contribution, the accuracy of the sample will depend directly on a one on one basis as the accuracy of the reference. A more accurate reference(at least two orders of magnitude lower) is needed to reduce this uncertainty contribution. Hence in most cases a larger reference is used to reduce this effect and ease the accuracy requirements on the reference at the cost of a slightly larger repeatability but a smaller combined uncertainty. The value of β which dominates all the measurements can be reduced by increasing the sampling rate (using simulation) for the test and reference windows. A sampling rate of 2400 Hz (faster camera) is found to give a β of about 400 nm for a 450 μm window with reference cavities being either another 450 micrometer or the 19.415 mm fused silica window used earlier.

Table 5- 5 : Measuring a 457.009 μm ± 1.1 μm test window with a 457.618 μm ± 1.1 μm reference window

Physical Thickness of sample (457.009 μm ± 1.1 μm)
455.6709
455.4971
455.5593
455.5802
455.5147
455.5636
455.6723
455.5812
455.5535
455.6697
455.5863 μm (AVERAGE)
0.064096 μm (STANDARD DEVIATION)

Table 5- 6: Uncertainty budget for 457.009 µm ± 1.1 µm test window

Main Parameter	Secondary Parameters	Absolute Uncertainty	Fractional Uncertainty
OPD_{T_Temp}	$n_T = 3.48314$ $\partial n_T / \partial T = 1.87 \times 10^{-4}/℃$ $L_T = 450\ \mu m$ $\partial L_T /(L_T . \partial T) = 4.6 \times 10^{-6}/℃$	26 nm	$60/10^6$
OPD_{R_Temp}	$n_R = 3.48314$ $\partial n_R / \partial T = 1.87 \times 10^{-4}/℃$ $L_R = 450\ \mu m$ $\partial L_R /(L_R . \partial T) = 4.6 \times 10^{-6}/℃$	26 nm	$60/10^6$
OPD_{R_calib}	1.1 µm	1.1 µm	$2.4/10^3$
β	Simulation	9 µm	$2/10^2$
ε_{Tuning}	Repeatability	64 nm	$1.4/10^4$
Combined Uncertainty for single pixel thickness		**9 µm**	**$2/10^2$**

5. 7 Summary

The OPD transform used in the commercial instrument was used in obtaining the physical thickness of various silicon artifacts (25 µm, 60 µm and 450 µm, reference window 19.415 mm fused silica) from a custom built wavelength scanning system thereby providing a proof of concept for sub-millimeter window measurements. The dominant source of uncertainty is the β value which is heavily dependent on the sampling rate of the camera (currently at 30 Hz) and through simulation has shown to reduce to by an order of magnitude for a sampling rate of 2400 Hz. The repeatability in the instrument is the next source of uncertainty and can be reduced by having the test and reference cavities of similar thickness (physical and material i.e. refractive index). In such a scenario the uncertainty will be dominated by the reference cavity accuracy. If an accurate reference is not available then a larger reference should be used to reduce

the uncertainty in the test sample. In such cases the repeatability will be larger compared to the case using similar reference and test cavities. The effects of temperature on the cavities offer the least uncertainty contribution in stable laboratory environments when the temperature variations are as low as 0.2 degrees over a couple of hours. Future work on this project and combination with another technique is provided in the next chapter on continuity.

CHAPTER 6: CONCLUSIONS AND CONTINUITY

6. 1: Conclusions

The study has presented length measurements of different artifacts transparent planar, transparent spherical and opaque planar along with a detailed uncertainty analysis. A detailed study of the instrument, the MST (Multiple Surface Transform) and the technique of wavelength scanning with a special Fourier transform, the OPD Transform was undertaken and the working was verified with a simulation based analysis with experimental inputs. The major contribution towards uncertainty for windows is from the β term which represents the uncertainty range for the estimated value of thickness over a given tolerance for perfect conditions (wavelength slope) in the technique followed by the uncertainty in knowing the calibrated value of the reference cavity for a given temperature and the repeatability in the instrument. A sub millimeter system was designed (using the OPD Transform) and an in house tunable laser, and detector and the thickness of different silicon windows was demonstrated as proof of concept. In this case too, the value of β dominated the measurement uncertainty and a simulation showed the measurement uncertainty to reduce by increasing the sampling rate.

6. 2: Continuity (extension of the project to include surface profile measurements)

In order to extend the measurement range from a single pixel to a surface profile, in house color corrected objectives (from Mitutoyo Corporation) along with

parabolic reflectors have been collected to be used for future research. A model of such a setup is as shown in Figure 6- 1.

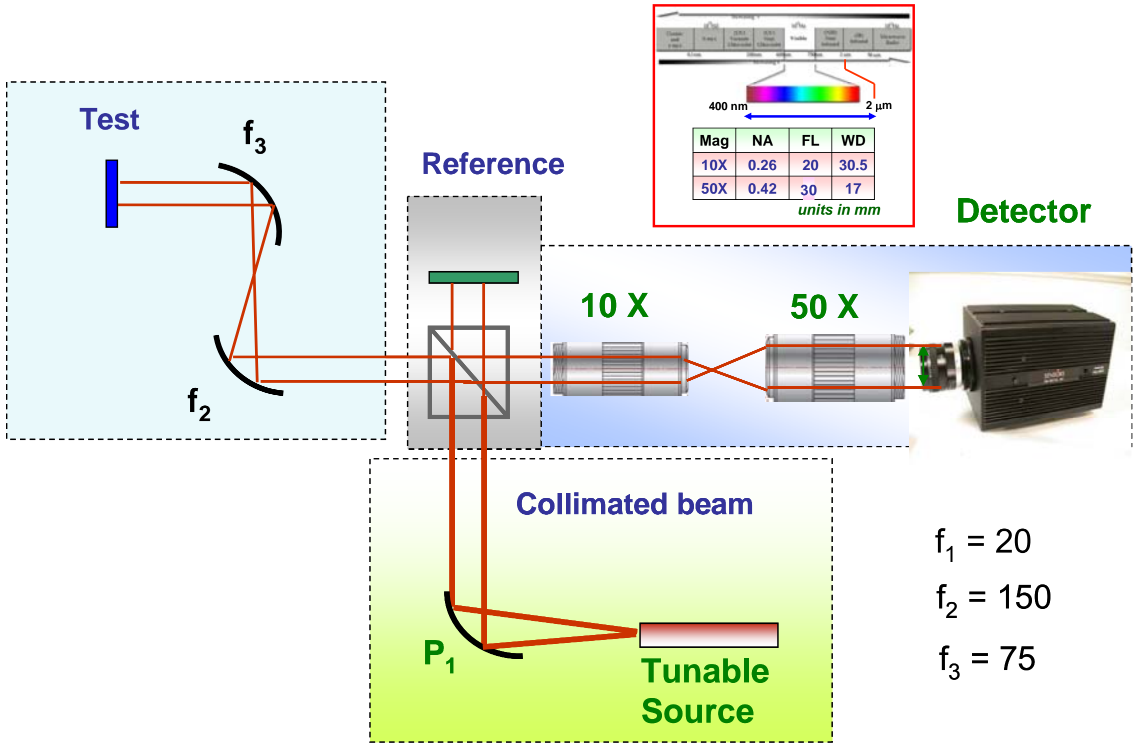

Figure 6- 1: Sketch of a future broadband tunable wavelength scanning system with reflective elements for beam shaping

The initial system sketch will provide a magnification of 3X with the sample footprint being 1.5 mm and the detector footprint being 4.5 mm. Since the proof of concept for a single pixel has been demonstrated, the system design will focus more on the optical and mechanical design constraints over the given tuning range.

6. 3 Wavelength scanning and reflectometry techniques

Another interesting avenue for thickness measurements below the minimum thickness using wavelength scanning with the OPD Transform has been demonstrated by combining the concept of wavelength scanning for tuning the laser and reflectometry (modeling) for analyzing the data. The minimum thickness limits in wavelength scanning using the OPD transform or any Fourier transform method is based on obtaining at least one cycle of the waveform over the measurement time. For thicknesses smaller than the minimum limit, a modeling approach can been implemented by using the principle of reflectometry. In [94] the authors have shown proof of concept by demonstrating the measurements of a 60 μm thick wafer (optical thickness ~ 200 μm) using the commercial wavelength scanning system (the MST) which has a minimum optical thickness limit of 600 μm. This technique can then be used in the sub-millimeter system to increase its dynamic measurement range well below the minimum thickness of 10 μm.

REFERENCES

Phase

[1] K. J. Gasvik, “ Interference” in Optical Metrology , John Wiley and Sons, Inc., New York, 2002.

[2] N. Bobroff, “Recent advances in displacement measuring interferometry”, Measurement Science and Technology, Vol 4, pp 907-926, 1993

[3] J.E. Greivenkamp and J.H. Bruning, “Phase Shifting Interferometry,” in Optical Shop Testing, Ed. D. Malacara, John Wiley and Sons, Inc., New York, 1992.

[4] K. Creath, “A comparison of Phase-Measurement algorithms,” in Proceedings of SPIE, 680, 1986

[5] P. De Groot, ““Derivation of algorithms for phase-shifting interferometry using the concept of a data-sampling window”, Applied Optics, Vol 34, pp 4723-4730, 1995

[6] L. Deck,"Fourier-Transform Phase-Shifting Interferometry",Appl. Opt.,Vol.42, pp 2354-2365, 2003

[7] F. Weigl,"Two-Wavelength Holographic Interferometry for Transparent Media Using a Diffraction Grating",Appl. Opt.,Vol.10, pp 1083-1086, 1971

[8] J. C. Wyant,"Testing Aspherics Using Two-Wavelength Holography",Appl. Opt.,Vol.10, pp 2113-2118, 1971

[9] C. Polhemus,"Two-Wavelength Interferometry", Appl. Opt.,Vol.12, pp 2071-2074, 1973

[10] R. Dandliker, Y. Salvade and E. Zimmermann,"Distance measurement by multiple-wavelength interferometry",Journal of Optics,Vol.29,pp 105-114, 1998

[11] R. Dändliker, R. Thalmann and D. Prongué,"Two-wavelength laser interferometry using superheterodyne detection",Opt. Lett.,Vol.13, pp 339-341,1988

[12] V. Mahal and A. Arie,"Distance measurements using two frequency-stabilized Nd:YAG lasers",Appl. Opt.,Vol.35, pp 3010-3015,1996

[13] J. E. Decker, J. R. Miles, A. A. Madej, R. F. Siemsen, K. J. Siemsen, S. d. Bonth, K. Bustraan, S. Temple and J. R. Pekelsky,"Increasing the Range of Unambiguity in Step-Height Measurement with Multiple-Wavelength Interferometry-Application to Absolute Long Gauge Block Measurement",Appl. Opt.,Vol.42, pp 567-5678 ,2003

[14] A. Olsson and C. L. Tang,"Dynamic interferometry techniques for optical path length measurements",Appl. Opt.,Vol.20, pp 3503-3507 ,1981

[15] H. Kikuta, K. Iwata and R. Nagata, " Distance measurement by the wavelength shift of laser diode light","Appl. Opt., Vol 25, pp 2976-2980, 1986

[16] O. Sasaki, T. Yoshida and T. Suzuki, " Double sinusoidal phase modulating laser diode interferometer for distance measurement", Appl. Opt., Vol 30, pp 3617-3621,1991

[17] G. Beheim and K. Fritsch, "Remote displacement measurements using a laser diode",Electron. Lett, Vol 21, pp 93-94, 1985

[18] A. J. den Boef, " Interferometric laser range finder using a frequency modulated diode laser", Appl. Opt. Vol 26, pp 4545-4550, 1987

[19] M. Suematsu and M. Takeda,"Wavelength-shift interferometry for distance measurements using the Fourier transform technique for fringe analysis",Appl. Opt.,Vol.30, pp 4046-4055 ,1991

[20] A. Hyamns, J Lait, Analysis of a frequency modulated continuous wave ranging system " Proceeedings IEEE 107, pp 365-372 (1960)

[21] W. Eickhoff and R. Ulrich, " Optical frequency domain reflectometry in single-mode fiber", Appl Phys. Lett. Vol 39, pp 693-695, 1981

[22] S. A. Kinglsey and D. E. N. Davies, "ODFR diagnostics for fibre and integrated-optic systems", Electron. Lett., Vol 21, 1985

[23] U. Glombitza and E. Brinkmeyer, "Coherent frequency-domain reflectometry for characterization of single mode integrated-optical waveguides", J. Lightwave Technol. Vol 11, pp 1377-1384, 1993

[24] M. Yoshida, K. Nakamura, and H. Ito, " A new method for measurement of group velocity dispersion of optical fibers using a frequency-shifted feedback fiber laser", IEEE Photon. Technol. Lett, Vol 13, pp 227-229, 2001

[25] T. J. Ahn, Y. Jung, K. Oh and D.Y. Kim,"Optical frequency-domain chromatic dispersion method for higher-order modes in an optical fiber", Opt. Express, Vol 13, pp 10040-10048, 2005

[26] M. Yoshida, T. Miyamoto,, N. Zou, K. Nakamura and H. Ito, "Novel PMD measurements method based on OFDR using a frequency-shifted feedback fiber laser", Opt Express, Vol 9, pp 207- 211, 2001

[27] M. Froggart, D. Gifford, S. Kreger, M. Wolfe and B. Soller, " Distributed strain and temperature discrimination in unaltered polarization maintaining fiber ", in Optical Fiber Sensors, OSA Technical Digest (CD) ,OSA 2006 Paper ThC5

[28] J. Thiel, T. Pfeifer and M. Hartmann, "Interferometric measurement of absolute distances of up to 40 m", Measurement,Vol.16, pp 1-6, 1995

[29] J. A. Stone, A. Stejskal and L. Howard, "Absolute Interferometry with a 670-nm External Cavity Diode Laser", Appl. Opt.,Vol.38, pp 5981-5994,1999

[30] K.-H. Bechstein and W. Fuchs,"Absolute interferometric distance measurements applying a variable synthetic wavelength", Journal of Optics,Vol.29, pp 179-182,1998

White Light interferometry

[31] S.W. Kim and G.H. Kim,"Thickness-Profile Measurement of Transparent Thin-Film Layers by White-Light Scanning Interferometry",Appl. Opt.,Vol.38, pp 5968-5973,1999

[32] B. Kimbrough, J. Millerd, J. Wyant and J. Hayes, "Low Coherence Vibration Insensitive Interferometer" , Katherine Creath, Joanna Schmit, e.ds., Proc SPIE, 6292 (1-12)

[33] Y.S. Ghim and S.W. Kim,"Thin-film thickness profile and its refractive index measurements by dispersive white-light interferometry",Opt. Express,Vol.14, pp 11885-11891 ,2006

[34]S. K. Debnath, M. P. Kothiyal, J. Schmit and P. Hariharan,"Spectrally resolved white-light phase-shifting interference microscopy for thickness-profile measurements of transparent thin film layers on patterned substrates",Opt. Express,Vol.14, pp 4662-4667 ,2006

[35] D. Kim and S. Kim,"Direct spectral phase function calculation for dispersive interferometric thickness profilometry",Opt. Express,Vol.12, pp 5117-5124 ,2004

[36] D. Kim, S. Kim, H. J. Kong and Y. Lee,"Measurement of the thickness profile of a transparent thin film deposited upon a pattern structure with an acousto-optic tunable filter",Opt. Lett.,Vol.27, pp 1893-1895, 2002

[37] K.N. J. a. S.-W. Kim,"Dispersive interferometry using femtosecond pulse laser for measuring refractive index and physical thickness of test samples",Interferometry XIII: Techniques and Analysis,Vol.6292,1-9,2006

Techniques for absolute distance measurements

[38] J. Degnan, “ Millimeter accuracy satellite laser ranging : A review”, in Contributions to Space Godesy to Geodynamics: Technology, Vol 25, pp 133-162,1993

[39] Ichiro Fujimay, Shigeo Iwasaki and Katuo Seta, “High-resolution distance meter using optical intensity modulation at 28 GHz” , Meas. Sci. Technol. Vol 9 ,pp 1049–1052, (1998)

[40] R. D. Peterson and K. L. Schepler,"Timing Modulation of a 40-MHz Laser-Pulse Train for Target Ranging and Identification",Appl. Opt.,Vol.42, pp 7191-7196,2003

[41] K. Minoshima and H. Matsumoto,"High-Accuracy Measurement of 240-m Distance in an Optical Tunnel by use of a Compact Femtosecond Laser",Appl. Opt.,Vol.39, pp 5512-5517,2000

[42] J. Ye, “Absolute measurement of a long, arbitrary distance to less than an optical fringe”,Opt. Lett.,Vol.29, pp 1153-1155 ,2004

[43] N. Schuhler, Y. Salvadé, S. Lévêque, R. Dändliker and R. Holzwarth, “Frequency-comb-referenced two-wavelength source for absolute distance measurement”,Opt. Lett.,Vol.31, pp 3101-3103, 2006

[44] A. Cabral and J. Rebordão, Accuracy of frequency-sweeping interferometry for absolute distance metrology Opt. Eng., Vol. 46, pp 073602 1-10, 2007

Techniques to reduce multiple beam interference in PSI

[45] K. Freischlad, “Large flat panel profiler”, in Flatness, Roughness and Discrete Defect Characterization for Computer Disks, Wafers and Flat Panel Displays, J.C. Stover, e.d., Proc SPIE, Vol 2862, pp 163-171, (1996)

[46] P. J. de Groot, "Grating interferometer for flatness testing", Opt. Lett.,Vol.21, pp 228-230,1996

[47] C. Ai, " Multimode-laser interferometric apparatus for eliminating background interference fringes from thin-plate measurements", U.S. patent 5,452,088 (19 September 1995)

[48] P. Dewa and A. Kulawiec, “ Grazing incidence interferometry for measuring transparent parallel plates”, U.S. patent 5,923,425 (13 July 1999)

[49] P. de Groot, “Measurement of transparent plates with wavelength-tuned phase-shifting interferometry”, App. Opt. Vol 39, pp 2658-2663, (2000)

[50] P. P. Sorokin and J. R. Lankard, Stimulated emission observed from an organic dye, chloro-alurninum phthalocyanine, IBM J. Res. Develop. 10, pp 162-163 (1966).

[51] F. P. Schäfer, W. Schmidt, J. Volze, Organic dye solution laser, Appl. Phys. Lett. 9, pp 306-309 (1966)

[52] O. G. Peterson et al., “CW operation of an organic dye solution laser”, Appl. Phys. Lett. 17 (6), 245 (1970)

[53] C. V. Shank and E. P. Ippen, “Subpicosecond kilowatt pulses from a modelocked cw dye laser”, Appl. Phys. Lett. 24, 373 (1974)

[54] R. L Fork, B. I. Greene and C. V Shank, “Generation of optical pulses shorter than 0.1 ps by colliding pulse modelocking”, Appl. Phys. Lett. 38, 671 (1981)

[55] J. A. Valdmanis et al., “Generation of optical pulses as short as 27 femtoseconds directly from a laser balancing self-phase modulation, group-velocity dispersion, saturable absorption, and saturable gain”, Opt. Lett. 10 (3), pp 131 -133, 1985

[56] N. Melikechi,"A two-wavelength dye laser with broadband tunability," Journal of Physics E: Scientific Instruments,Vol.20, pp 558-559,1987

[57] D. Bradley, A. Durrant, G. Gale, M. Moore and P. Smith,"Characteristics of organic dye lasers as tunable frequency sources for nanosecond absorption spectroscopy," Quantum Electronics, IEEE Journal of,Vol.4, pp 707-711,1968

[58] Encycopedia of Laser Physics and Technology
http://www.rpphotonics.com/dye_lasers.html

[59] L. L. Deck,"Multiple-surface phase-shifting interferometry", Optical Manufacturing and Testing IV,Vol.4451, pp 424-431,2001

[60] S. R. Chinn, E. A. Swanson and J. G. Fujimoto, “ Optical coherence tomography using a frequency-tunable optical source”, Opt. Lett. Vol 22, pp 340-342 (1997)

Techniques for reducing non linearity in the laser

[61] E. Moore and R. McLeod, “Correction of sampling errors due to laser tuning rate fluctuations in swept-wavelength interferometry,” Optics Express, Vol 16, pp13139-13149,2008

[62] K. Tsuji, K. Shimizu, T. Horiguchi, and Y. Koyomada, “ Spatial-resolution improvement in long range coherent optical frequency domain reflectometry by frequency sweep linearization”, Electrn. Lett. Vol 33, pp 408-410, 1997

[63] K. Iyama,L.T. Wang and k. Hyashi, " Linearizing optical frequency sweep of a laser diode for FMCW reflectometry", J. Lightwave Technol. Lett, Vol 6, pp 1466-1468, 1994

[64] K.Y. Huang and G. M. Carter, " Coherent optical frequency domain reflectometry (OFDR) using a fiber grating external cavity laser", IEEE Photon. Technol. Lett. Vol 6, pp 1466-1468, 1994

[65] L. T Wang, K. Iyama, F. Tsukada, N. Yoshida and K-I. Hayashi, „ Loss measurement in optical waveguide devices by coherent frequency modulated continuous- wave reflectometry", Opt. Lett. Vol 18, pp 1095-1097, 1993

[66] M. Kobayashi, K. Takada, and J. Noda, "Optical frequency encoder using polarization maintaining fiber", J. Lightwave Technol, Vol 8, pp 1697-1702, 1990

[67] K. Takada, " High resolution OFDR with incorporated fiber-optic encoder", Vol 4, pp 1069-1072, 1992

[68] U. Glombitza and E. Brinkmeyer, " Coherent frequency-domain reflectometry for characterization of single-mode integrated-optical waveguides", J. Lightwave Technol, Vol 15, pp 1131-1141, 1997

[69] H. Rosenfeldt, C. Knothe, J. Cierullies and E. Brinkmeyer, " Evolution of amplitude and dispersion spectra during the fiber bragg grating fabrication", in Bragg gratings, Photosensitivity and Poling in glass waveguides, OSA Technical Digest Series (Optical Society of America, 2001)

[70] O. H. Waagaard, "Spatial characterization of strong fiber Bragg gratings using thermal chirp and optical-frequency-domain reflectometry", J. Lightwave Technol, Vol 23, pp 909-914, 2005

[71] L. Deck,"Absolute distance measurements using FTPSI with a widely tunable IR laser," Interferometry XI: Applications,Vol.4778, pp 218-226,2002

[72] L. Deck, "Frequency transform phase shifting interferometry," US Patent 6882432

[73] L. Deck, " FTPSI using a widely tunable 1550nm telecom laser", Zygo *RandD* tech memo, pp 1-16, 2001

[74] QDI Lambda Light CW and DM 1550 nm DFB Laser module, provided by Zygo Corporation, pp 1-4, 2002

[75] L. Perret and P. Pfeiffer,"Sinusoidal nonlinearity in wavelength-sweeping interferometry",Appl. Opt.,Vol.46, pp 8074-8079,2007

[76] J. Talamonti, R. Kay and D. Krebs, " Numerical model estimating the capabilities and limitations of the fast Fourier transform technique in absolute interferometry", Applied Optics, 35, pp 2182-2191, 1996

[77] I. H. Malitson,"Interspecimen Comparison of the Refractive Index of Fused Silica",J. Opt. Soc. Am.,Vol.55, pp 1205-1208,1965

[78] Dispersion equations for Optical Materials, Melles Griot

Techniques for measuring gauge blocks

[79] T. Doiron and J. Beers, "The Gauge Block Handbook", National Institute of Standards and Technology

[80] A. Korolev, "Measurement of Gage Blocks on a Kosters interferometer ", Measurement Techniques, 44, pp 709- 712, 2001

[81] M. Tsai, H. Huang, M. Itoh and T. Yatagai, "Fractional Fringe Order method using Fourier Analysis for Absolute Measurement of Block Gauge Thickness", Optical Reveiew, 6, pp 449-454, 1999

[82] Y. Ishii and S. Seino, "New method for interferometric measurement of gauge blocks without wringing onto a platen", Metrologia, 35, pp 67-73, 1998

[83] Y. Kuriyama, Y. Yokoyama, Y. Ishii and J. Ishikawa, "Development of a New Interferometric Measurement System for Determining the Main Characteristics of Gauge Blocks", Annals of the CIRP, 55, pp 563- 566, 2006

[84] J. Jin, Young-Jin. Kim, Yunseok Kim, C. Kang and S. Kim , " Absolute length calibrationof gauge blocks using optical comb of a femtosecond pulse laser ", *Interferometry XIII: Techniques and Analysis*, Katherine Creath, Joanna Schmit, eds., *Proc. SPIE,* 6292, pp. 62920O1-8, 2006

[85] E. Thwaite, "Phase Correction in the Interferometric Measurement of End Standards," Metrologia 14, 53-62, (1978)

[86] Landolt-Bornstein: Zahlenwerte und Functionen, I1 Band, 8. Teil Optiche Konstaten und Reflexionsvermogen von Legierungen, Berlin, Heidelberg, New York: Springer 1962

[87] http://www.tf.uni-kiel.de/matwis/amat/elmat_en/kap_3/illustr/t3_7_1.html

[88] Y. Okada and Y. Tokumaru, "Precise determination of lattice parameter and thermal expansion coefficient of silicon between 300 and 1500 K," J. Appl. Phys. 56, pp 314-320 1984

[89] B. Frey, D. Leviton, T. Madison, “Temperature-dependent refractive index of silicon and germanium NASA Goddard Space Flight Center, MD, pp 1-10, 1994

[90] A. Suratkar, Y. Ghim, A. Davies, “Uncertainty analysis on a commercial wavelength scanning interferometer measuring absolute distances,” . Proceedings of the SPIE Interferometry XIV: Techniques and Analysis. Edited by Schmit, Joanna; Creath, Katherine; Towers, Catherine E, Volume 7063, pp. 70630R-70630R-12 2008 *(Request from Editor Joanna Schmit)*

[91] ToBeSubmitted: A. Suratkar, Y. Ghim, A. Davies, “Uncertainty analysis for thickness measurements of transparent artifacts using wavelength scanning interferometry,” Measurement Science and Technology 2009

[92] A. Suratkar, A. Davies, F. Farahi, “New interferometric technique to measure the length (thickness) of opaque objects using a commercial interferometer,” Proceedings of the SPIE, Optical Manufacturing and Testing VII. Edited by Burge, James H.; Faehnle, Oliver W.; Williamson, Ray., Volume 6671, pp. 66710N-11, 2007.

[93] ToBeSubmitted: A. Suratkar, A. Davies, F. Farahi, “Improving coarse measurements of gauge blocks using wavelength scanning interferometry,” APPLIED OPTICS 2009

[94] ToBeSubmitted: Y. Ghim, A. Suratkar, A. Davies, “Wavelength scanning interferometer for 3D topographical thickness measurement of silicon wafer” OPTICS LETTERS, 2009